Geological controls on the evolution of Asian climate with specific reference to topography, ice sheets and CO_2

Despoina Zoura

Submitted in accordance with the requirements for the degree of
Doctor of Philosophy

The University of Leeds

School of Earth and Environment

September 2019

The candidate confirms that the work submitted is his/her/their own, except where work which has formed part of jointly authored publications has been included. The contribution of the candidate and the other authors to this work has been explicitly indicated below. The candidate confirms that appropriate credit has been given within the thesis where reference has been made to the work of others.

The work in Chapter 3 of the thesis has appeared in publication as follows:

Zoura, D., D. J. Hill, A. M. Dolan, S. J. Hunter, Z. Tang, and A. M. Haywood. 2019. "Atmospheric Carbon Dioxide, Ice Sheet and Topographic Constraints on Palaeo Moisture Availability in Asia." *Earth and Planetary Science Letters* 519:12–27.

I was responsible for setting up and running the model and for all the analyses presented in the paper.

The other authors provided feedback on the general experimental design and applicability of the methods and interpretation of the results.

The work in Chapter 4 of the thesis is currently in review by Global and Planetary Change and has received favourable reviews from the editor and reviewers.

Zoura D., A.M. Haywood, D.J. Hill, A.M. Dolan, Z. Tang. "The role of Central Asian uplift in East Asian Monsoon circulation and its palaeoclimate implication.

I was responsible for setting up and running the model as well as for all the analyses presented in the paper.

The contribution of the other authors was providing feedback on the interpretation of the results.

Acknowledgements

Foremost, I would like to express my sincere gratitude to my supervisors, Prof. Alan M. Haywood, Dr. Daniel J. Hill, Dr. Aisling M. Dolan and Dr. Zihua Tang for the continuous support, guidance, encouragement, insightful comments and stimulating discussions throughout my PhD. Their expertise was invaluable in the formulating of the research topic, and I could not have imagined having a better supervisory team for my PhD study.

I would also like to thank my colleagues and friends from the Institute of Geology and Geophysics, Chinese Academy of Sciences (IGGCAS) for the collaboration and the willingness to help me during my visits there.

In addition, I would like to thank my family and friends for their support and for providing happy distractions from my research.

This work was funded by the Strategic Priority Research Program of the Chinese Academy of Sciences (XDB26020401) and the National Natural Science Foundation of China (41472151).

Abstract

The hydrological regime in East and South Asia is dominated by the monsoons, whilst central Asia is characterized as arid. Defining the timing of the onset of aridity and the intensification of the monsoons in Asia, has generated significant debate over the years. The uplift of the Tibetan Plateau, the retreat of the Paratethys Sea, the atmospheric carbon dioxide (CO_2) decrease, and the associated global cooling after the Eocene/Oligocene transition are all considered to be major drivers of Asian aridity and monsoonal intensification. Here, a series of sensitivity simulations of a fully coupled ocean–atmosphere climate model (HadCM3) are carried out to investigate the effect of the atmospheric CO_2 variability, the uplifts of the Tibetan Plateau, Mongolian Plateau and Tian Shan orogen, and the Greenland and Antarctic ice-sheets formation, on Central Asian aridity, the East Asian Monsoon circulation and monsoon driven precipitation. Results show that increasing of the CO_2 causes wetter conditions for the East Asian and South Asian Monsoons and a steeper transition from non-monsoonal to monsoonal conditions in South Asia, while Arid East Central Asia becomes wetter during the non-monsoonal months. Results also show that even though ice-sheet coverage and CO_2 changes play a role on the Asian climate and its sub-systems, the latitudinal position and elevation of the Tibetan Plateau are the primary drivers for the Asian climate evolution. Absence of high-elevation in Asia shows increased surface temperatures, and decreased moisture availability and precipitation over Asia. Additionally, with the Tibetan Plateau at lower elevations, the westerlies flow zonally limiting the precipitation over East Asia to the summer months. Above an elevation threshold of 3000 m, simulations show a shift to a modern-like East Asian Monsoon circulation and Arid Central Asia conditions suggesting that the shift towards modern-like conditions over Asia is controlled by the high-elevation Central Asia.

Contents

List of Figures

List of Tables

List of abbreviations/acronyms

AECA: Arid East Central Asia

AI: IPCC (2007) Aridity index

DJF: December, January, February

EAM: East Asian Monsoon

EOT: Eocene/Oligocene Transition

GCM: General Circulation Model

I_{DM}: De Martonne index (aridity index)

JJA: June, July, August

MAM: March, April, May

MP: Mongolian Plateau

SAM: South Asian Monsoon

SON: September, October, November

TP: Tibetan Plateau

TS: Tian Shan orogen

Referencing style

The referencing style used in this thesis is the Leeds Harvard.

Chapter 1: Introduction

1.1 Project rationale

Asia is Earth's largest and most populous continent covering about 30% of the planet's total land area and 8.7% of its total surface while accounting for 60% of the world population. Asian climate is diverse, with climates ranging from arctic and subarctic to tropical. Environmental conditions in South and East Asia are dominated by the monsoons which represent a major component of the global climate system(Clift and Plumb, 2008; Webster et al., 1998), whilst central Asia is characterized by arid conditions with desertification threatening over 25% of China's landmass (Normile, 2007). In contrast to modern monsoon variability which is relatively well understood, Cenozoic variability and dynamics remain enigmatic (Ao et al., 2016) and it is important to understand these mechanisms in order to predict future changes more accurately. Internal forcing such as the Tibetan Plateau (TP) uplift, global cooling leading to ice sheet formation, Paratethys Sea retreat, land – sea distribution changes, eustatic fluctuations, monsoonal strength variability and reduced moisture transport have all been proven to play a role in driving the Asian climate change throughout the Cenozoic (Bosboom et al. 2014; Caves et al. 2015; Licht et al. 2014; Lippert et al. 2014). However, little is known about the relationship between these mechanisms, aridity onset and monsoon intensification.

With that in mind, this project's rationale is to provide for the first time a systematic approach to understanding Asian climate evolution by studying the main forcing factors (namely, the TP uplift, the ice-sheet formation and the atmospheric carbon dioxide (CO_2) values) through a set of sensitivity simulations designed to define each of these factor's role to the evolution of Asian climate throughout the Cenozoic.

1.2 Modern Asian climate and the importance of the monsoons

The climate of Asia is vastly diverse, encompassing polar, temperate, arid and tropical zones (Fig.1). However, the most prominent feature of Asian climate is the monsoonal system. The word “monsoon” is derived by the Arabic word for season and is usually defined as a seasonal wind reversal accompanied by changes in precipitation (Ramage, 1971). Fundamentally, monsoonal climates are characterized by dry winters and wet summers and a wind reversal from easterlies to westerlies.

The strongest and most well-known monsoons are those that affect India/Southeast Asia and East Asia, henceforward referred to as the South Asian Monsoon (SAM) and East Asian Monsoon (EAM) respectively. Those two subsystems are of great importance as they affect more than half of the world’s population and have a great impact on the society and economy of the affected countries (IPCC, 2007). Specifically, with agriculture being the most common form of land-use in the majority of the monsoon dominated regions in Asia, the seasonal variability of monsoon associated precipitation is a key factor to the economy of the region. In recent years, the erratic nature of the monsoons has caused droughts, floods and other extreme weather events that caused disturbances to the community (i.e. Hong Kong drought in 1963; China flood event in 1931 etc). Furthermore, recent work has linked the monsoonal variability to civilization changes during the past 5700 years around the Indus Valley region (Kathayat et al., 2017). It is thus essential to understand the monsoonal mechanisms and patterns not only in present day but through the Cenozoic where available proxy data can be used to evaluate the models and mechanisms proposed, so that uncertainties and biases in future predictions can be constrained.

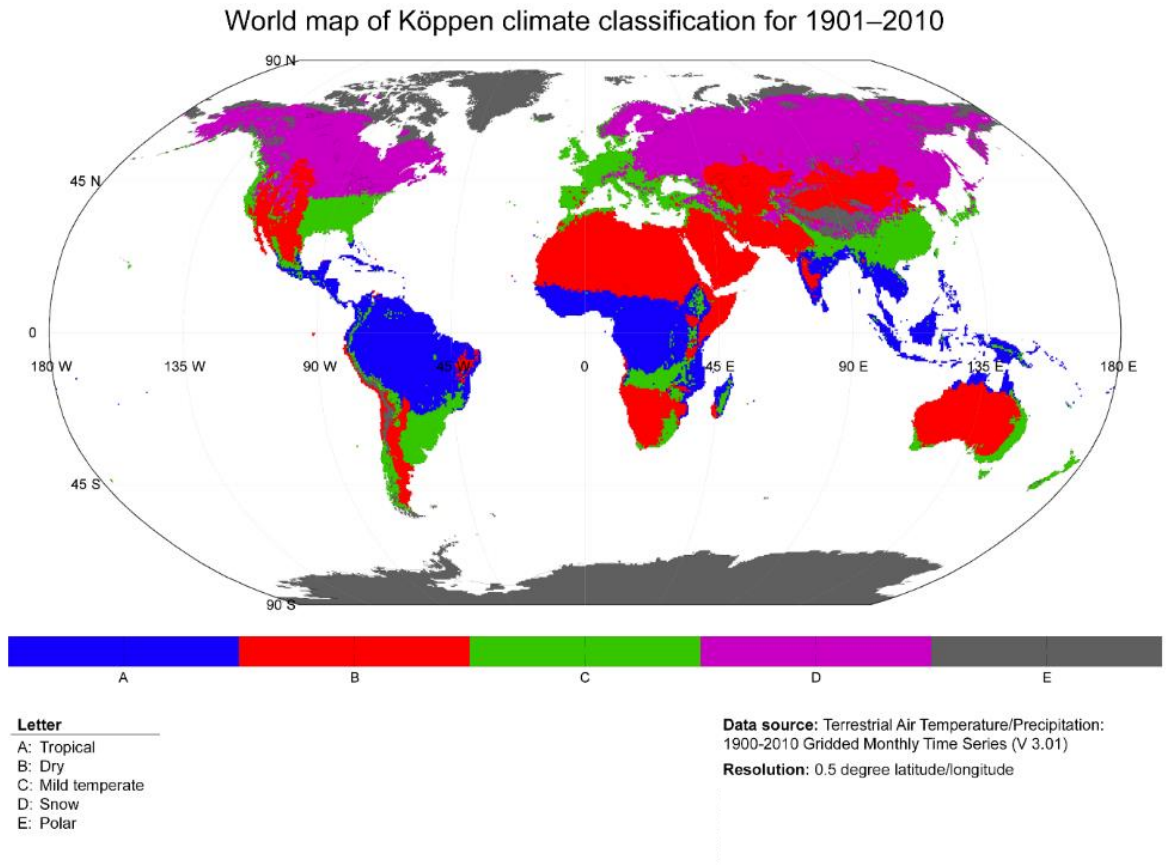

Figure 1: The five major climatic types according to the Köppen-Geiger climate classification. Asia presents with all 5 climate types namely A: tropical, B: Dry, C: Mild temperate, D: Snow and E: Polar. Plot from Chen and Chen 2013.

1.3 Palaeogeographic evolution of Eurasia during the Cenozoic

Initially, it is useful to describe the geological history and uncertainties associated with this region. Asia constitutes two broad Cenozoic deformation zones: the India-Asia collision zone in the east and the Arabia-Asia collision in the west (Yin, 2010). Despite decades of study, controversy remains over basic aspects that formed the Asian continent since the Paleogene period. One of the most debated subjects being the exact onset age of the collision which ranges from 65 Ma (Yin and Harrison, 2000) to approximately 50 Ma (Najman et al., 2001; Rowley, 1996).

Cenozoic tectonics of Asia is most dramatically expressed by the development of the TP. Wang et al. (2008) suggests that the central plateau (the Lhasa and southern Qiang-tang basins) was uplifted by the Late Paleogene (40 Ma). Predating that uplift and based on paleomagnetic estimates there seems to be a substantial surface uplift of the TP (Lippert et al., 2014). To the south, the Himalaya rose during the Neogene (23.3 Ma). To the north, the Qilian Shan rapidly uplifted in the Late Cenozoic. These ranges constitute the modern southern and northern margins, respectively, of the TP. Several studies indicate that the southern TP (i.e., the Lhasa block) established its current elevation in the late Cretaceous (England and Searle 1986; Kapp et al. 2007; Leier et al. 2007; Murphy et al. 1997). Central and northern Tibet on the other hand, experienced significant crustal shortening within 10 Ma from the onset of the collision.

According to a tectonic review by Yin (2010) deformation of the Asian continent during the Cenozoic can be divided in the following periods. From 60-40 Ma, the first phase of the deformation is mainly concentrated in front of the northward indenting Indian continent. The period of 30-20 Ma marked important events like the formation of the Tian Shan (TS) orogen, the extension in the North China Sea and the partitioning of the Palaeo-Qaidam basin into the Hoh Xil and Qaidam basins (Fig. 2).

The Hoh Xil basin is part of the north-central TP. It is characterized by low-gradient fluvial and lacustrine facies laying as a possible analogue of the Qaidam or Tarim foreland basin systems (Wang et al., 2008). The Hoh Xil basin has an average elevation of ~5 km which is about 2 km higher than the Qaidam basin that has an average elevation of ~2900 m (Fig. 2).

Tarim basin is most known for its size of approximately 530,000 km^2 and active sand dunes (Sun et al., 2015). The Tarim basin is constrained by three mountain ranges: The Kunlun range, Pamir Mountains and TS to the South, West and North respectively. The Tarim basin was part of the Paratethys Sea until the late Eocene (40-37 Ma) when tectonic events led to

the retreat of the Sea to the northwest (Licht et al., 2014). Bosboom et al. (2014b) suggest that the Tarim Basin was hydrologically connected to the Tethyan marine realm until at least the earliest Oligocene and had not yet been closed by uplift of the Pamir–Kunlun orogenic system to the southwest.

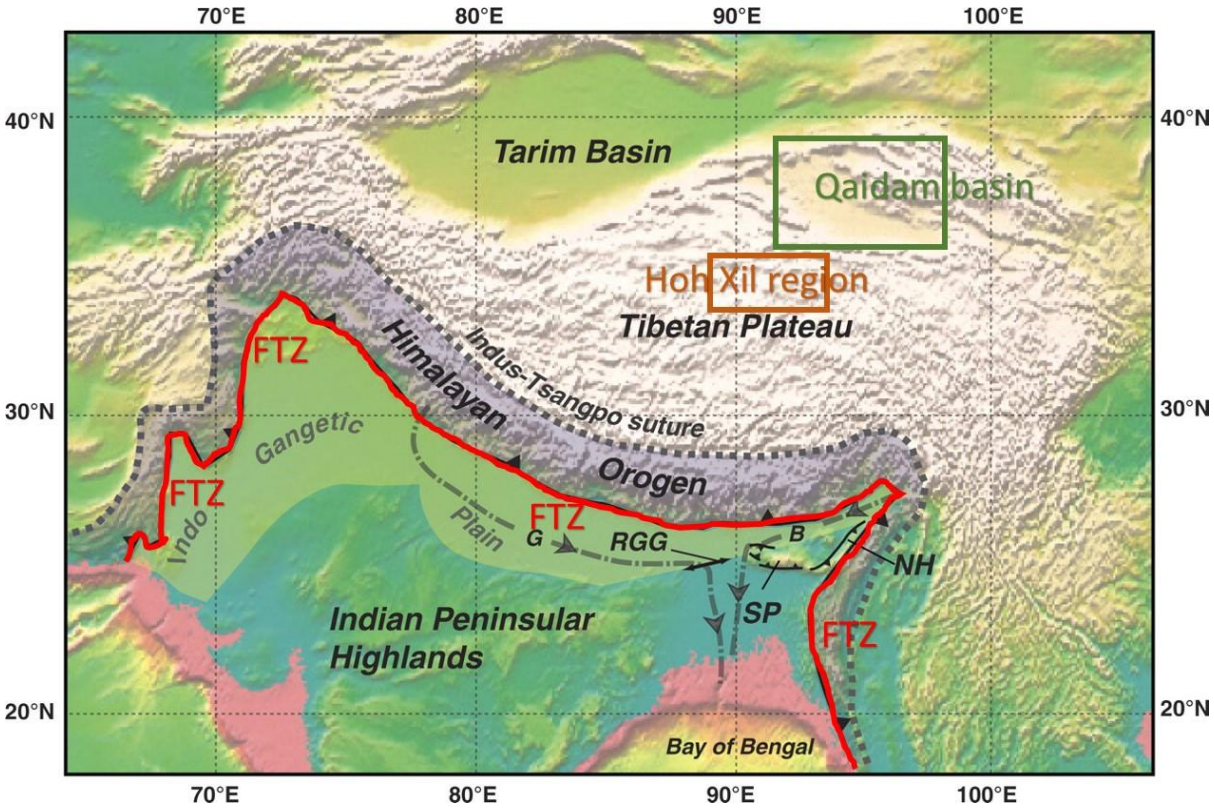

Figure 2: Outline of the Himalayan orogen between the Indus-Tsangpo suture zone and frontal thrust zone (FTZ) in the South and the locations of the Tarim Basin, Qaidam basin, Hoh Xil Basin, Shillong Plateau (SP), Rajmahal-Garo Gap (RGG), and Naga Hills (NH), The Ganges River (G) and Brahmaputra River (B) both flow across the Rajmahal-Garo Gap into the Bay of Bengal (modified from Yin, 2010).

1.3.1 Eocene

Between the late Cretaceous (100 Ma) and early Eocene (56 Ma) time, an Andean mountain range developed along the southern margin of the Eurasian plate (Wang et al., 2008). According to Molnar et al. (2010) middle Eocene was characterised by a high terrain area of approximately 4000m height, thousands of kilometres long and perhaps 200 to 400 km wide, laying at 10°N (±5°) at ~90°E -20°N (±5°) at ~70°E along the southern margin of Eurasia. Lippert et al. (2014) also demonstrated the existence of an Eocene proto-plateau but they narrow down the palaeolatitude estimation to ~19° ±4° N using a so-called conservative approach (Fig. 3). Oxygen isotope data for the Eocene suggest that the southern and central part of the TP had reached high elevation compared to the northern part of the plateau that remained low (Sun et al. 2015). Rowley and Currie (2006) suggest that the growth of the plateau is progressive and moves northward for elevations between 4-5 km at a rate of about 20km/Ma since middle Eocene (46.2 Ma). At the same time, the Tethys Ocean north of India has been already closed by the India-Asia collision and a new shallow epicontinental sea has been created. This sea was connected to the Indian Ocean to the South, the Mediterranean to the West and the North Sea basin through a shallow water connection via the Danish-Polish trough (Rögl, 1998) (Fig. 3).

Lhasa and Qiangtang terranes formed the proto-TP and were at or near their current elevation since 40 Ma (Wang et al. 2008). Palaeoelevation estimates derived from the Lunpola basin inside the Qiangtang terrane (Fig. 4) are currently the oldest data indicating that parts of the plateau were highly elevated (approximately 4000m) by the late Eocene to early Oligocene (Rowley & Currie, 2006). Further to the North, studies from the Hoh Xil basin are controversial concerning the elevation of the basin during the Late Eocene. DeCelles et al. (2007) contradict the first palaeoelevation estimates of 2 km by Cyr et al. (2005) and by re-evaluating the data using lower empirically based lapse rates argue that the basin was 4.7-5 km high during Late Eocene.

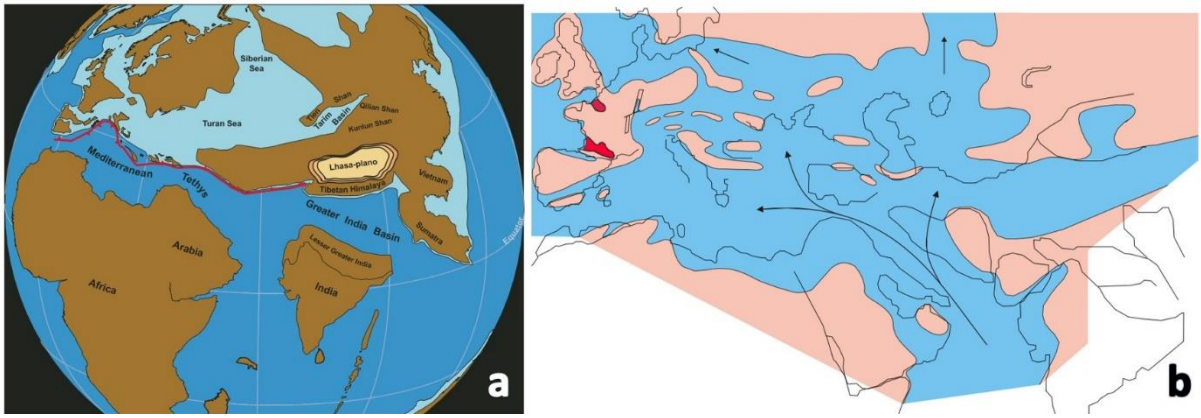

Figure 3: a) Early Eocene palaeogeographic reconstruction at the time of collision between the Tibetan Himalaya and the southern margin of Asia by Lippert et al. (2014), introducing the high proto-plateau in southern Tibet. b) Eocene palaeoceanographic reconstruction showing the extend of the Paratethys to the central Asia and water connections with the Mediterranean, Indian Ocean and North Sea (Rögl, 1998).

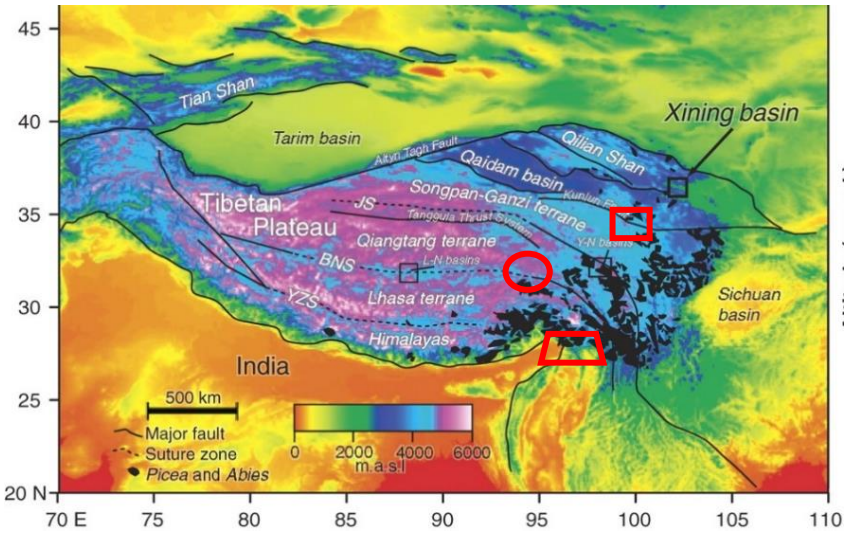

Figure 4: Topographic map of Tibetan Plateau (TP) region with major tectonic features (YZS— Yarlung Zangpo suture; BNS—Bangong-Nujiang suture; JS—Jinsha suture; N— Nima basin; Y-N—Yushu-Nangqiang basins). Qiangtang and Lhasa terrains are shown in the central TP with elevations exceeding 5.000 m. Hoh Xil and Lunpola basins and Indus-Yarlung suture zone are shown in the red box, circle and trapezoid respectively (modified after Dupont-Nivet et al. 2008).

Although most of the researchers agree in the existence of an early proto-plateau in the southern margin of Asia a new constrain is introduced by Lippert et al. (2014) for the palaeolatitude of this feature in Eocene times. For example, the Indus-Yarlung suture zone (IYSZ) with a modern location at 29°N, 88°E palaeolatitude is estimated at 21° ±4° N from early to middle Eocene (56-47 Ma) and 24.7° ± 3.8°N in late Eocene to Early Oligocene. Similarly, the Lhasa terrane transitioned northward to its present latitude at 29°N only in the past 50 Ma with a palaeolatitude of 16°-22°N since 110 Ma.

While southern Tibet has remained approximately at its present height for as long as we can measure palaeoelevations - 35±5 Ma (Rowley and Currie 2006), the elevation history of northern Tibet is hardly constrained at all (Molnar et al. 2010). Finally, for the central TP indications show elevation in excess of 4 km since Late Eocene to Early Oligocene (35±5 Ma ago) (Rowley and Currie 2006).

1.3.2 Oligocene

Although we cannot quantify the elevation history of the TP, we can synthesize the conclusions of studies all over this area and propose a new palaeogeographical reconstruction for the Oligocene taking under consideration the new palaeolatitude and palaeoelevation data. Prior to approximately 25 Ma (Late Oligocene) intracontinental deformation in Asia was confined mostly inside Tibet (Yin 2010). Starting from Asia's southern margin it seems likely that around 30 Ma a huge area extending from 20-25°N to nearly 40°N had a mean elevation as high as 1000m (Molnar et al. 2010). With that mean elevation as a base, we can add the Central Tibet elevation which was estimated in excess of 4 km for the Early Oligocene (Rowley and Currie 2006). In addition, oxygen isotope studies in the Lunpola basin suggest that the region was 4-4.6 km high by early Oligocene (Wang et al. 2008). Nima basin, between the Lhasa and Qiangtang terranes was also high and dry,

similar to the modern environment by Early Oligocene (DeCelles et al., 2007). Finally, to the North, in Hoh Xil Basin even though palaeoaltimetry estimates are equivocal the minimum elevation is estimated to be 2000 m whereas the maximum 5000 m. The Tarim and Junggar basins are most likely linked as one unified basin, before the formation of TS range (Yin et al., 2008). The uplift of TS began at 24-20 Ma (Yin et al., 1998) although Molnar et al. (1993) argue that it started at 8 Ma (Fig. 5).

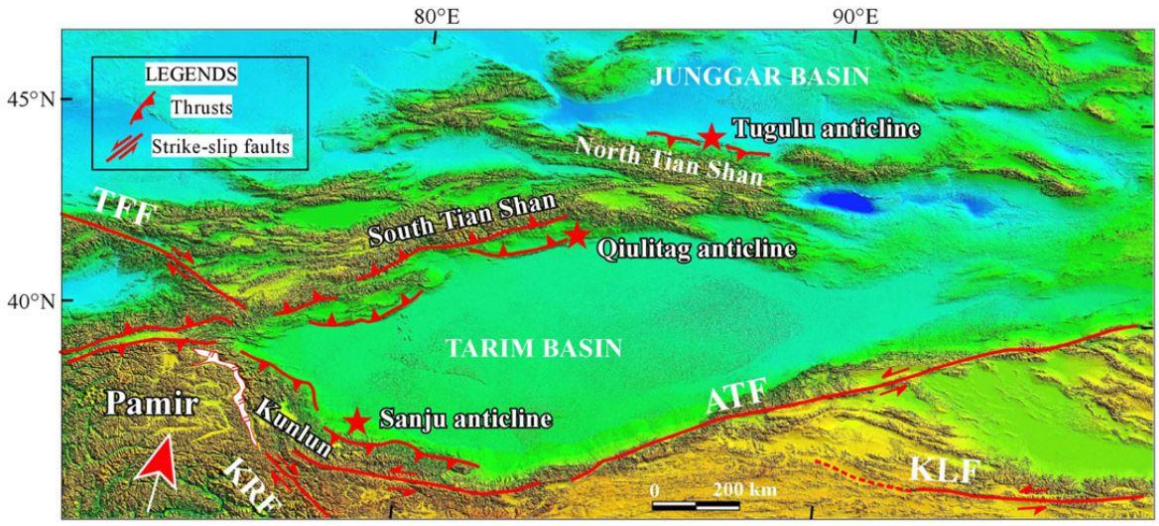

Figure 5: Digital elevation model showing a simplified tectonic framework (Sun et al., 2015). *Tarim and Junggar basin are two independent basins separated by the Tian Shan (TS) range.*

At the Eocene – Oligocene boundary, Paratethys was separated from the Mediterranean due to the increased continentalization of Europe. During Early Oligocene (Early Kiscellian), the connection between them was established with two narrow straits while both Seas were connected to the Atlantic to the North and West respectively (Rögl, 1998). Paratethys was also extending to the East into Central Asia through a narrow seaway, although, this connection is uncertain (Fig. 6 A-D).

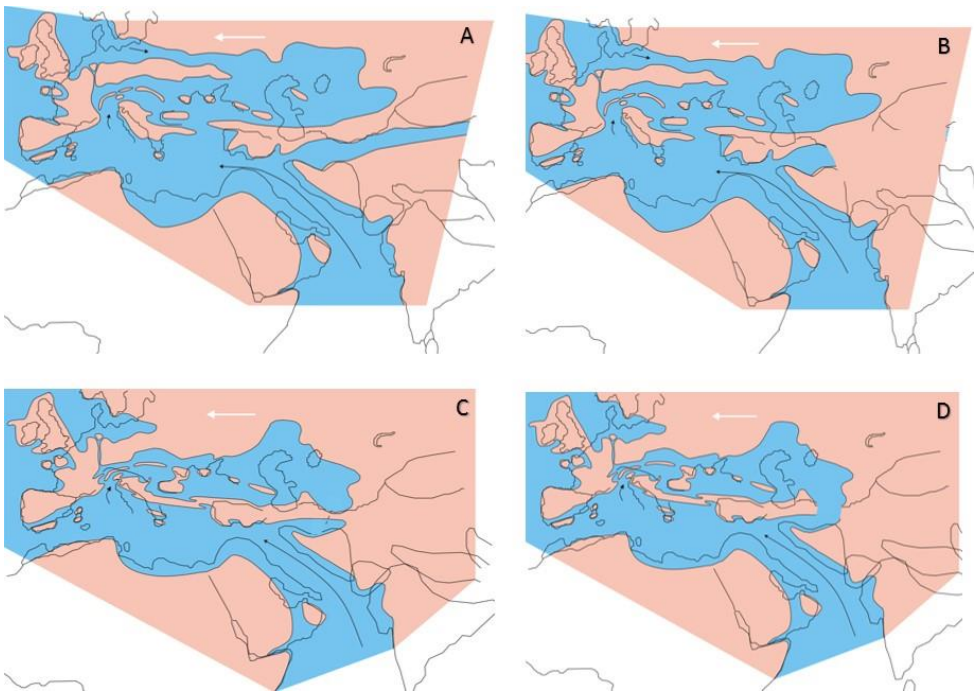

Figure 6: Palaeoceanographic boundary condition sketches for the Oligocene, modified after (F. Rögl, 1998). *A: Paratethys extending in Central Asia through a narrow strait, B: Paratethys connection to Central Asia closed, C: Paratethys connection to the Mediterranean is established through a narrow strait to the West, D: Paratethys connection to the Mediterranean is established by two straits to the Southwestern and South-eastern extend of the Sea respectively.*

1.3.3 Miocene

The second phase of Cenozoic deformation in the Himalaya started during the Early Miocene and has been ongoing ever since (Hodges, 2000). In the Middle to Late Miocene (18-8 Ma) studies show a major change in the Tibetan deformation pattern (Coleman and Hodges, 1995; Taylor and Yin, 2009). Extensional faults during Miocene created the sea of Okhotsk to the East of Asia (Yin 2010). The onset of the TS uplift at 8 Ma (Molnar et al. 1993) is contradictive to other studies as discussed above but new neotectonic studies and magnetostratigraphic analyses suggest that the uplift of TS may have accelerated since the early Miocene (Tang et al., 2016; Yin et al., 1998). On the north-eastern margin of the TP, specifically in the Qilian Shan and associated ranges (Fig. 4) both early and later evidence

place the uplift during the Late Miocene (Lease et al., 2007; Meyer et al., 1998; Tapponnier, 2001). The final major tectonic event for the Miocene is the collision of the Pamir orogen with the TS orogen at 5.3 Ma ago (Fig. 7).

During the past 15 Ma, the TP has grown outward on its north-eastern and eastern sides (Molnar et al. 2010). Several studies suggest that these margins of the plateau have risen to their present-day heights since approximately 15-10 Ma (Molnar and Stock, 2009). At the same time estimates show an elevation of ~1000 m for the Northern Tibet (Molnar et al. 2010). Oxygen isotope-based palaeoaltimetry studies from the Tethyan Himalaya suggest that it was near modern elevation by the Mid-Miocene (Garzione et al. 2000; Rowley et al. 2001). There are also studies in the Namling-Oiyung basin suggesting that the elevation of the southern TP has remained at approximately 4.6 km since 15 Ma ago (Currie et al. 2005; Spicer et al. 2003).

During the Early Miocene (23 Ma) the general configuration of the Paratethys did not change and the connection to the Indian Ocean and the Mediterranean remained open. Further into the Miocene (approx. 18 Ma) important tectonic events such as the collision of the Arabian plate with the Anatolian plate resulted in the closing of the seaway between the Mediterranean and the Indian Ocean. In Middle Miocene, the Paratethys was connected to the Mediterranean with one seaway in Slovenia while the connection to the Indian Ocean at that time is debatable (Rögl, 1998). Finally, in the Late Miocene and as the continentalization of Europe continued the Paratethys become completely isolated and shrunk significantly (Rögl, 1999).

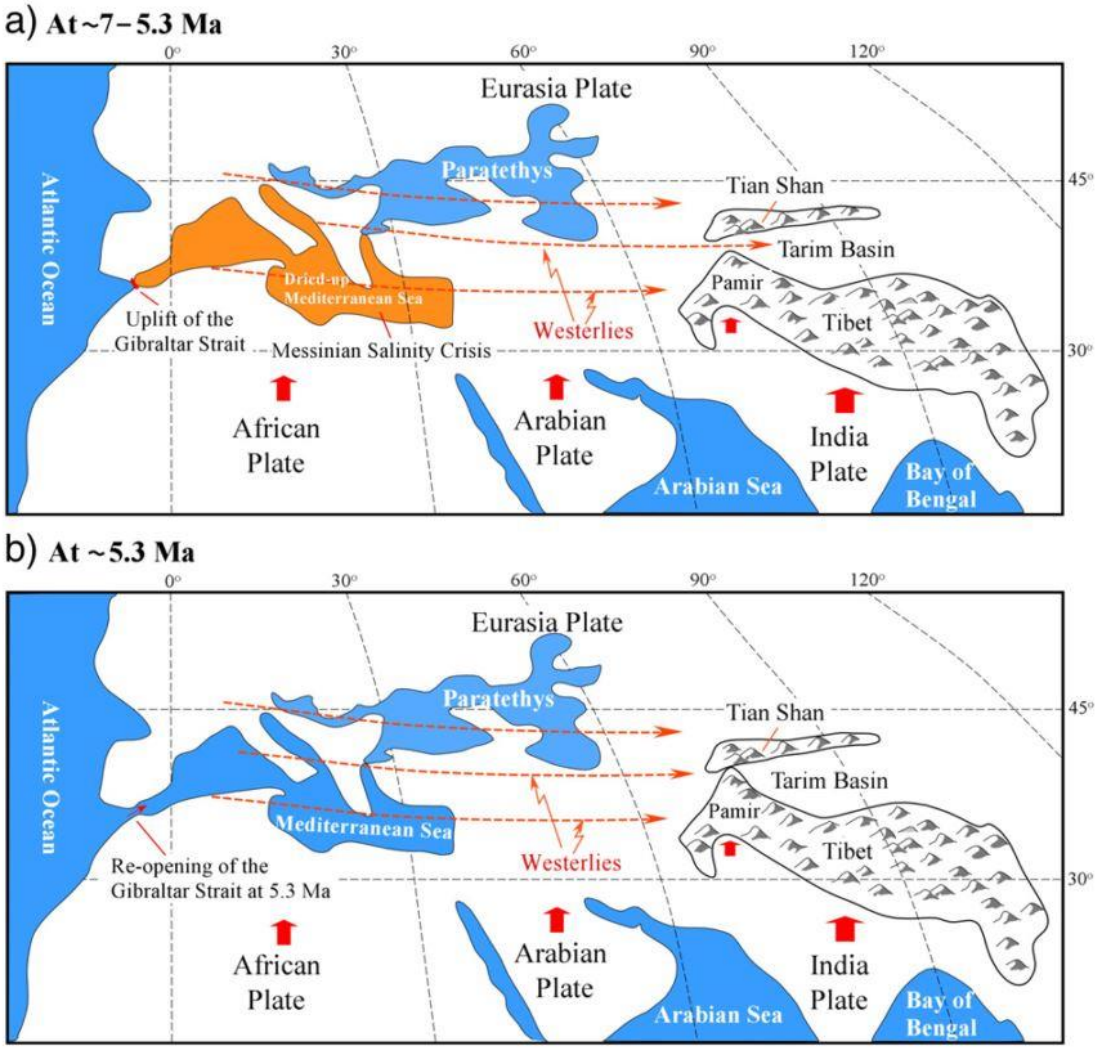

Figure 7: Schematic maps showing the closing of the Tarim Basin to the West due to Pamir orogen and TS collision during the Latest Miocene. (a) Regimes of sea distribution, extent of the dried-up Mediterranean Sea, and the positions of the Pamir and TS orogens. (b) The northward indentation of the Pamir salient finally led to the collision with the TS orogen at ~5.3 Ma, together with the uplift of the surrounding mountains (after Sun et al. 2015).

1.4 CO_2 evolution during the Cenozoic

CO_2 is a primary driver for climatic change on a global scale, and even though in the recent years CO_2 levels are directly measured providing a detailed record, that is not the case for the rest of the Cenozoic era. In a broad context, the carbon cycle on large time scales can be defined as the exchange of carbon between rocks, the atmosphere, biosphere oceans and soils (Royer et al., 2001). Over the years, many techniques and methods have been

developed for reconstructing Cenozoic atmospheric CO_2, but each with limitations. The different temporal resolution recorded in different types of proxies such as paleosols, boron isotopes, phytoplankton carbon isotopes etc., the dating accuracy, and the lack of many continuous records, lead to significant discrepancies between proxies. For example, in the early '00 CO_2 proxy estimates for the Eocene were ranging from 300 ppm to 3000 ppm (Beerling and Royer, 2011). However, recent advances and further development of those methods are producing promising results for specific proxies (IPCC, 2007).

The early Eocene (56 Ma) is considered as the warmest period of the past 65 Ma (Pagani et al., 2005). During the transition from Palaeocene to Eocene, large-scale volcanic outgassing of CO_2, combined with magmatism, regional metamorphism and suspected methane release from wetlands and/or gas hydrate reservoirs are suggested forcings that drove the thermal maximum events from 55 Ma to 50 Ma ago (Pearson and Palmer, 2000), reaching its pick at 50 Ma ago. Estimates of CO_2 concentration for this period vary significantly but the consensus is that atmospheric CO_2 was in excess of 1000 ppm (i.e. Hansen et al. 2008; Pagani et al. 2005) (Fig. 8). Recently, in an effort to further constraint the atmospheric CO_2 values during the early Cenozoic, Anagnostou et al. (2016), analysed foraminiferal calcium carbonate $\delta^{11}B$. The results showed atmospheric CO_2 concentrations during the Early Eocene Climate Optimum (EECO, 50.3 - 52.6 Ma) at 1400±470 ppm. Furthermore, nahcolite proxies in evaporite deposits suggest new upper and lower limits of CO_2 concentration during the EECO at 1260 and 680 ppm respectively (Jagniecki et al., 2015).

Following the climatic optimum, there was a prolonged period of cooling with CO_2 values rapidly decreasing leading to a shift from greenhouse to icehouse conditions at the Eocene to Oligocene Transition (EOT). Researchers are in agreement with the declining CO_2 trend following the Eocene, however, estimates for the EOT are largely unconstrained with researchers placing CO_2 values at ~1500 ppm to 450 ppm (Pearson et al. 2009), 1700 – 900 ppm (±100) (Heureux and Rickaby, 2015). More recently, new proxy records combined with

advances in proxy science, place the CO_2 at less than 770 ppm during the EOT (Anagnostou et al., 2016; Zhang et al., 2013). Furthermore, CO_2 reconstructions based on stomatal proxies indicate even lower concentrations (~410 ppm) during the EOT, values that are considerably lower than reconstructions based on marine proxies (Steinthorsdottir et al., 2016).

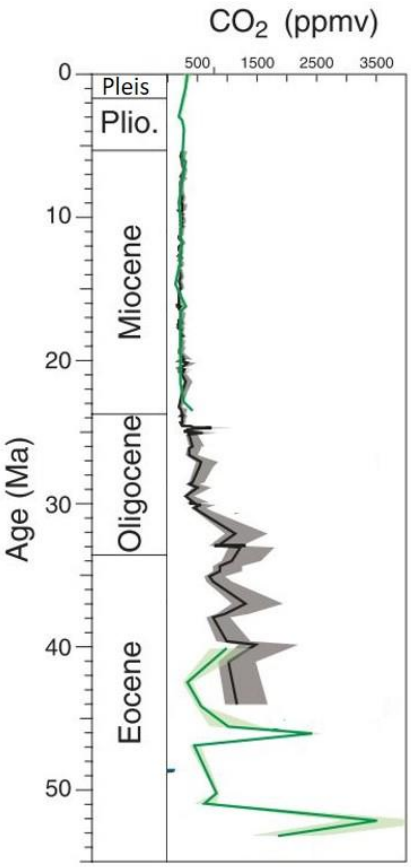

Figure 8: Synthesis of atmospheric CO_2 estimates. Black line shows estimates obtained from alkenones (Pagani et al., 2005). *Green line is based on boron isotopes* (Pearson and Palmer, 2000). *Graph modified from* Miller et al. (2009).

Data available for the Oligocene are sparse, however, results from a continuous record of the past 40 million years from ODP Site 925 (Zhang et al., 2013) indicate that after the EOT and until the Late Oligocene there was a long-term decrease in atmospheric CO_2.

Reconstructions derived from boron isotopes, algal alkenones, and stomatal density of fossil leaves, suggest values ranging from 200 – 1000 ppm for the Oligocene however the uncertainties are large (Henderiks and Pagani, 2008; Pagani et al., 2005; Pearson et al., 2009; Roth-Nebelsick et al., 2012; Sun et al., 2017; Zhang et al., 2013).

Atmospheric CO_2 concentrations present with a long-term decreasing pattern which continues well into the Miocene (Fig. 8). New data suggest that CO_2 concentration at the Oligocene-Miocene boundary was as high as ~650 ppm (Steinthorsdottir et al. 2019), followed by a drop during the early Miocene. Since the early Miocene, atmospheric CO_2 values have remained below 500 ppm and present with a more stable pattern than before (Pearson and Palmer, 2000).

1.5 Ice-sheet evolution throughout the Cenozoic

The glacial history of the Cenozoic is largely unconstrained when it comes to the pre-Pleistocene era (Zachos et al. 1992). With the absence of direct geological evidence, ice sheet reconstructions are based on proxy records such as oxygen isotopes and marine microfossils that can be difficult to interpret beyond the Pleistocene timescales and ice-sheet models.

During the Early-Middle Eocene, Antarctica experienced warm and wet climates with no indication of ice-sheet formation (Francis et al., 2009), vegetated and with annual mean temperatures above 0^{o}C (DeConto and Pollard, 2003). The consensus that the onset of Antarctic glaciation occurred during the EOT (33.9 Ma), is supported by the observed increase in benthic foraminiferal $\delta^{18}O$ values that correspond to cooling and growth of the ice sheet volume (Coxall et al., 2005; Zachos et al., 2001), marking the transition from greenhouse to icehouse conditions on Earth. The Antarctic glaciation onset is described as rapid and occurring in two-steps (Coxall and Wilson, 2011; Coxall et al., 2005), while the East Antarctic continental interior is believed to be the point of initiation (Barrett, 1996). The ice

sheet growth is attributed to either tectonic forcings such as the opening of ocean gateways, or to decreasing CO_2 values combined with favourable for ice-sheet growth orbital configurations (i.e. Cramer et al. 2009; DeConto and Pollard 2003; Pearson et al. 2009). Furthermore, mineralogical and geochemical composition of grains collected during the ODP Site 696 provided the first evidence for the presence and continuity of ice in the Late Eocene extending from the mountainous interiors to South of the Weddell Sea (Carter et al., 2017).

The early glaciation of the Arctic remains a controversial subject with most studies pointing towards Middle Miocene (Winkler et al., 2002) (Fig.9). However, more recent studies have provided sedimentary evidence of glacial ice that researchers place between 38 to 30 Ma ago (Eldrett et al., 2007), when temperatures and atmospheric CO_2 were significantly higher. Additionally, sediments dated from middle Eocene to early Oligocene collected at ODP site 913, show evidence of ephemeral glaciation on Greenland and the Arctic Sea during the middle Eocene through early Oligocene (Tripati and Darby, 2018). Furthermore, sediment core spanning from Late Palaeocene to present taken from the Arctic Ocean (IODP ACEX) shows evidence of ice-rafted debris in the Middle Eocene (Moran et al., 2006). However, these recent studies that suggest a bipolar ice world after the EOT are in direct contradiction with modelling studies that have shown that the threshold CO_2 value for Northern Hemisphere glaciation is ~280 ppm, significantly lower than any proxy reconstruction for the same period (DeConto et al., 2008).

After the EOT and until the Middle Miocene, glaciation was marked by ice volume fluctuations similar in scale to those of the Pleistocene ice sheets of the Northern Hemisphere (National Research Council 2008) and indicate a highly dynamic glacial environment in both poles (i.e. Holbourn et al. 2014, 2015, 2018; Jovane et al. 2019). During the middle-Miocene (~ 14 Ma ago) deposits and marine isotope records show a second stepwise decrease of the Pacific oceanic waters that led to further glacial expansion

(Holbourn et al. 2005; Lewis et al. 2007). This is consistent with results from the Arctic Ocean that show an increase on the occurrence of ice rifted debris (Moran et al., 2006).

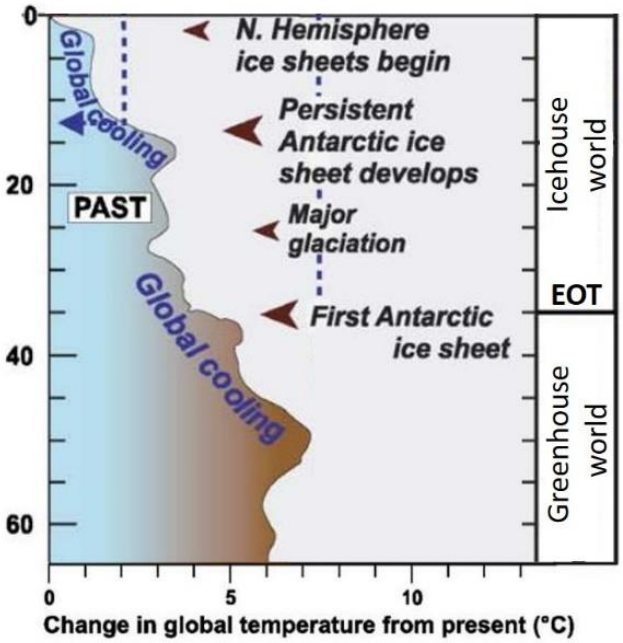

Figure 9: Antarctic ice-sheet evolution synoptic overview throughout the Cenozoic. Temperature curve from Crowley and Kim 1995. The EOT refers to the Eocene to Oligocene Transition that marks the shift from greenhouse to icehouse world. Even though the Northern Hemisphere glaciation was suggested to have started during the Pleistocene, recent studies place it during the Late Eocene. (Figure modified from Escutia et al. 2005).

1.6 Paleoclimatic evolution of the Asian continent during the Cenozoic

Geological records have shown that the Cenozoic was a time of dramatic tectonic and climatic change in Asia. The India-Asia collision, the TP uplift, the retreat of the Paratethys Sea and the global cooling and associated decrease in atmospheric CO_2 values, have all had an effect on the evolution of the Asian climate that led to the formation of modern-like atmospheric circulation over Asia.

During the early Eocene there was a series of global warming events adding to the long-term warming trend. Reconstructions from proxy data identified the Early Eocene Climate Optimum as the warmest period of the Cenozoic era (Hollis et al. 2009, 2012; Zachos et al. 2008). From the Paleogene to Early Eocene the climate of Asia was dominated by a broad arid band from Central Asia to the East (e.g. Guo et al. 2008; Sun and Wang 2005), and it was characterized as warm, while the monsoon circulation was weak and limited in a narrow region around the coast (Lu and Guo, 2014). The Eocene to Oligocene transition (EOT) (33.5-34 Ma) marked a significant change in earth's climate with the transition from greenhouse to icehouse conditions. The EOT shift is recorded in marine sediments that show a large and widespread ocean cooling (Liu et al. 2009; Zachos et al. 2001), and onset of Antarctic ice-sheet formation (Coxall et al. 2005; Goldner et al. 2014).

Recent studies of palynological and palaeoenvironmental proxy data (foraminifera, bivalves, calcareous nannofossils etc.) suggest that during the Eocene the inland aridity was formed and subsequently intensified towards the end of the Late Eocene (i.e. Bosboom et al. 2014; Guo et al. 2014; Miao et al. 2016). On the other hand there have been many studies linking the aridification of inland Asia to the global cooling during the EOT (i.e. Dong et al. 2013; Dupont-Nivet et al. 2007; Wang et al. 2013).

Sun and Wang (2005), compiled data from 125 sites over China and showed a reorganization of the climate system. Specifically, during the Eocene and the Oligocene, East Asia is dominated by a broad arid belt, whereas around the Oligocene to Miocene boundary this arid belt is spatially limited to the Northwest (Fig. 10). The arid belt dominating Central Asian climate during the Paleogene experienced significant fluctuations during the Eocene that intensified in the Oligocene. Furthermore, sedimentary records from the Xining basin also showed that inland Asia was characterized by dry conditions prior to the EOT but with warm and humid intervals, while pollen data from Qaidam basin, NE of the TP, have also shown relatively dry conditions during the Eocene and Late Oligocene (Wang and Fan, 1999). Early

Oligocene is characterized by a limited distribution of sediments over Asia, however, the data available suggest that the climate over East Asia is also dominated by the arid belt but appears with a shrinkage in terms of width (Sun and Wang 2005).

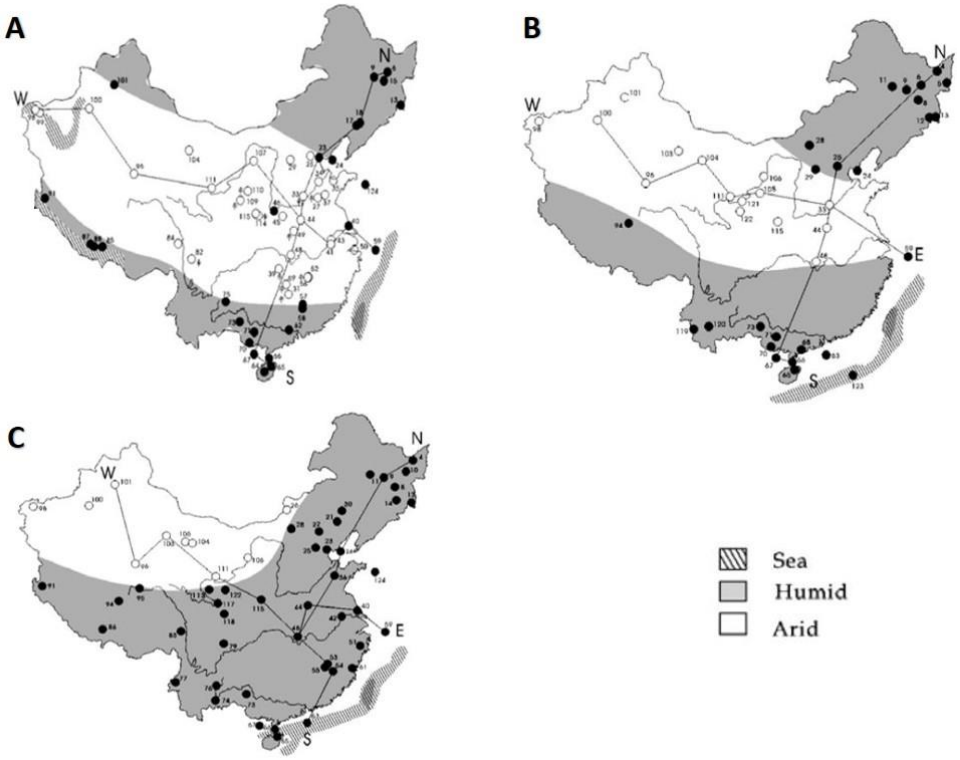

Figure 10: Evolution of climate zones in China during A) the Eocene, B) the Oligocene and C) the Miocene. Reconstructions are based on palynological and palaeobotanical data, modified from Sun and Wang (2005).

Continental and marine proxy records can provide great insights on the climate of Asia during the Cenozoic. However, using proxy data for reconstructing monsoonal strength can be a complicated and difficult task (Clift and Plumb, 2008). Firstly, the two monsoons dominating the climate of Asia are distinctly different. The South Asian Monsoon (SAM) presents with a tropical monsoon circulation where precipitation is associated with the Intertropical Convergence Zone (ITCZ) (Gadgil, 2003). On the other hand, the East Asian Monsoon precipitation is associated with frontal systems and the jet stream (Molnar et al. 2010). The different manifestation of these monsoons can not be captured by a single proxy, and that,

combined with the difficulty in dating sedimentary records which are usually scattered or discontinuous, proves a challenge for studies reconstructing the monsoonal variability and strength especially before the Pliocene times. Thus, in order to reconstruct the monsoonal evolution, researchers have used a wide variety of proxy data that capture individual characteristics of the monsoonal system.

The first study that provided data for the monsoonal evolution over large time scales was the ODP expedition 117 in the Arabian Sea (Prell et al. 1991). The sampled cores combined with terrestrial records, showed enhanced upwelling associated with a strengthening of the monsoon during the Late Miocene (~8Ma), which was interpreted as the timing of monsoonal onset (An et al., 2001; Prell et al., 1991). However, subsequent studies using longer marine cores from the South China Sea and the North Pacific, and terrestrial data such as the Red Clay Formation of the Loess Plateau provide reconstructions that show monsoon intensification dating back to at least the Oligocene/Miocene or early Miocene (Guo et al., 2002; Miao et al., 2013; Rea, 1994; Srivastava et al., 2012; Sun and Wang, 2005). Up until this point, the absence of continuous and wide spread proxy records over Asia for the Oligocene and earlier times, limited our ability to define if the evident change during the Oligocene – Miocene boundary corresponds to monsoonal onset or an era of monsoonal intensification. However, Shukla et al. (2014), analysed lacustrine deposits from India that suggest the existence of a pronounced South Asian Monsoon existed prior to the collisional uplift. Furthermore, Licht et al. (2016) studied dust deposits from 33-42 Ma when the TP was at lower elevation, the Paratethys Sea has not yet retreated to the west and the CO_2 values were higher and showed that dust-sources and near-surface circulation in Central Asia was present with only minimal changes since at least 42 Ma ago.

1.7 Asian climate reconstruction with the use of models

While geological records provide insights into the Asian climate and its evolution during the Cenozoic, the mechanisms that control the formation and evolution of Asian monsoons and aridity remain a controversial subject. To address the absence of data and the uncertainties of proxy interpretation, there has been extensive research on the evolution of Asian climate from a palaeoclimate modelling point of view.

The first attempts of using numerical methods for weather predictions can be dated back to the beginning of the 20th century, however it was not until 1956 that computing power became sufficient for the creation of the first 3-D General Circulation Model (GCM) (Phillips, 1956). In the 1970s the interest on the climates of the past led to the first experiments using Atmospheric GCMs (AGCM) focusing on the Last Glacial Maximum (e.g. Alyea 1972; Manabe and Hahn 1977; Williams et al. 1974). Since then, the use of models in palaeoclimate reconstructions as well as the models themselves have matured in capacity and capability (Haywood et al., 2019).

Understanding the global monsoons and sub-systems is a challenge for researchers in both past and modern-day context. One of the cornerstones in gaining a better understanding of the monsoon dynamics and behaviour has been the use of coupled ocean-atmosphere GCMs as the air-sea interactions are established forcings for the monsoon (Wang et al., 2005).

Studies show that the large-scale Asian monsoons already existed during the Paleogene (Caves et al., 2015; Licht et al., 2014, 2016; Quan et al., 2013). One of the first climate modelling studies of the Eocene epoch, showed that monsoonal strength over Asia was limited, due to the existence of the shallow epicontinental Paratethys Sea that reduced the land-sea temperature contrast (Ramstein et al., 1997). Furthermore, Huber and Goldner (2012), using boundary conditions with two different TP elevation configurations and assuming a high elevation plateau during the Eocene, showed that high TP alters the regional

circulation in the monsoonal region, and that the monsoonal system migrates slightly northward and intensifies. However, others suggest that these monsoons were only tropical and restricted to the South (Li et al., 2018; Spicer et al., 2017).

Over the years there are many hypotheses formed about the forcing mechanisms of the Asian Monsoons and the Central Asian aridity. One of the widely accepted theories is that the TP was a key factor in monsoonal formation and aridity establishment by blocking the flow of moisture from the ocean to the inland, enhancing the land-sea temperature gradient and affecting the atmospheric circulation and in turn the precipitation over Asia (Liu and Dong, 2013; Liu and Yin, 2002). However, other studies suggested that the Paratethys Sea retreat played a role possibly as important as the TP uplift in forming the monsoon climate (Ramstein et al. 1997; Zhang et al. 2007a, b). Additionally, studies have also suggested that the global cooling during the Eocene to Oligocene Transition has also influenced the Asian monsoons and aridity significantly (Dupont-Nivet et al. 2007; Lu et al. 2010).

More recently, Liu et al. (2017, 2019), ran a series of simulations from mid-Paleocene to present day, with and without topography and with different atmospheric CO_2 values, suggesting that the timing and causes of formation of the monsoons in South Asia and East Asia are different. Specifically, they showed that the TP uplift was the primary control mechanism for the EAM and they suggested that the formation of the SAM occurred in the Late Eocene and the onset was controlled by the northward propagation of Indian continent into the tropical latitudes of the Northern Hemisphere.

However, none of the proposed hypothesis can fully explain the evolution of the monsoons during the Cenozoic. That is largely due to the uncertainties of the boundary conditions that models use. Uncertainties in palaeoelevation/palaeobathymetry, latitudinal position of high-elevation, ice sheet coverage, land – sea distribution and poorly constrained atmospheric CO_2 levels during the Cenozoic make it difficult for palaeoclimate modelers to provide

definitive answers on the questions concerning the timing, causes and controlling mechanisms of the Asian monsoons and aridity. With that in mind, the approach in here will be solely based on sensitivity simulations to explore the effects of the TP uplift, ice sheet coverage and CO_2 changes without the uncertainties of palaeogeographical boundary conditions.

1.8 Aims and objectives

The overall aim of this project is to provide a better understanding and new insights on the effect of three of the major forcing factors driving climatic change over Asia. Specifically, through a series of 13 sensitivity simulations, we explore the role of the TP uplift, atmospheric CO_2 change and the ice-sheet formation, on the East Asian Monsoon, Central Asian aridity and its onset and the South Asian Monsoon. To reach that aim there are a number of objectives to be met:

- Carry out sensitivity experiments with different ice-sheet coverage boundary conditions to study how Asian aridity and the monsoons are affected by changes in ice coverage.

- Simulate Asian climate with different atmospheric CO_2 values to explore if Asian aridification and monsoonal intensification are controlled by CO_2 decrease.

- Carry out a series of sensitivity experiments with changing TP elevation, to explore the impact of the Central Asian uplift on the established aridity and monsoonal circulation of the continent.

- Simulate Asian climate with boundary conditions changed both in combination and isolation to study the relative contribution of each factor to climatic change in Asia.

- Carrying out simulations with 5 intermediate elevation configurations for the TP and Central Asian region to define the elevation threshold for changes in the climate patterns over Asia, and determine the role of high elevation as a palaeoclimate forcing altering the westerly jet.

- Finally, using all the simulations carried out for this thesis, we determine the required geological and atmospheric boundary conditions that could have led to inland Asian aridity and what are the main forcing factor that controls the onset of aridification.

1.10 Structure of the thesis

This chapter provides an overview of the modern Asian climate, the Asian climate throughout the Cenozoic and the main forcing factors that affect its evolution from the Eocene through the Miocene times. Proxy reconstructions and underlying uncertainties of the boundary conditions in terms of palaeogeography, atmospheric CO_2 levels and ice-sheet coverage are also discussed.

Chapter 2 contains the HadCM3 model description and evaluation, the experimental design of this study and the climatic variables and techniques used to analyse the results presented in the subsequent chapters.

Chapter 3 explores three major forcing factors (CO_2, topography and ice sheet coverage) through a series of sensitivity experiments to determine each factor's effect on the evolution

of Asian climate, focusing on the East Asian Monsoon region, the South Asian Monsoon region and Arid East Central Asia.

Chapter 4 focusses on the role of the TP uplift in East Asian monsoon circulation, and specifically the westerly jet and associated monsoonal precipitation.

In Chapter 5, the sensitivity experiments are used to explore driving mechanisms for the onset and intensification of the aridity in Central Asia through aridity indices and the Köppen climate classification.

Finally, Chapter 6 contains a summary of the results and future work.

Chapter 2: Methods and experimental design

2.1 Model description and evaluation

The Hadley Centre Coupled Model version 3 (HadCM3) has been used to carry out the simulations for this study. HadCM3 is a General Circulation Model (GCM) that was developed in 1999 by the UK Met Office and was the first climate model that did not require flux adjustments (Gregory and Mitchell, 1997). It is widely used for both palaeoclimate reconstruction and future projections (i.e. IPCC assessments).

The HadCM3 model consists of a dynamically coupled atmosphere, ocean and sea-ice model (see Gordon et al., 2000 for further details). The horizontal resolution of the model is 3.75^{o} x 2.5^{o} for the atmosphere which corresponds to 278 km x 295 km at 45^{o} latitude and 278 x 417 km at the equator and 1.25^{o} x 1.25^{o} for the ocean. The atmosphere and ocean are represented by 19 and 20 vertical levels respectively. The majority of the 19 atmospheric layers are distributed in less than 10 km altitude (13 layers in total), whereas 9 of them are distributed between 0 and 5 km (Pope et al., 2001).

The atmospheric physics have a 30-minute time step and the coupling to the ocean component occurs once per simulated day. The radiation scheme includes six and eight spectra bands for the shortwave and longwave radiation respectively.

HadCM3 can produce precipitation from two schemes. Namely the convection scheme and the large-scale precipitation scheme. The large-scale precipitation and cloud scheme is formulated in terms of an explicit cloud water variable following Smith (1990). The orography and gravity wave parameterization include the effects of flow blocking, trapped lee waves, and high drag states (Gregory et al. 1998; Pope et al. 2000).

In this study, HadCM3 uses the MOSES 1 (Met Office Surface Exchange Scheme) land-surface model. The MOSES 1 land-surface scheme has an interactive plant photosynthesis module

and soil thermodynamics that can simulate the freezing and melting of soil water, surface runoff and soil drainage (Cox et al., 1999). Additionally, the surface albedo is a function of snow depth, vegetation type and temperature over the ice and snow. The thermodynamic scheme of the sea-ice model includes snow-cover. Ice is advected by the surface ocean current, and when the depth exceeds 4 m, convergence is prohibited (Cattle et al., 1995).

HadCM3 has been used successfully in the representation of modern Asian climate as shown by Dabang et al. (2005) where the comparison between GCM outputs focused on the East Asian climate showed that HadCM3 can reproduce with success both annual and seasonal precipitation and surface air temperature. Furthermore, studies of precipitation and tropical Sea Surface Temperature (SST) for all four seasons yield a well-represented monsoon (Inness and Slingo 2003; Turner et al. 2005). However, when compared with modern climatologies the model presents with biases such as the cold bias in the northern high-latitudes (Pope et al., 2000), and the warm bias in the Southern Ocean (Gordon et al. 2000). Nonetheless, HadCM3's response to doubling of the atmospheric CO_2 is near the average value among the models that were used for the IPPC 4th assessment (Solomon et al., 2007). Furthermore, HadCM3 was one of the models with the least bias between the 24 GCMs that were part of the Coupled Model Intercomparison Project (CMIP5) in simulating seasonal and spatial precipitation and temperature patterns over the TP and is able to detect the summer monsoon signals and westerly wind systems over the same area (Su et al., 2013).

HadCM3 has also been used successfully in several different palaeoclimate modelling studies from Quaternary times to the Early Eocene (Haywood and Valdes, 2004; Lunt et al., 2007; Tindall et al., 2010) and it has been shown that it is an appropriate tool to study the Asian climate, especially in terms of precipitation (Lunt et al. 2010).

The Pre-industrial control experiment carried out for this study, also yields a well-represented Asian climate in terms of precipitation seasonality, wind reversal and monsoonal domain. The simulated Pre-industrial annual precipitation cycle averaged over

India and Eastern China when superimposed on observational data from 1979-2008 shows a good correlation (Fig. 11).

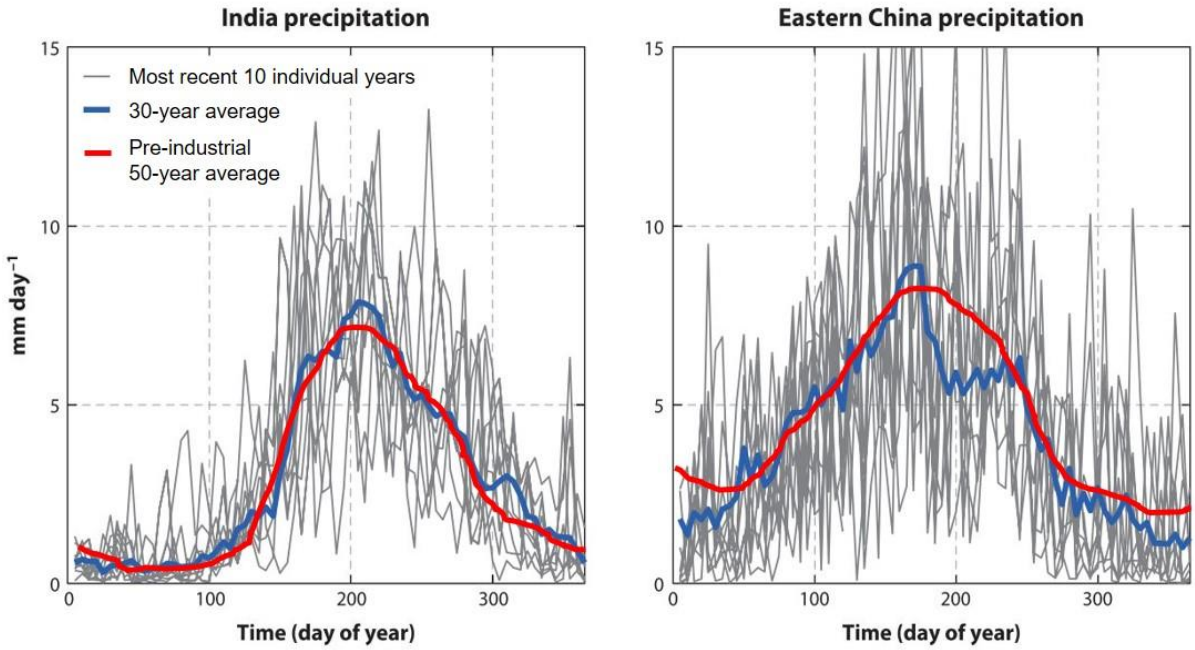

Figure 11: Annual cycles of precipitation for India (left) and eastern China (right). The red line shows the 50-year average from the Pre-industrial control experiment, the blue line averaged 30-year observed data from the Global Precipitation Climatology Project and the grey line the last 10 individual years of the data set (1998 – 2008). Plot modified after Molnar et al. (2010). Precipitation in mm/d.

Additionally, HadCM3 is able to simulate very well the seasonal precipitation pattern of the East Asian Monsoon region as well as the northward propagation of the rainfall (see Chapter 4 for details). That is also evident when compared with observational data (Fig. 12).

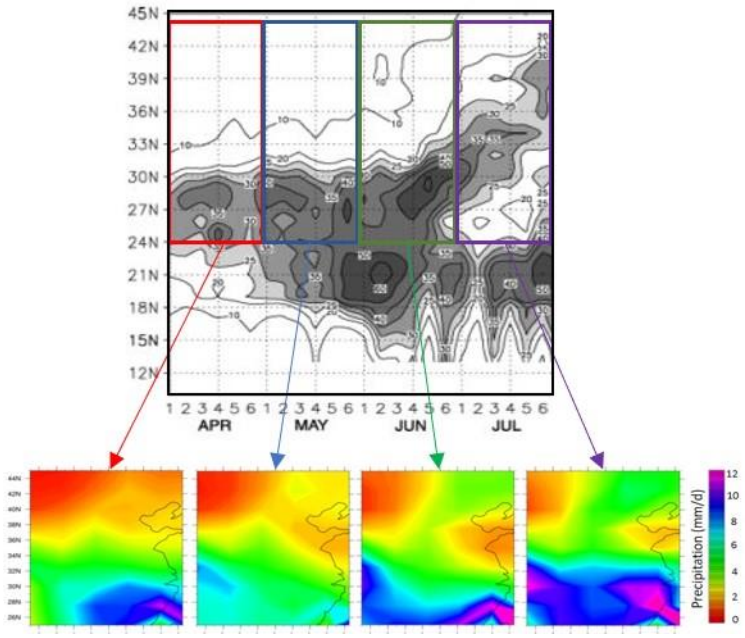

Figure 12: Precipitation over East Asian Monsoon region. Top: April to July averaged from 1961-1990. Figure adapted from Yanai and Chan (2005), Bottom: Pre-Industrial control experiment. Our control experiment successfully simulates all precipitation stages of the EAM precipitation. Precipitation in mm/d.

Finally, the Pre-industrial experiment also simulates one of the most prominent features of the Asian Monsoon, the characteristic wind reversal from easterlies over the coast of East Africa to westerlies over the Indian subcontinent (Fig. 13).

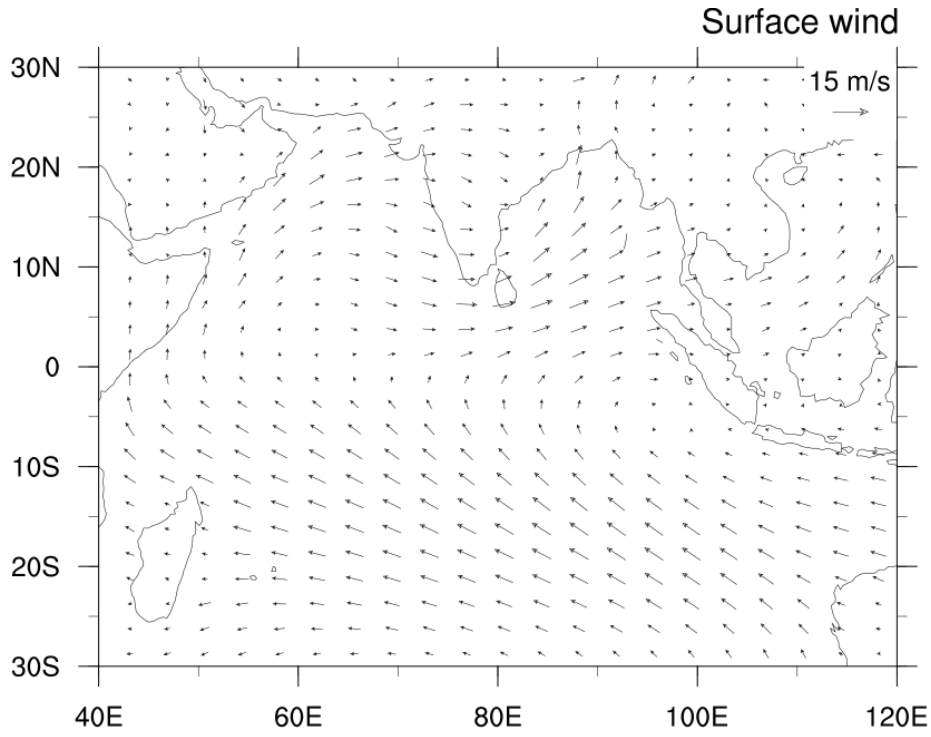

Figure 13: Surface winds (m/s) during May as simulated in the Pre-industrial experiment. The characteristic wind reversal marking the monsoonal onset is successfully simulated.

2.2 Experimental design and boundary conditions

The experimental design for this thesis was divided in two parts. Firstly, 8 simulations were performed, including a pre-industrial experiment (Fig. 14c). Pre-industrial atmospheric CO_2 concentration levels for the control experiment (PreInd) were set to 280 ppm. To assess Asia's hydrological sensitivity to rising CO_2 values two more simulations are performed with 2 x PreInd CO_2 and 4 x PreInd CO_2 values (2piCO2, 4piCO2). The selected atmospheric CO_2 values are within the suggested range during the EOT (450 – 1500 ppm) (Pearson et al., 2009b). 2piCO2 values are below the threshold for Antarctic glaciation (700 – 840 ppm) (DeConto et al., 2008) and within the range of suggested values for Mid to Late Oligocene (Pagani et al., 2005), while 4piCO2 values are consistent with Early Oligocene values (Pearson et al., 2009b). Asian climate response to ice-sheet coverage is explored through the No

Greenland Ice Sheet (NoGrIS) and the ice-free (NoIce) simulations (Fig. 14d), where the Greenland ice sheet and both the whole Antarctic and Greenland ice-sheets are removed respectively. To investigate the effects of the TP uplift on the Asian climate alone, we changed the regional topography of the TP to flat (FlatTP) (Fig. 14b) and to an Oligocene-like TP topography (Fig. 14e). The Oligocene-like topography used in this set of experiments, uses Oligocene palaeoelevation estimates derived from Markwick (2007) implemented over the area 62.5^{o}E and 125^{o}E and 20^{o}N – 52.5^{o}N. The Oligocene-like topography places the high-elevation TP at lower latitudes than present day, hence providing us with the opportunity to explore not only the response to elevation changes but also to the latitudinal distribution of high elevation topography. Finally, in the simulation called Combo we simulate a combination of the abovementioned changes in boundary conditions. Specifically, the TP topography is set to match the one of the Oligocene, CO_2 values are set to 2 x the PreInd level and ice is removed globally (Fig. 14c). All other boundary conditions, apart from those explicitly mentioned, are kept at pre-industrial values.

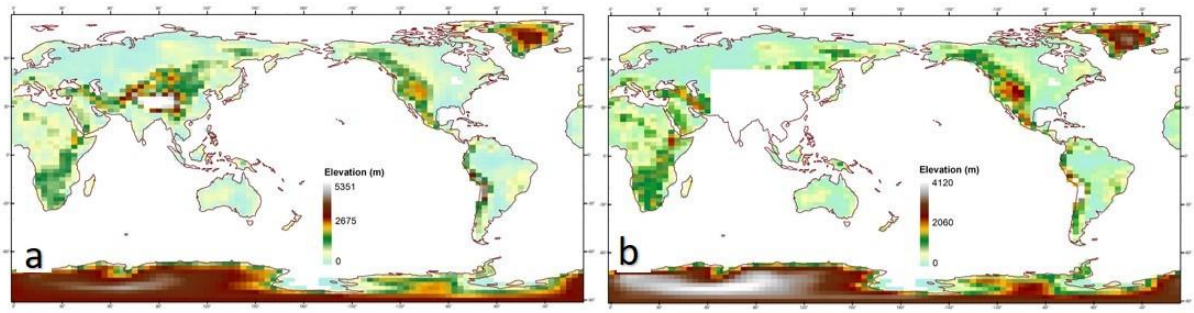

c

Experiment name	atm. CO_2	Topography	Greenland ice sheet	Antarctica ice sheet
PreInd	Pi (280 ppmv)	pi	modern extent	modern extent
2piCO2	2 x pi	pi	modern extent	modern extent
4piCO2	4 x pi	pi	modern extent	modern extent
NoGrIS	pi	pi	ice-free	modern extent
NoIce	pi	pi	ice-free	ice-free
FlatTP	pi	flat TP	modern extent	modern extent
OligTP	pi	Oligocene TP	modern extent	modern extent
Combo	2 x pi	Oligocene TP	ice-free	ice-free

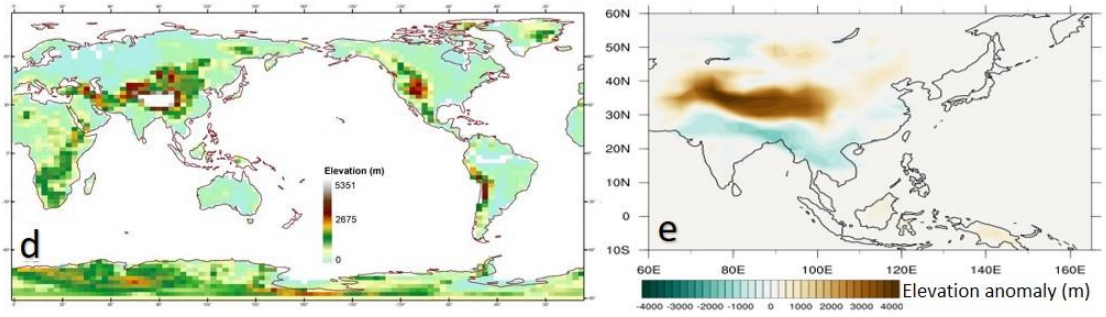

Figure 14: Boundary conditions for the simulations in this study: a) Pre-industrial topography, b) Flat TP, d) No ice Greenland and Antarctic, e) Elevation anomaly between OligTP and PreInd experiments (PreInd – OligTP) (Elevation scales are common only for a and d), c) boundary conditions used for all the experiments.

The results from these 8 experiments suggested that even though the other forcing factors contribute to climatic change over Asia, the TP is the main driver. To that end, the second part of the experimental design was focused on changing boundary conditions for the high-elevation Central Asia (namely the TP, Mongolian Plateau (MP) and TS orogen). Specifically, we decrease elevations from modern by 96%, 77%, 58%, 38% and 19% (hereafter referred to as TP5000, TP4000, TP3000, TP2000 and T1000 respectively). The number following "TP" in the experiment name denotes the maximum elevation of the TP in each experiment in metres (Table 1). Additionally, we carried out a simulation with no orogens in Central Asia where TP, TS and MP were set to sea-level (hereafter referred to as FlatTP). Finally, a simulation with Oligocene-like elevation (OligTP) in Central Asia (after Markwick 2007) was

completed, where the TS and MP were at elevations lower than 1000 m (see Fig 14a), and the TP was at approximately 2300 m elevation but was located at a lower latitude (Fig.14b). The changing elevation in the model is implemented over the area between 62.5°E and 125°E and 20°N – 52.5°N (Fig.14).

All other boundary conditions for each experiment were kept constant and specified as pre-industrial (PreInd). Specifically, atmospheric CO_2 was set to 280 ppm, vegetation type and distribution was specified as being modern, as was the land-sea distribution, ice-sheet coverage and topography for the rest of the globe, outside of the geographical domain specified above. The experiments were not designed to represent a specific geological period of the past, but since the influence of the TP, TS and MP are considered predominant for the evolution of East Asian climate during the Cenozoic, our experimental design represents an appropriate methodology to better understand regional uplift and how uplift controlled the way that the Asian climate regime developed. Each simulation was performed for 500 simulated years with the final 50 years used to derive the required climatological means for subsequent analysis.

Experiment name	**Maximum TP elevation**	**Maximum MP elevation**	**Maximum TS elevation**
PreInd	5351	2425	4100
FlatTP	sea level	sea level	sea level
TP1000	1016.69	460.75	779
TP2000	2033.38	921.5	1558
TP3000	3103.58	1406.5	2378
TP4000	4120.27	1867.25	3157
TP5000	5136.96	2328	3936
OligTP	2364	900	1100

Table 1: List of experiments with maximum elevation (metres above sea level) for the TP, MP and TS orogen respectively.

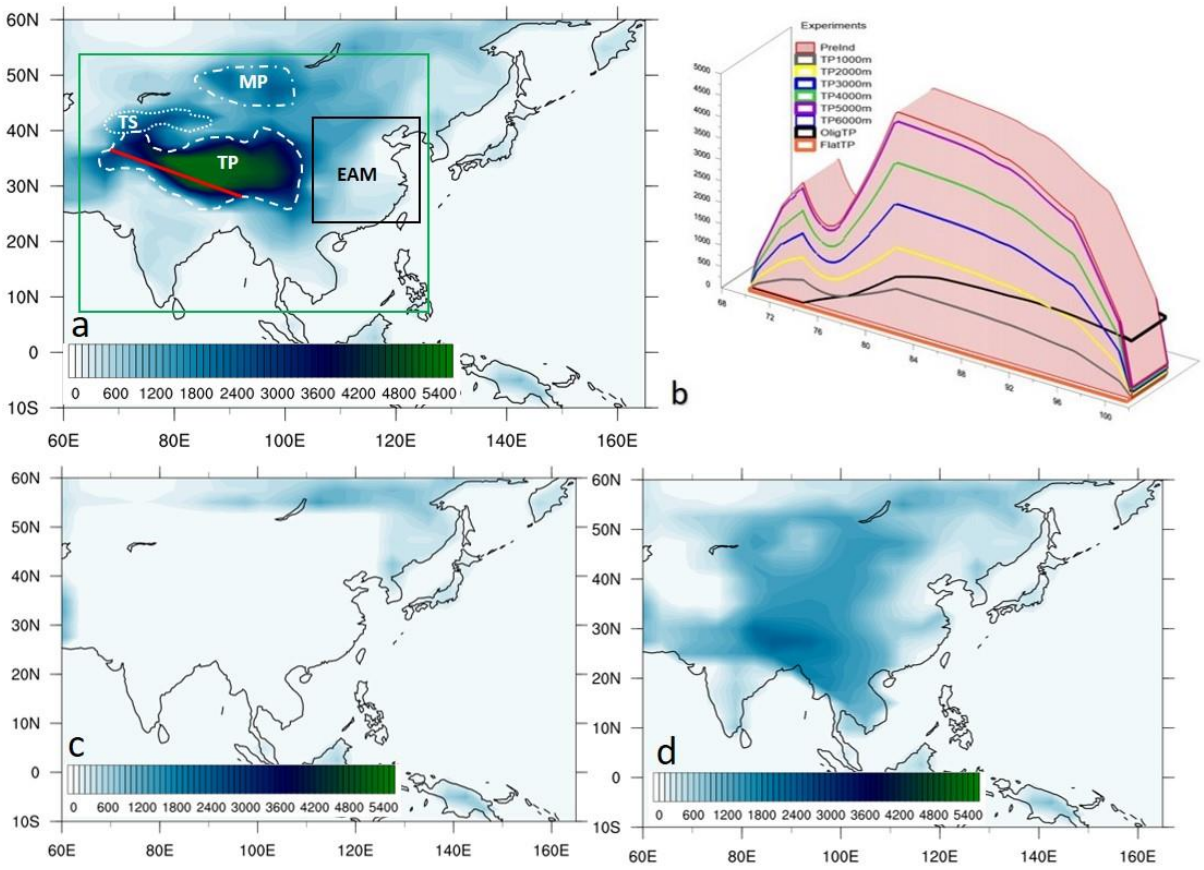

Figure 15: a) Pre-industrial (PreInd) elevation. The dashed line shows the TP, dotted line the TS, dash/dot line the MP, black box shows the region used to analyse the EAM patterns, and the green box the area over which the elevation is decreased for all the experiments (see section 2.2 for details); the red line shows the axis along which elevation profiles are shown in b. b) Elevation profiles for the simulations carried out by this study along the (red) axis shown in a). c) flattened TP, TS and MP topography d) Oligocene-like elevation (after Markwick, 2007).

2.3 Climatological variables and analysis techniques

When considering the sensitivity of the Asian climate to different forcings, it is important to be aware of the diversity of climates present in Asia. For example, the environmental conditions over South and East Asia are dominated by the monsoons, while Central Asia is characterized by arid conditions (Fig. 1). Analysing variables over the whole of Asia can only provide a general view of the pattern and magnitude of change, but the underlying causalities and mechanisms cannot be easily understood without studying the two main

monsoonal systems of Asia individually (Fig. 16). The first step is to spatially define the monsoonal domain. In general, different studies have used different extents for the monsoon domain according to the variable they focus on. For example, Parthasarathy et al. (1994) used the seasonally averaged precipitation over only the Indian subcontinent to develop the All-Indian Summer Rainfall index. Webster and Yang (1992) studying the wind shear and the Outgoing Longwave Radiation (OLR) selected the domain from 0°-20° N, 40°-110° E. Wang et al. (2008) defined an East Asian – Western North Pacific index extending from 5° – 15° N, 90° – 130° E and from 20° – 30° N to 110° – 140° E. For the purposes of this study we focus on the monsoons over Asia during boreal summer. Namely, we study the SAM and the EAM separately, as they differ in both climatology and variability (Cherchi et al., 2011). Using the domains as defined by Webster et al. (1998) and Wang (2005) for the SAM and EAM respectively, we averaged the monthly precipitation over these regions in an effort to not only assess the monsoonal change, but also the climate response over Asia under non-monsoonal circulation. Finally, in order to study the forcings that drive aridity over Central Asia we also analyse the same variables for the Arid East Central Asia (AECA) region located at 75° – 105° E, 35° – 55° N (Hong et al., 2014) (Fig. 16).

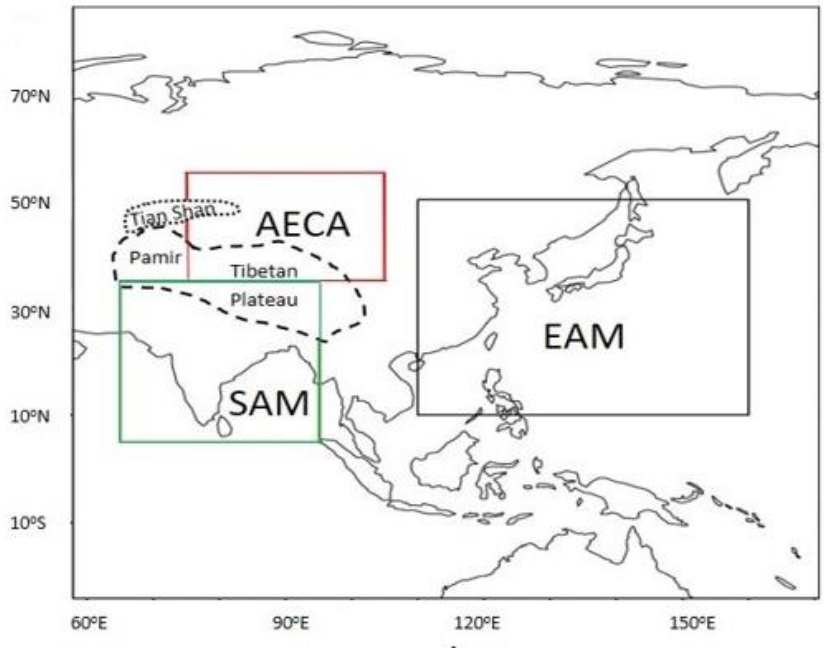

Figure 16: Green box: South Asian Monsoon region (SAM), red box: Arid East Central Asia region (AECA) and black box: East Asian Monsoon region (EAM). The map also shows the spatial extent of the TP, TS and Pamir orogens.

2.4 Aridity indices and the Köppen climate classification

The term aridity is defined as a deficiency of moisture but there is no universally accepted boundary between different degrees of arid and the thresholds between arid and semiarid are not explicitly defined. To avoid confusion in defining arid climates in this study, the widely known IPCC (2007) and De Martonne (1926) Aridity Indices and the Köppen (1936) climate classification are used. Instead of describing climate with absolute values for different parameters, the relationship between those parameters of the climate with specific earth system components, such as the vegetation (i.e. Köppen classification) is studied. This approach has two main advantages. First, it presents palaeoclimate modelling results in a way that they can be directly compared with proxy data, and secondly it provides an insight into climatic patterns by producing classification maps that combine information from multiple parameters at once. The latter is crucial as Zoura et al. (2019) showed that the relative significance of each forcing is dependent on the hydroclimatic parameter studied.

Thus, producing classifications that are a product of multiple hydroclimatic parameters helps eliminate such a dependency.

The IPCC (2007) aridity index (AI) is solely based on annual precipitation making it a simple and effective metric. According to the AI, arid environments receive less than 250 mm of precipitation during the year, while the threshold for semiarid environments is 250 – 500 mm/year. Similarly, the De Martonne (1926) aridity index (I_{DM}) uses the annual precipitation and temperature to define climates from arid to very humid as shown in Eq. 1, where P is the average annual precipitation and T the average annual temperature.

$$I_{DM} = \frac{P}{T+10} \quad \text{(Eq. 1)}$$

The Köppen Classification uses monthly temperature and precipitation data and divides the climate in 5 main climate categories (namely tropical, dry, temperate, continental and polar), which can be further divided in 31 sub-types (Köppen, 1936).

It was first introduced in 1900, and has since been widely used, as it is an ideal diagnostic tool to monitor changes in the climatic condition over various timescales (de Noblet, 1997; Rubel and Kottek, 2010; Willmes et al., 2017) not only for observational data but also in modelling studies (i.e. Chen and Chen 2013; Gao and Giorgi 2008; Li et al. 2018a). For this study, we will use the Köppen classification, not only to define arid regions (both hot and cold) but also to analyse the interannual variation of the last 50 simulated years of each experiment in an effort to differentiate between the spatially stable and unstable arid climates over Asia. Based on the approach described in Chen and Chen (2013), here, a spatially unstable climate is defined when the type of the climate over a region has changed at least once during the last 50 simulated years. To obtain more detailed maps with better resolution than the model output, we followed the methodology for re-gridding the model output data and applying the Köppen classification that is described and discussed in detail in Willmes et al. (2007). As the focus of this study is the aridity over Asia, other climate types

are masked out. The masking also makes it easier for the reader to compare the indices with the Köppen classification as the arid climates are the only common climatic types between them.

Finally, both indices and the Köppen classification were chosen as they have all been extensively used in the past to represent the different climate types and changes over different time scales, but more importantly, they are ideal as they are all using temperature and precipitation, parameters that are well-represented in HadCM3 (Inness and Slingo 2003; Dabang et al. 2005; Lei et al. 2014).

Chapter 3: Atmospheric carbon dioxide, ice sheet and topographic constraints on palaeo moisture availability in Asia.

Introduction

This chapter provides the first systematic approach on the effects of three of the major forcing factors of Asian climate during the Cenozoic. Through a series of sensitivity simulations that take into account the TP uplift, the atmospheric CO_2 changes and change in ice-sheet coverage (Fig. 15), this chapter focuses on three individual regions that are part of the complex Asian regime. Simulations are used to investigate the effects of each factor on the SAM, the EAM and the AECA (Fig. 16) as well as the relative contribution of each factor in the annual precipitation cycle, the surface temperature and the moisture availability.

The objectives of this chapter are to explore i) how are Asian aridity and the monsoons affected by changes in ice-sheet coverage? ii) Is Asian aridification and monsoonal intensification controlled by CO_2 decrease? iii) What is the impact of the Himalayan orogen and TP uplift on the established aridity in Central Asia and monsoonal circulation of the continent? iv) What is the relative contribution of each factor to climatic change in Asia?

3.1 Control simulation (annual precipitation and seasonal surface temperature)

The East Indian Monsoon region receives most of its rainfall from June to September (Parthasarathy et al., 1994). The annual precipitation (Fig. 17) and temperature cycle (Fig. 17) over the SAM region is successfully simulated in the preindustrial control experiment. Surface temperature and precipitation maximum values are reached during boreal summer (JJA) (Fig. 17). During boreal winter (Fig. 17), precipitation is focused around the equator and to the South. During spring maximum precipitation migrates to the northeast towards the

eastern part of China. In JJA precipitation is located in the tropical zone, around 20°N and as the summer gives way to autumn, precipitation is retreating away from the continental Asia and towards the Indian and Pacific Ocean (Fig. 17).

The annual mean precipitation is higher in the EAM region in comparison to the AECA and SAM regions (Fig. 17). For all three regions the driest months are during boreal winter after which we observe an abrupt monsoon onset and a subsequent increase until peak rainfall is reached in late spring/early summer (for the AECA), and summer for SAM and EAM regions. (Fig. 17). The coldest period over Asia is during boreal winter with negative values reached in the temperate zone. However, the tropics and subtropics are constantly warm with temperatures higher than 25°C (Fig. 17). The only season with surface temperatures over Asia always above 0°C is the boreal summer (Fig. 17).

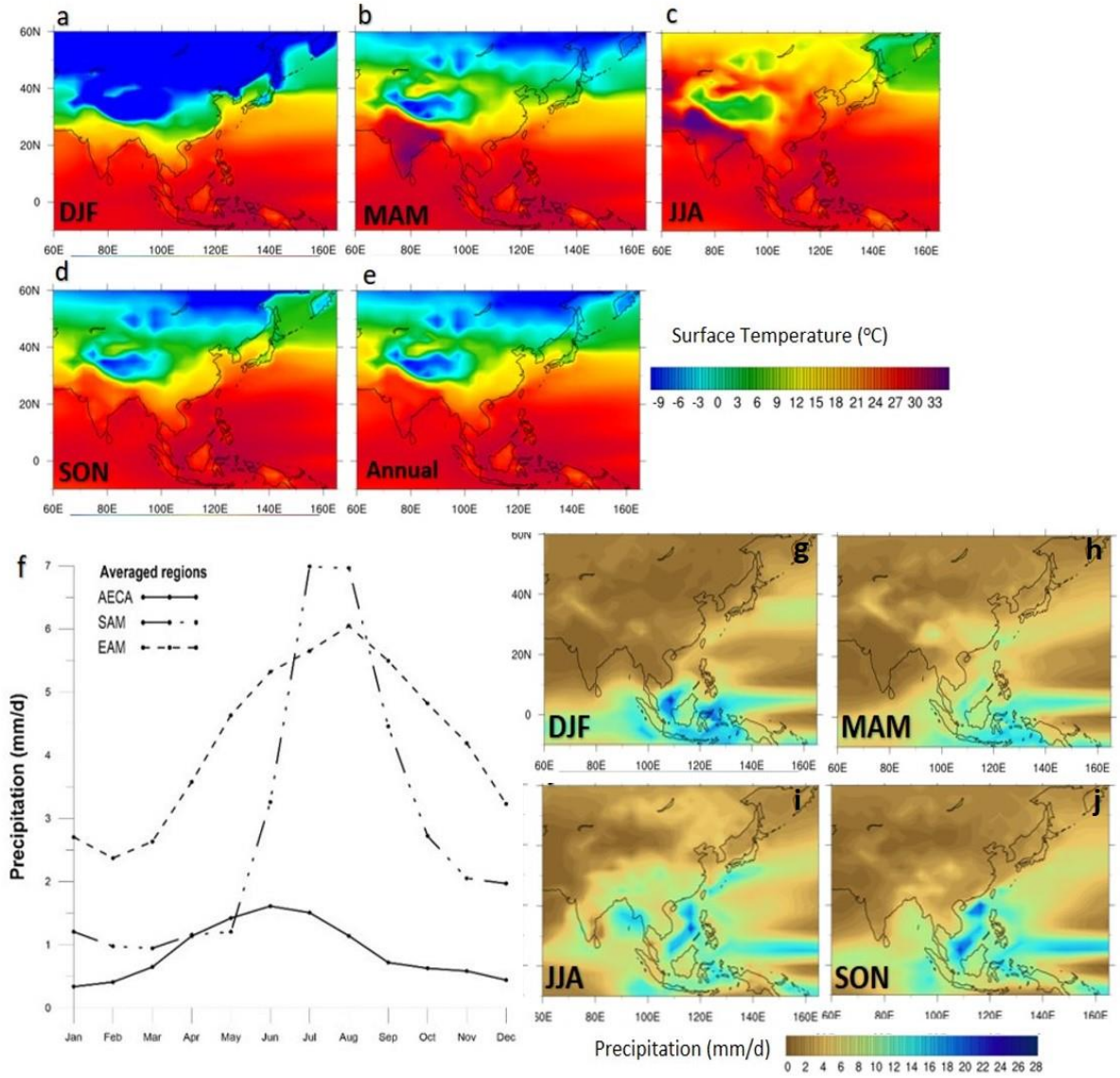

Figure 17: a–e: Seasonal and annual surface temperature (°C) over the Asian continent and surrounding oceans. a) December – February (DJF), b) March – May (MAM), c) June – August (JJA) and d) September – November (SON), e) Annual mean surface temperature. f) simulated PreInd annual precipitation cycle for the Arid East Central Asia (AECA, solid line), the South Asian Monsoon region (SAM, dash/dot line) and the East Asian Monsoon (EAM, dashed line), g-j: Seasonal simulated PreInd precipitation (mm/d) over the Asian continent and surrounding oceans.

3.2 Impact of changing boundary conditions on the South Asian Monsoon

Analysis of the annual precipitation cycle over the SAM region for each of the experiments reveals a variety of responses to the different boundary condition changes (Fig. 18a-b) applied within the climate model. All simulations, except for the FlatTP, yield maximum precipitation values during July and August (Fig. 18a). After a doubling of atmospheric CO_2 July is no longer the month with the highest rainfall as values for August increase by 20% making August the month with the highest contribution to annual precipitation (Fig. 18b). However, this is not the highest increase observed in the 2piCO2 simulation as May precipitation over the SAM is 23% higher than in the PreInd. Quadrupling of CO_2 results in an increase from May until November with the highest increase simulated reaching 88% in May (Fig. 18b). Similarly to the 2piCO2 simulation, from January to April the model simulates a decrease of up to 37% (Fig. 18b). The only distinction between the double and quadruple CO_2 annual cycle patterns occurs in the monsoonal months. Specifically, during June and July the 2piCO2 precipitation is lower than the PreInd, whilst in 4piCO2 the same months are wetter by up to 35% (Fig. 18b). The removal of ice sheets plays a more important role over the SAM region under non-monsoonal circulation. Specifically, the months of Oct-Feb are wetter and during May (the month marking the monsoonal onset), the model simulates the largest change in precipitation indicating a more abrupt transition from non-monsoonal to monsoonal conditions (Fig. 18a-b).

Flattening of the TP changes the month with the highest precipitation values from July-August to May, but this is not the only notable change. Precipitation during January to April is minimal amongst all simulations (-70% the PreInd), accounting for the driest non-monsoonal months simulated (Fig. 18b). May and June receive more precipitation in the FlatTP simulation with higher values than the PreInd. However, the monsoonal months in the FlatTP simulation are generally drier with precipitation from July-September being the

lower in comparison to all the other simulations (Fig. 18a). With the TP set to an Oligocene-like elevation, the most substantial change is predicted for May and June with precipitation increasing by more than 200% and 70% respectively (Fig. 18b). With that increase in magnitude May is now contributing more than 10% in the annual rainfall indicating a steeper transition from non-monsoonal to monsoonal circulation (Fig. 18a).

Simulated seasonal and annual temperature changes in response to altered boundary conditions do not show the same variations as precipitation (Fig. 19, S1, S2). The 2piCO2 and 4piCO2 simulations result in a higher annual surface temperature by up to 6^{o} and 12^{o}C respectively over the whole Asian continent and surrounding oceans (Fig. 19a, b). The SAM region becomes cooler by up to 1.5^{o}C in the NoGrIS simulation with the surface temperature over the Bay of Bengal and the Northern part of the Indian Ocean showing almost no change compared to the PreInd (change less than 0.5^{o}C) (Fig. 19c). Removal of both the Greenland and Antarctic ice sheets leads to a cooling over the SAM region (Fig. 19d). The Indian landmass cools by up to 3^{o}C. However, the southern flanks of the Himalayas experience higher temperatures of the same magnitude as the decrease compared to the PreInd (Fig. 19d). FlatTP simulated surface temperature is higher than the PreInd by 4^{o}C over India, whilst the southern flanks of the Himalayas reach the highest simulated temperature with +13^{o}C compared to the PreInd (Fig. 19e). For the SAM region the TP removal raises the surface temperature. The Bay of Bengal and the northernmost part of the Indian Ocean are simulated to have lower temperatures (up to -2^{o}C compared to the PreInd) leading to a higher land – sea thermal contrast (Fig. 19e). The Bay of Bengal and Indian Ocean in an Oligocene-like elevation setting show almost no change compared to the PreInd, while the Northern and Southern part of the Indian subcontinent cools by up to 9^{o}C (Fig. 19f). Finally, in the Combo simulation the SAM region yields higher temperatures in both the Indian continent and the surrounding seas with a narrow strip of lower temperatures of about 5^{o}C, parallel to the TP (Fig. 19g).

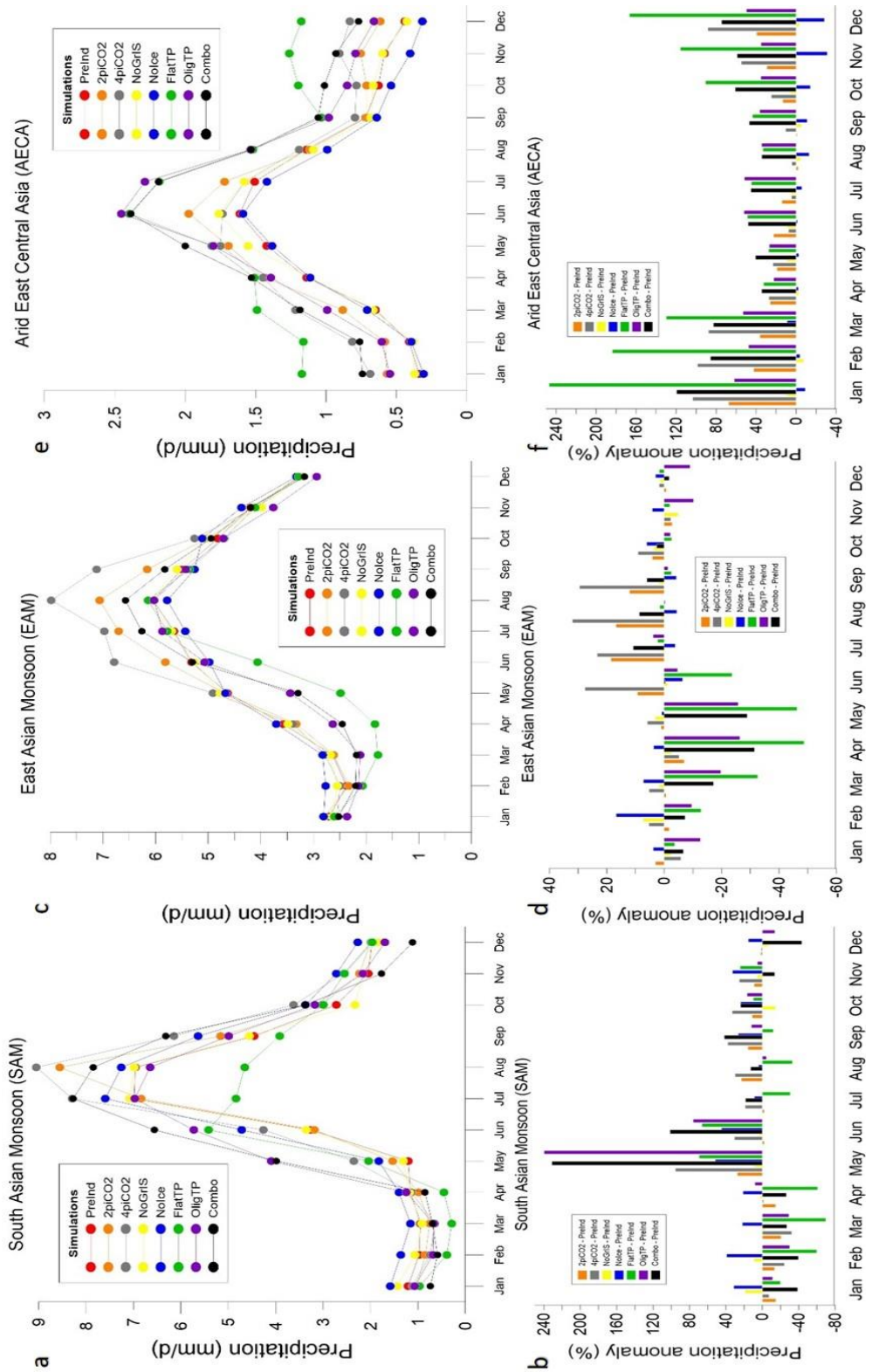

Figure 18: Averaged simulated monthly precipitation (mm/d) over: a) the SAM c) the EAM and e) the AECA regions and simulated percentage increase (positive values) and decrease (negative values) in precipitation for each experiment compared to the pre-industrial control experiment for b) the SAM d) the EAM and f) the AECA regions.

3.3 Impact of changing boundary conditions on the East Asian Monsoon

Doubling of atmospheric CO_2 produces wetter conditions from May to September by up to 18%, while non-monsoonal months experience small fluctuations that do not exceed 8% of the PreInd (Fig. 21 c-d). Quadrupling of the CO_2 leads to higher monsoon related precipitation (May - September) with a notably high percentage increase (30%), while the non-monsoonal months (October to April) show changes that are less than 10% of the PreInd values (Fig. 19d). Under ice free conditions, the EAM region receives more precipitation during non-monsoonal months by up to 17% for February, while the monsoon related precipitation shows a slight decrease throughout the monsoonal period by up to 6.5% of the PreInd value (Fig. 19d). In the FlatTP simulation, precipitation is constantly lower than the PreInd with the exception of July and August where the model predicts a slight increase that does not exceed 2.5%, and thus can be considered negligible (Fig. 19d). Oligocene-like elevation for the TP results in the same pattern as in the FlatTP but with precipitation changes (relative to the PreInd) being less than in the FlatTP simulation. Specifically, non-monsoonal months show the highest decrease, by up to 27%, whereas as in the FlatTP simulation the change during the monsoonal months can also be considered negligible with values of less than +3% (Fig. 19d). Where all changes have been made simultaneously (Combo) the resulting change in precipitation is more complex. Specifically, boreal winter and spring (December – May) experiences significantly lower precipitation (by up to -52%), even though precipitation for the monsoonal months (from July to September) shows higher values (the increase does not exceed 10% of the PreInd value) (Fig. 19d).

For the EAM region, surface temperature under higher CO_2 values is almost 6^{o}C greater over the Eastern Asian landmass, while the increase in the north-eastern Pacific is higher than PreInd by 2-3^{o}C (Fig. 19a). In 4piCO2, the model simulates a constant increase in temperature with values reaching double the 2piCO2 values, and the Pacific Ocean cooler than the Eastern

Asia landmass (Fig. 19b). Removing the Greenland ice sheet leads to lower temperatures for the whole EAM region with a temperature decrease of up to -3°C compared to the PreInd (Fig. 19c). NoIce conditions seem to mostly affect the northern and western part of the EAM region, while the Pacific Ocean experiences almost no change except for some small areas in proximity to the Eastern Asian landmass (Fig. 19d). The flattening of the TP generates elevated surface temperatures by up to 7°C in the mid and high latitudes of the EAM region, but the Pacific Ocean at 20°N shows with a cooling of up to 2.5°C (Fig. 19e). The OligTP simulation produces lower temperatures over the majority of the EAM region with values up to 2°C. However, the northern part of the EAM and parts of the Asian landmass are warmer by up to 2°C compared to the PreInd experiment (Fig. 19f). The EAM region for the Combo simulation yields higher temperatures by up to 6°C. The highest temperature changes are located in eastern China and around Japan while the surface temperature increases over the Pacific Ocean do not surpass 3°C (Fig. 19g).

3.4 Impact of changing boundary conditions on the Arid East Central Asia

The response of the AECA to boundary condition changes is distinctly different to the regions analysed previously. In general, all of the simulations, except for the NoIce, produce wetter conditions over the AECA with the largest change seen in the experiment FlatTP (Fig. 21 e-f). Doubling atmospheric CO_2 increases the precipitation throughout the year, but the largest increase is simulated during non-monsoonal months (i.e. Jan, Feb) (Fig. 22 e). Precipitation is also constantly higher in the 4piCO2 during all simulated months. From October to April Central Asia receives more precipitation (up to 100% more than the PreInd) (Fig. 22f). Removal of the Greenland ice-sheet leaves the AECA almost unaffected with precipitation difference from the PreInd never exceeding 10% (Fig. 20f,21f). Completely removing the ice-sheets from both Greenland and Antarctica (NoIce) produces a decrease in precipitation

throughout the year (Fig. 21e). Specifically, even though the months marking the monsoonal onset do not show large differences from the PreInd, from July to August the model simulates a constant decrease in precipitation that reaches its largest value during November (-31%). The FlatTP simulation produces the largest increase in precipitation for the AECA region, with non-monsoonal months experiencing a large increase in rainfall with values more than two times the PreInd (Fig. 21f). Lower elevation of the TP (OligTP) also leads to increased precipitation throughout the year, but in contrast to the FlatTP simulation the increase is almost uniform throughout the whole year with an average of 42% (Fig. 19). This uniform increase is not seen in the Combo simulation. Non monsoonal months receive more rainfall than the PreInd, which in some cases is greater than 100% the PreInd (Fig. 21f).

Surface temperature changes over the AECA region show the highest increase and decrease for any of the regions considered (Fig. 19). In 2piCO2, the AECA region becomes warmer by 6^{o}C on average, and this increases to 12^{o}C when CO_2 is quadrupled (Fig. 19a-b). Even though removing the Greenland ice-sheet generates a generally warmer climate, the AECA region shows only small fluctuations in temperature (Fig. 19c). The removal of both ice-sheets creates a complex pattern of surface temperature response with some areas experiencing higher than the PreInd temperatures and others lower (Fig. 19 d). The magnitude of this change is ±5^{o}C. Flattening of the TP generates the highest change in the AECA region (Fig. 19e). Notably the region over the TP is warmer by up to 13^{o}C, while the rest of the AECA region shows an increase of up to 8^{o}C. The NW part of the AECA (North of the TS orogen) is cooler than the PreInd by at least 3^{o}C. Oligocene–like topography raises the surface temperature over the TP just as in the FlatTP, with the main difference being the spatial extent of this warming (Fig. 19f). In this case the region north of the TP is cooler by up to 5^{o}C, but in the north-eastern part of the AECA there is significant region with higher temperatures (Fig. 19f). Finally, the combination of the boundary condition changes (Combo) generates much warmer conditions in the AECA (compared to the PreInd) (Fig. 19g). Even though the

TP is set to Oligocene elevation the spatial extent of the high surface temperatures over the TP is similar to the FlatTP simulation, while to the north of the AECA temperatures are also significantly higher (more than 8^{o}C) (Fig. 19g).

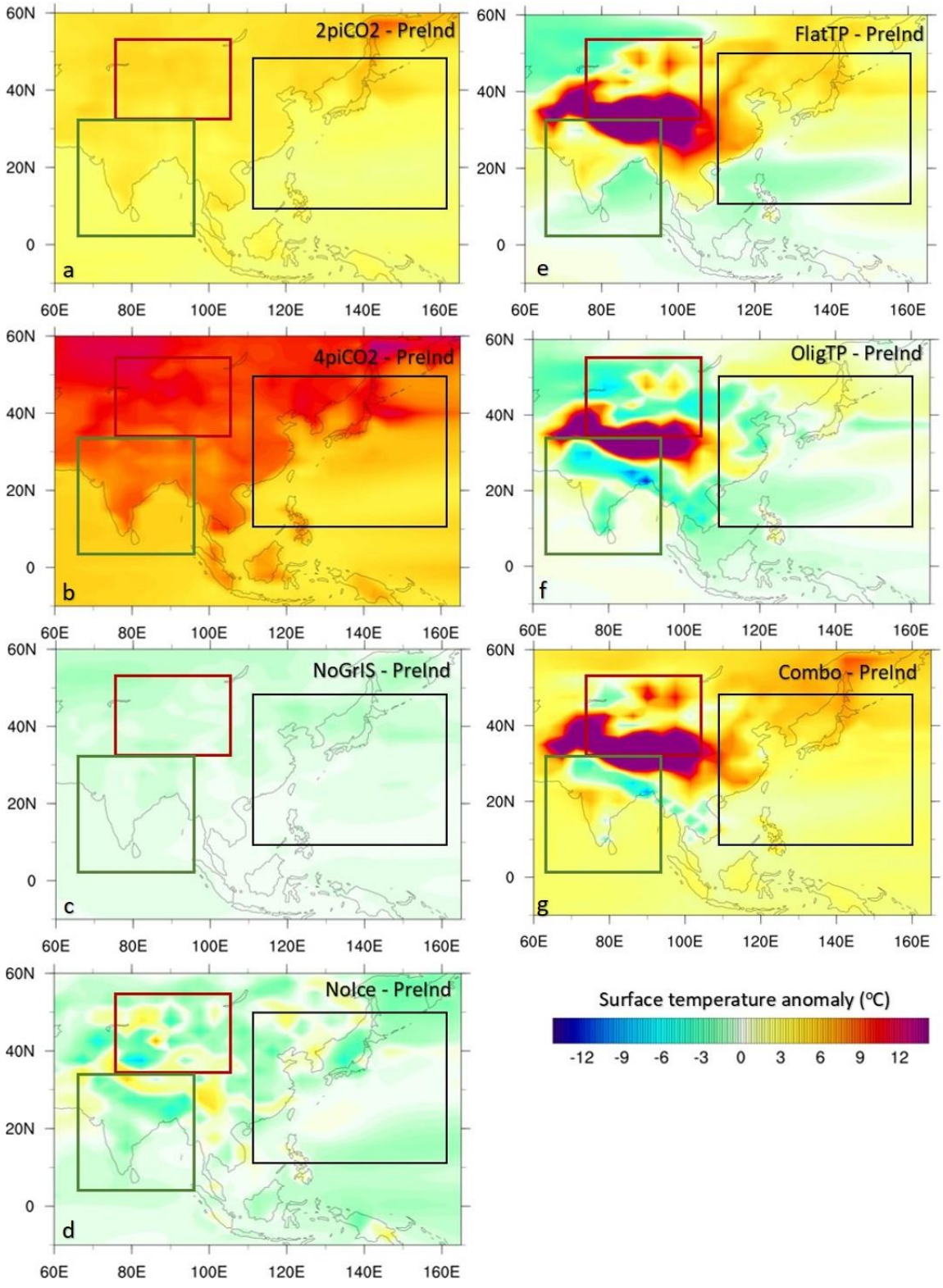

Figure 19: Simulated annual surface temperature anomaly (°C) compared to the PreInd for: a) 2piCO2, b) 4piCO2, c) NoGrIS, d) NoIce, e) FlatTP, f) OligTP and g) Combo simulation. The SAM, EAM and AECA regions are denoted by the green, black and red boxes respectively.

3.5. Discussion

3.5.1 Boundary condition effects on climate and the monsoons

Increased atmospheric CO_2 leads to enhanced heating of the Earth (Fig. 19a-b) (IPCC, 2001) and its radiative forcing alters the atmospheric heat distribution and hydrological cycle (Cherchi et al., 2011). The land-sea thermal contrast is the basic forcing mechanism for the SAM, and an increased contrast can be expected to strengthen monsoon circulation (Turner et al. 2011).

The modelled monsoonal precipitation under elevated CO_2 concentrations increases over the SAM and EAM regions, consistent with previous modelling studies (i.e. Annamalai et al. 2007), and is a product of enhanced moisture transport from a warmer Indian Ocean towards the Asian continent (Ueda et al., 2006). Our results indicate increased monsoonal precipitation for both the 2piCO2 and 4piCO2 simulations for the SAM and EAM regions following the "wet-get-wetter response" (Held and Soden, 2006; Fig. 20b-c). This suggests that precipitation in regions that already have strong moisture convergence and precipitation will be enhanced (Chou et al., 2009). During the monsoonal months, the moisture availability over the SAM and EAM shows an increase consistent with higher precipitation (Fig. 21b-c), while the high pressure systems over the AECA and East EAM regions retreat to the West and East respectively (Fig. 22b-c). In the PreInd simulation the low pressure system associated with precipitation is located above the TP, while, in 2piCO2, the low pressure system expands to the North and East of the TP (Fig. 22b). Additionally, the precipitation simulated over the SAM region in 4piCO2, where surface temperature reaches higher values throughout the year (Fig. 19b), shows a precipitation enhancement following the traditional monsoon period suggesting a possible extension in the duration of the monsoon. At the same time the beginning of the monsoonal period (May) receives more precipitation leading to a steeper transition from non-monsoonal to monsoonal conditions

(Fig. 18a, 22). The AECA in both the 2piCO2 and 4piCO2 simulations does not receive more precipitation under monsoonal circulation, while Precipitation – Evaporation (P – E) shows a localized decrease without significant change in the pattern from the PreInd (Fig. 21b-c). Under non-monsoonal circulation, moisture availability over the SAM and EAM regions shifts from positive (during the monsoons) to negative, even over the landmass of the EAM region where precipitation shows an increase (Fig. 24b-c). However, the adjacent Indian Ocean now shows increased moisture availability. Interestingly, during non-monsoonal months the AECA receives more precipitation by at least 0.5 mm/d (for 2piCO2) up to 1 mm/d (for 4piCO2), which in an arid area corresponds to an increase of 34% and 71% respectively (Fig. 23b-c). Correspondingly, from Oct – Apr, P – E over the AECA indicates enhanced moisture availability and therefore less arid conditions with increasing CO_2 values (Fig. 24 b-c). During the non-monsoon months the high-pressure system over Central Asia shrinks and migrates northwards producing lower pressure over the AECA region compared to the PreInd (Fig. 25b-c).

The removal of the Greenland ice-sheet creates only localised changes and does not seem to affect Asian climate in a significant way (Fig. 20d). In NoIce the simulated surface temperature is lower than in the PreInd for most of the SAM, EAM and AECA regions (Fig. 19d). However, monsoonal precipitation exceeds the PreInd demonstrating that the land-sea thermal contrast is not the only driver of monsoon intensification. This can be explained if we see the monsoon as a manifestation of the ITCZ seasonal migration in response to the positioning of the maximum insolation (Gadgil, 2003). Our simulation reveals that the removal of the Antarctic ice-sheet yields a warmer equatorial Indian Ocean during boreal summer, leading to a migration of the ITCZ to the North towards inland India. Furthermore, reinforced southerlies and westerlies carry moisture from the North part of the Indian Ocean and Bay of Bengal towards inland south Asia increasing the moisture availability, not only

over the SAM region but also over the landmass of the EAM and the area located in between those systems (Fig. 21e, 21e).

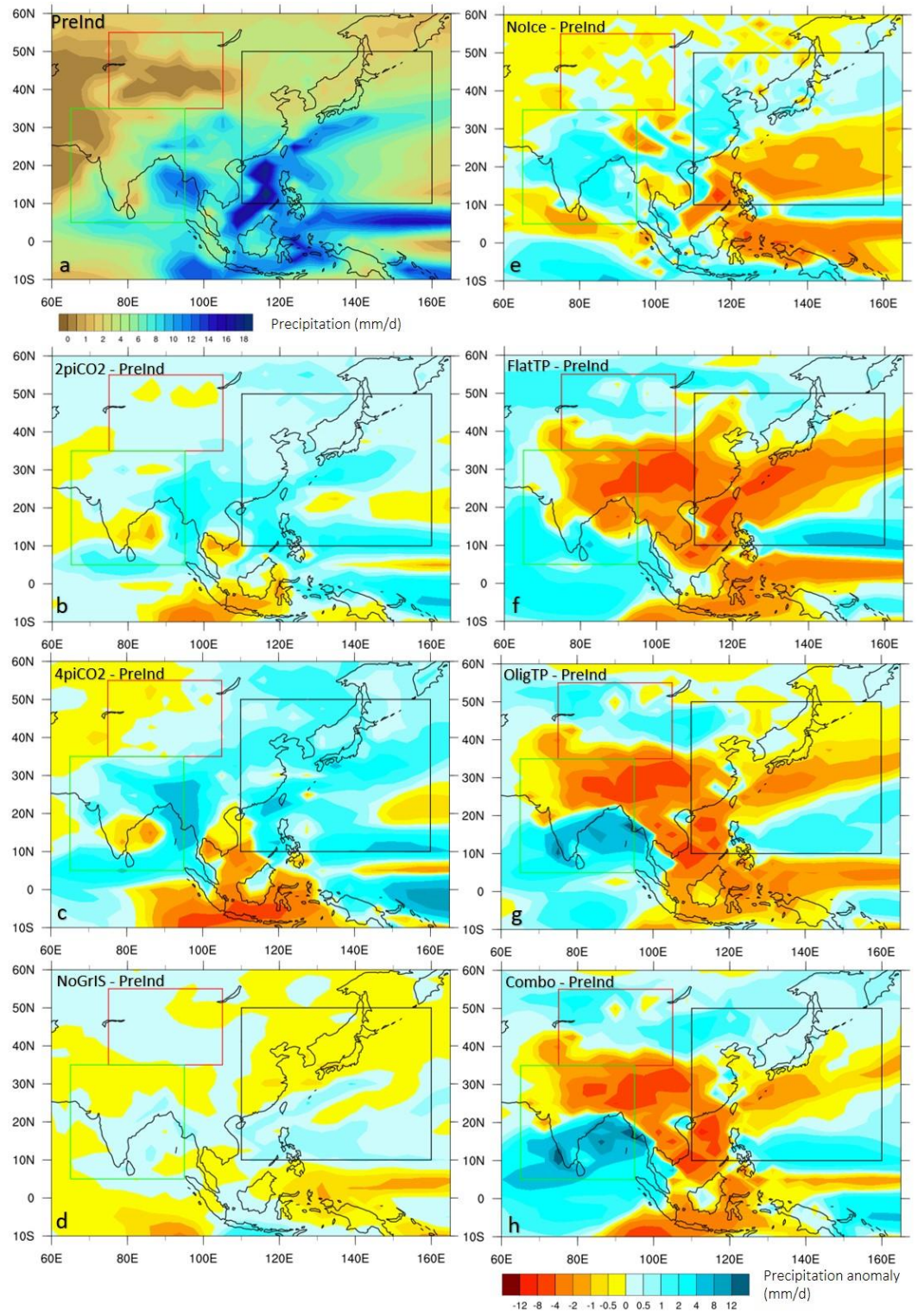

Figure 20: a) Simulated monsoonal (May – September) precipitation (mm/d) for the PreInd. Simulated monsoonal precipitation anomaly (mm/d) compared to the PreInd for: b) 2piCO2, c) 4piCO2, d) NoGrIS, e) NoIce, f) FlatTP, g) OligTP and h) Combo simulations. The SAM, EAM and AECA regions are denoted by the green, black and red boxes respectively.

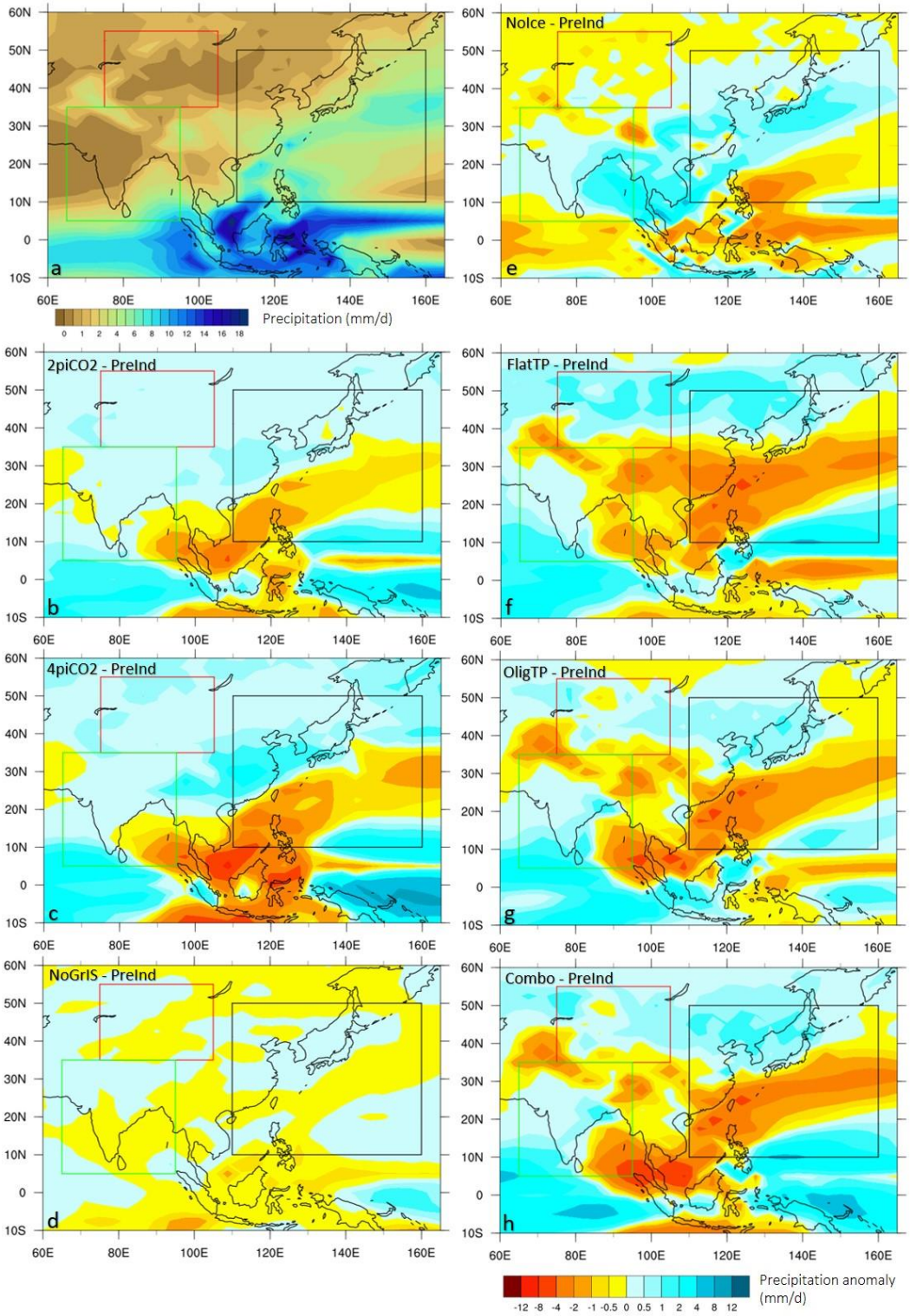

Figure 21: a) Simulated non-monsoonal (October – April) precipitation (mm/d) for the PreInd. Simulated non-monsoonal precipitation anomaly (mm/d) compared to the PreInd for: b) 2piCO2, c) 4piCO2, d) NoGrIS, e) NoIce, f) FlatTP, g) OligTP and h) Combo simulations. The SAM, EAM and AECA regions are denoted by the green, black and red boxes respectively

During the monsoonal months, moisture availability and mean sea level pressure does not show a large difference from the PreInd (Fig. 20e, 21e) for all the three regions.

With the TP flattened temperatures over the land are constantly higher throughout the year (Fig. 19 e), however, in opposition to the 2piCO2 and 4piCO2, where the temperature change is almost uniform above the Asian landmass and precipitation was intensified, in FlatTP the Asian monsoon related precipitation becomes weaker (Fig. 18a-d). Precipitation rates are the lowest amongst all simulations performed, and for the first time we observe a shift of this magnitude in the moisture availability over Asia (Fig. 21, 23f). This can be attributed to the up to 13^{o}C higher than PreInd temperatures over the whole Asian landmass (Fig. 19e). Notably, during monsoonal months, the AECA reaches the lowest values of P – E with a change not only in the magnitude but more importantly in its spatial distribution (Fig. 21f). The position of the negative moisture availability zone falls between the two low pressure systems that are created over Asia when the TP is removed (Fig. 22f). With no orographic barrier in place, atmospheric pressure systems over Asia from Oct – Apr is centred at 50^{o}N while in the FlatTP simulation, is centred at 35^{o}N, with less spatial extent and lower values (Fig. 25f). Nevertheless, during non-monsoonal months the AECA shows positive moisture availability and as a result precipitation reaches the highest percentage of increase compared to the PreInd (on average 144% increase from Oct-Apr) (Fig. 24f). This increase can be attributed to the change in moisture availability as westerlies are enhanced over the AECA since the high-pressure system is displaced to the South and the area of the pressure change is within the AECA region (Fig. 25f).

In the OligTP simulation, the EAM region receives less precipitation than in PreInd indicating a weaker monsoon where moisture availability from the adjacent water bodies is decreasing (Fig. 21 g, 17c-d). With the TP set to Oligocene elevation the SAM precipitation intensifies especially in the beginning of the monsoon (May-June) (Fig. 18a). Wetter conditions are also simulated for the AECA that combined with the different moisture availability and low-

pressure patterns (compared to the FlatTP), indicates that there is a threshold to the TP elevation that is controlling the aridity and monsoon intensity (Fig. 21g, 21g) that was probably established after the Oligocene. Even under non-monsoonal circulation the AECA is constantly wetter by up to 60% (Fig. 18f) also suggesting that the aridity over the region was established after the Oligocene.

Finally, in the Combo simulation we observe that the simulated climate over Asia is mainly driven by the topography change rather than the CO_2 increase or the ice-sheet formation (Fig. 21h, 23h).

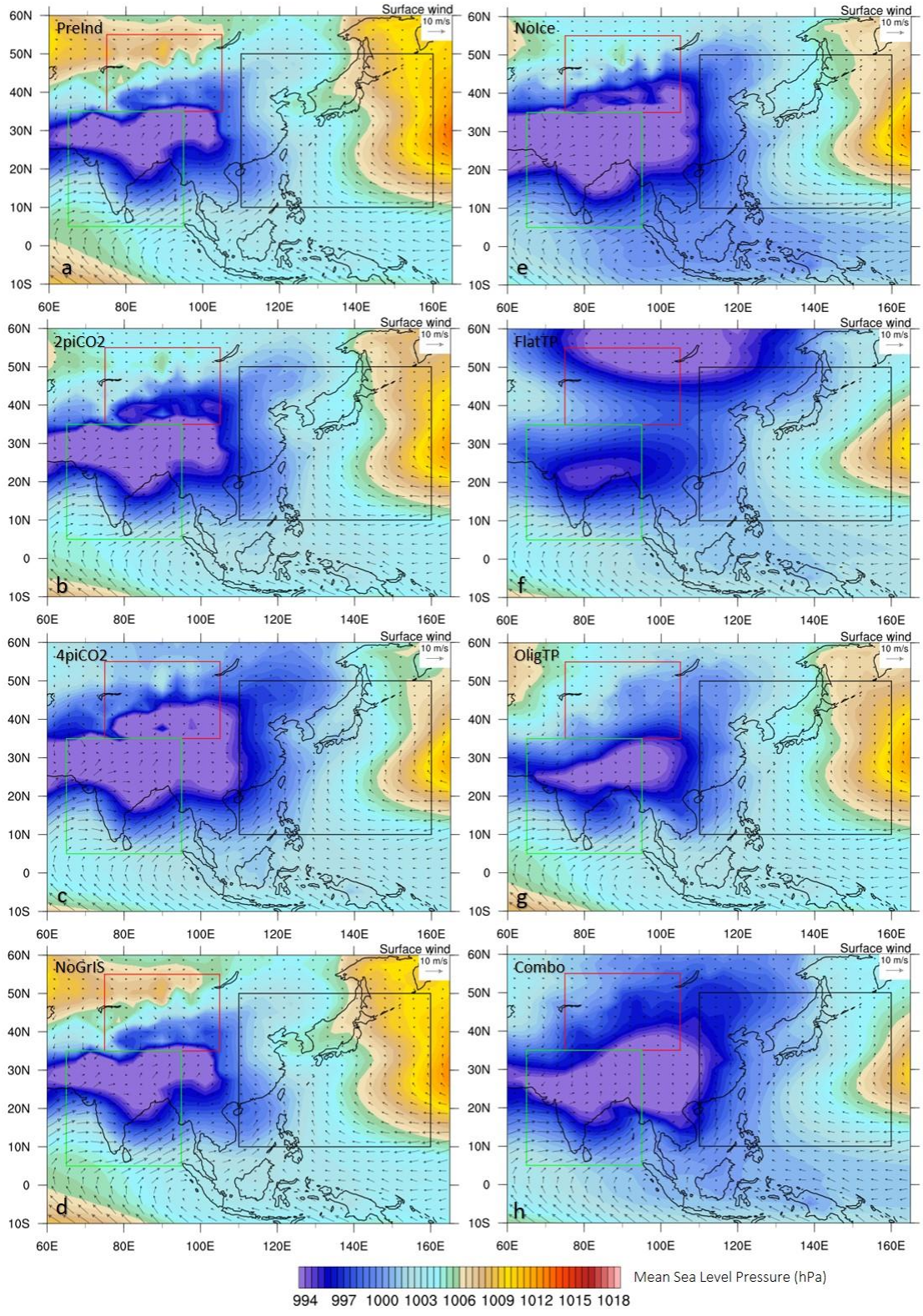

Figure 22: Simulated monsoonal (May - September) Mean Sea Level Pressure (hPa) and surface winds (m/s) for: a) PreInd b) 2piCO2, c) 4piCO2, d) NoGrIS, e) NoIce, f) FlatTP, g) OligTP and h) Combo simulations. The SAM, EAM and AECA regions are denoted by the green, black and red boxes respectively.

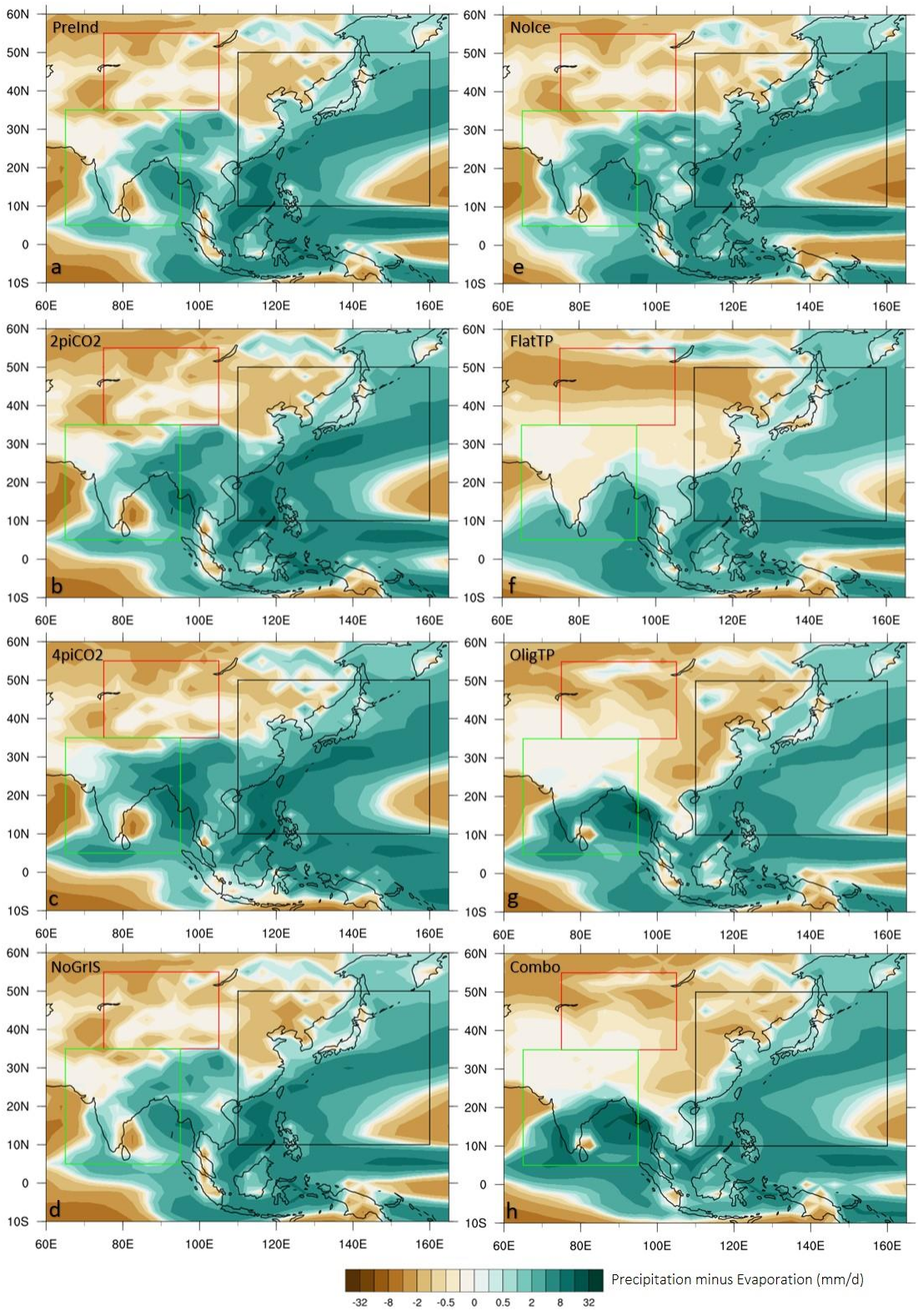

Figure 23: Simulated monsoonal (May – September) Precipitation – Evaporation (P – E) (mm/d) for: a) PreInd b) 2piCO2, c) 4piCO2, d) NoGrIS, e) NoIce, f) FlatTP, g) OligTP and h) Combo simulations. The SAM, EAM and AECA regions are denoted by the green, black and red boxes respectively.

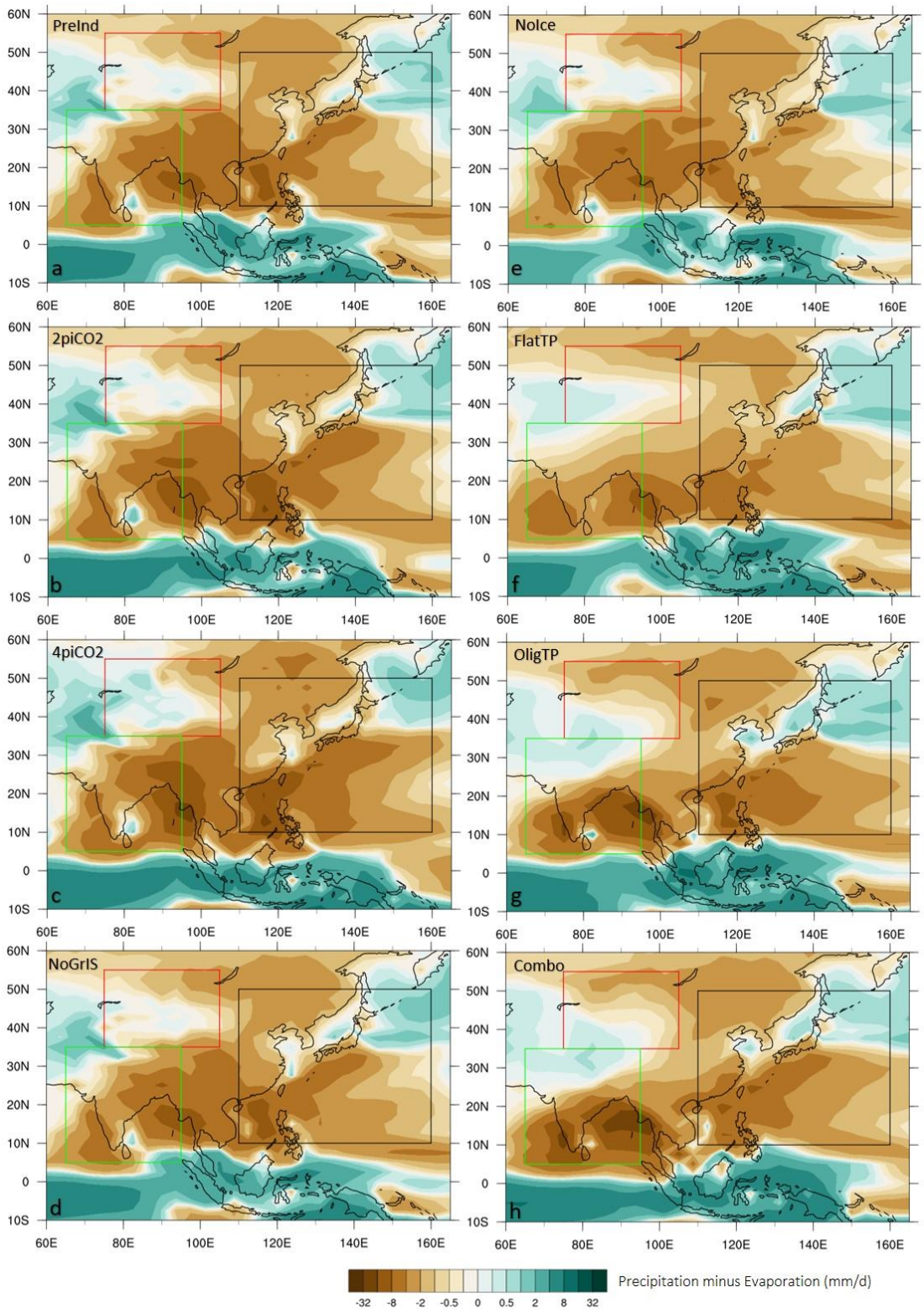

Figure 24: Simulated non - monsoonal (October – April) Precipitation – Evaporation (P – E) (mm/d) for: a) PreInd b) 2piCO2, c) 4piCO2, d) NoGrIS, e) NoIce, f) FlatTP, g) OligTP and h) Combo simulations. The SAM, EAM and AECA regions are denoted by the green, black and red boxes respectively.

3.5.2 Significance of results for understanding the development of aridity in Asia during the Cenozoic

Changes in atmospheric CO_2 concentration, Antarctic ice-sheet coverage and TP elevation have all been determined to be important drivers for the precipitation that the SAM and EAM regions receive, not only during monsoonal months but during non-monsoonal months (Fig. 20, 22). Nevertheless, the AECA region seems to remain unaffected by all changes to boundary conditions except for the TP elevation for both monsoonal and non-monsoonal months. In a palaeoclimate context it has been well established that the differential uplift of the TP, together with associated land/sea distribution changes as well as the global cooling at the EOT, played a significant role in the climatic evolution of the Asian continent in general. However, aridification of inland Asia is interpreted as a combination of the global oceanic cooling and ice-sheet growth, the TP uplift and the retreat of the Paratethys Sea (Bosboom et al. 2014a,b; Licht et al. 2014; Lippert et al. 2014). The sensitivity experiments indicate that the Asian aridification is solely controlled by the TP uplift rather than changes in CO_2 and ice-sheet formation. From the precipitation and P – E results analysed in this study, it is clear that climate reconstructions from proxy records can be challenging to interpret for a number of reasons. Firstly, the nature of climate variability recorded by different proxies varies. Some proxy systems (either physical/chemical or biological) may record annual environmental conditions averaged over long timescales. Others may provide information useful to deduce seasonality and the relative strength of the monsoons. So, understanding the nature of what proxy system is actually recording in the environment will be central in any comparison to the climate model results shown here. Secondly, given the spatially heterogeneity seen in our model results, the geographical location of any proxy data record will be an important predetermining factor in the environmental reconstruction itself. For example, during the monsoonal period in the 4piCO2 experiment, the AECA region receives more precipitation on average. However, the western part of the same region is drier compared to the PreInd

(Fig. 20c). Thus, extrapolation from a single proxy record from the west part of the AECA could lead to a completely different environmental reconstruction than a proxy collected from the eastern part of the same region. Finally, depending on what each proxy records (i.e. precipitation or P – E), the most important driver can be different. Specifically, if one focusses on P – E in the EAM region for the OligTP simulation during non-monsoonal months (Fig. 24g), we would expect to have greater moisture availability in the environment. However, the results for precipitation alone (which declines relative to the PreInd), would suggest otherwise (Fig. 23g).

Finally, in order to understand and decipher the forcings and underlying mechanisms that drove the aridity and monsoonal circulation after the EOT in more detail, it is necessary to perform an additional series of fully realistic Oligocene simulations, whereby the effect of individual boundary condition changes can be fully factorized.

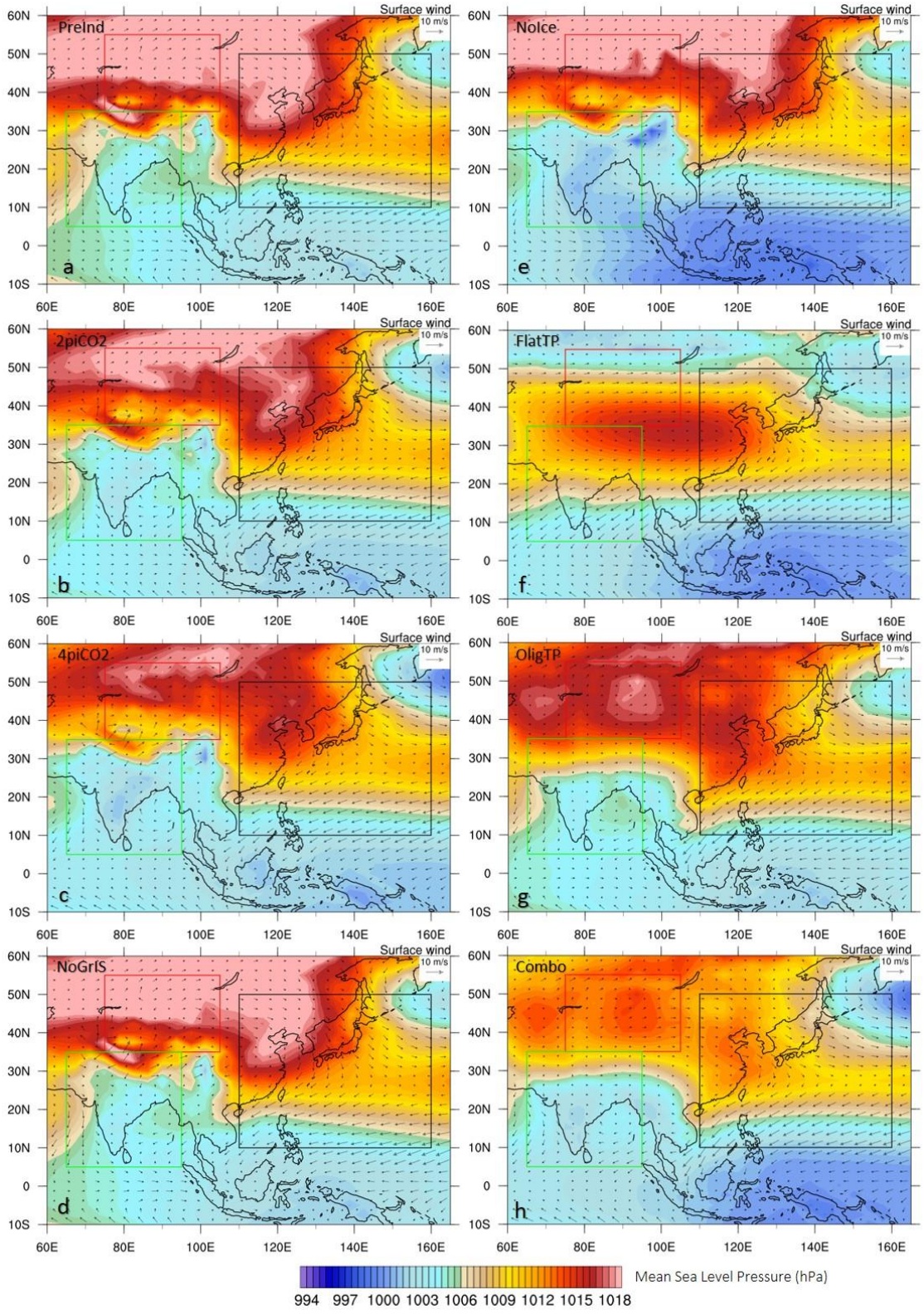

Figure 25: Simulated non-monsoonal (October - April) Mean Sea Level Pressure (hPa) and surface winds (m/s) for: a) PreInd b) 2piCO2, c) 4piCO2, d) NoGrIS, e) NoIce, f) FlatTP, g) OligTP and h) Combo simulations. The SAM, EAM and AECA regions are denoted by the green, black and red boxes respectively

3.6 Conclusions

An attempt to determine the effect of three different factors to Asian climate (CO_2, ice-sheet coverage and TP uplift), using HadCM3 is made for this study. The model shows that CO_2 increase leads to enhanced monsoonal precipitation for both the SAM and EAM and wetter conditions over AECA throughout the year. The Greenland ice-sheet seems to not affect Asian climate. However, the specification of Antarctic ice-sheet produces a wetter AECA, stronger SAM conditions but weaker EAM related precipitation. TP uplift corresponds to an intensified SAM but weakens the EAM region's precipitation through the year. A combination of boundary condition changes seems to follow the OligTP simulation's general pattern with wetter conditions over the AECA, throughout the year, a steeper transition from non-monsoonal to monsoonal precipitation for the South, and a weaker precipitation over East Asia during the boreal winter. This suggests that the TP, even though other changes contribute, is the main driver for climatic change over Asia. Finally, by studying different hydroclimatic parameters (i.e. Precipitation vs Precipitation – Evaporation) it is shown that the relative significance of each forcing is dependent on the parameter studied itself, a fact that should be taken into consideration when interpreting proxy records for palaeoclimate reconstructions.

Chapter 4: The role of Central Asian uplift in East Asian Monsoon circulation and its palaeoclimate implication

Introduction

Following the results in Chapter 3 that suggest the TP uplift is the primary driver for climatic change over Asia, this chapter focuses on the East Asian Monson region using a new set of seven simulations starting with flattening of the high-elevation Asia and increasing it stepwise up to the Pre-Industrial elevation, creating 5 intermediate stages of an idealised uplift (Table 1). The characteristic EAM stages that are associated with the westerly wind circulation and the frontal systems are tracked for each of the experiments and the hypothesis that precipitation over the EAM region is controlled by the westerly-jet latitudinal position is tested.

The objectives of this chapter are to explore i) the seasonal variability of the westerly jet and associated precipitation over East Asia, ii) the elevation threshold for changes in the climate patterns over Asia and iii) the westerly jet latitudinal position in relation to the uplift to determine the role of high elevation as a palaeoclimate forcing altering the jet.

4.1 East Asian Monsoon precipitation

The rainfall pattern from April to July over East Asia can be divided in the following four stages: 1) persistent rainfall in April over the South EAM region, 2) Pre-Meiyu phase in May, 3) Meiyu rainfall in June where rainfall shifts northward and 4) second northward jump of the rainfall that marks the end of the Meiyu stage (Chiang et al. 2014; Molnar et al. 2010). The term Meiyu is associated with the subtropical front that brings summer rainfall over the EAM region and is one of its most prominent features.

With boundary conditions set to PreInd and TP5000, simulated precipitation from April to July follows the modern-like seasonal variability and spatial extent described above (Fig. 26). Furthermore, experiments show that spring rainfall over East Asia is absent with topography set to less than TP2000, indicating dry conditions during spring (Fig. 26). Greater elevation produces an increase in spring rainfall South of the Yangtze river (approx. 31^{o}N), characteristic of the first stage of the EAM (Fig. 26). The tipping point from the dry conditions to the persistent spring rainfall, and thus the formation of stage 1 of the modern EAM, is seen in experiment TP3000. In TP3000, spring precipitation is significantly decreased in terms of extent and intensity than experiment PreInd, and conditions resemble the PreInd pattern when elevation surpasses that of TP4000. In the OligTP experiment, spring rainfall over the south part of the EAM region is close to PreInd in terms of intensity but is more limited spatially and mainly affecting the southeast EAM (Fig. 26). Interestingly, even though in terms of "absolute" elevation the OligTP is set to less than that of TP3000, stage 1 of the EAM is not absent.

The FlatTP to TP2000 experiments produce dry conditions during the second stage of the EAM (Fig. 26), and again TP3000 is the threshold elevation for a shift to wetter conditions that can be characterized as the pre-Meiyu phase, even though limited to the southeast of the region. The OligTP simulation shows the precipitation zone extending to the west and north, indicative of stage 2 EAM circulation (Fig. 26).

During the Meiyu phase, all experiments show a precipitation increase and northward propagation (Fig. 26). Lower elevation produces weakened and spatially limited precipitation (i.e. FlatTP), but as we move to the higher elevation experiments the pattern becomes increasingly similar to the PreInd.

Finally, in July rainfall propagation into the higher latitudes is evident in experiments TP3000 or above even though weaker compared to the PreInd (Fig. 26). This is not the case for the

FlatTP simulation where precipitation is spatially confined to the lower latitudes. The OligTP experiment shows a relatively dry zone over the central EAM region, however the South and North are significantly wetter (Fig. 26).

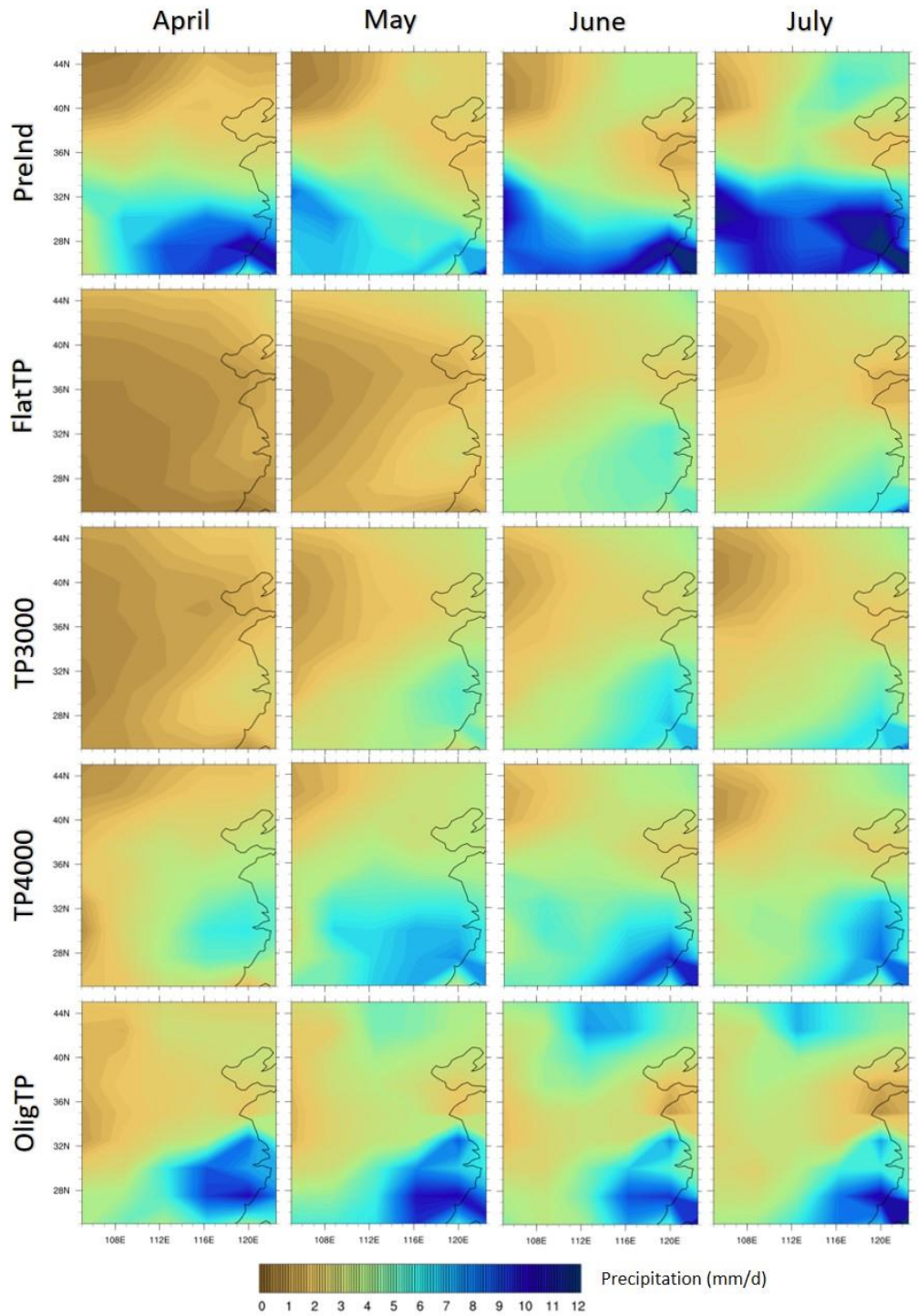

Figure 26: April to July monthly total precipitation rate (mm/d).

4.2 Westerly jet and meridional temperature gradient

In simulations with elevation higher than TP3000, the latitudinal position of the westerly jet follows the modern-day seasonal variation (Fig. 27). In April the jet over the EAM region is located at 34^{o}N, during May it shifts northward by 2 degrees, in June the jet migrates to the north of the TP and finally, during July the jet acquires its northernmost latitudinal position further north from the TP. However, simulations with lower elevation show a different pattern. Specifically, in experiments FlatTP to experiment TP2000, the westerly jet latitudinal position shifts northwards by only 2^{o} from April to July and does not propagate into the higher latitudes (Fig. 27), as the westerlies are not impeded by the TP, and temperature gradient is not as strong with the absence of high elevation over Central Asia (Fig. 28). The four jumps in the westerly jet latitudinal position are also evident in the OligTP experiment. However, due to the difference in the latitudinal distribution of the TP elevation the westerly jet does not reach as far north compared to the PreInd, with its northernmost position being at 40^{o}N (Fig. 27).

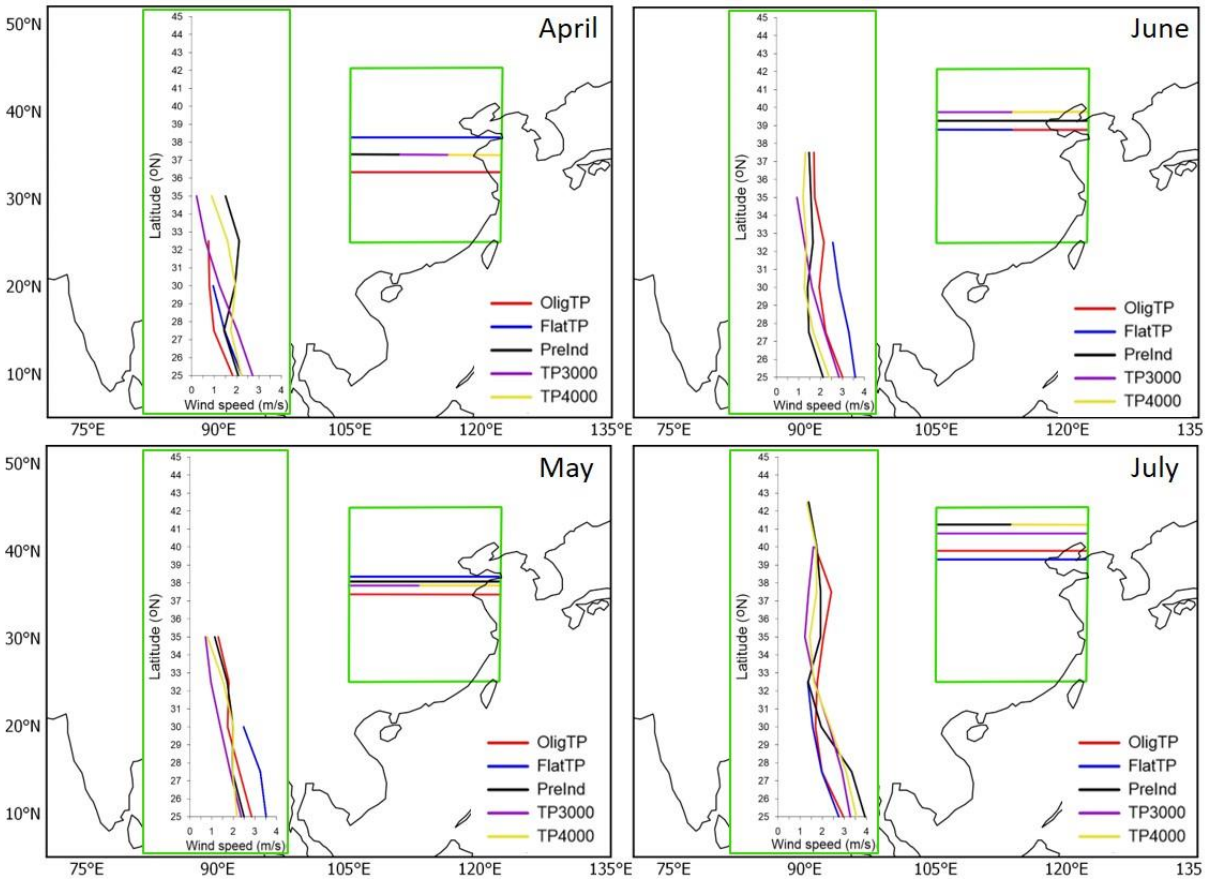

Figure 27: Map plots show a schematic of the latitudinal position of the westerly jet (horizontal lines) for months April – July, over the EAM region (green box) for each experiment. PreInd (black), FlatTP (blue), TP3000 (magenta), TP4000 (yellow), OligTP (red). The integrated graph plots show the latitudinal propagation and windspeed (m/s) of the low-level southerlies/south-easterlies averaged over the EAM region. Notably, the northward propagation of the low-level southerlies/south-easterlies is controlled by the latitudinal position of the westerly jet. Experiments TP1000, TP2000 and TP5000 are not shown, as their results are similar to the FlatTP for the first two and the PreInd for the latter. The westerly jet position (or jet occurrence) is defined at a location where the wind speed is a local maximum (exceeding 30 m/s) between 100 and 500 hPa (Chiang et al. 2014; Schiemann et al. 2009). *The propagation of the low-level winds is given by the position in which the directionality changes from south/south-east to westerlies.*

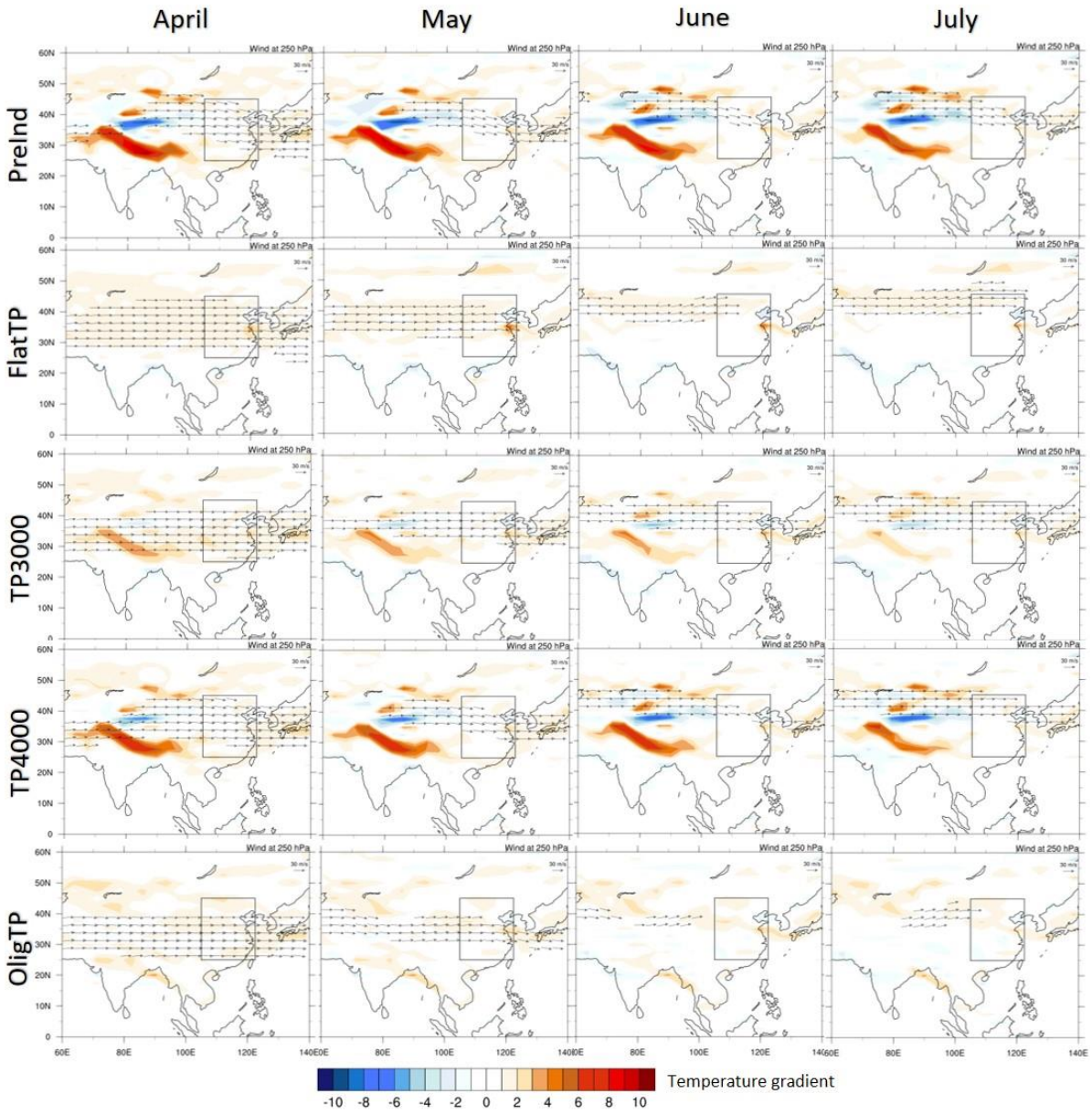

Figure 28: Meridional surface temperature gradient (°C) April – July and 250hPa winds (m/s). Westerlies with speed less than 30 m/s, which is the lower threshold for a jet occurrence, are masked out. The meridional gradient is defined as dT/dLat.

4.3 850 hPa winds and moisture availability

It has been well established by previous studies that changes in the elevation of the TP cause a change in wind circulation over Asia, not only in the upper troposphere but in the lower as well. In both PreInd and TP4000 experiments, easterlies and south-easterlies are dominating

the South of the EAM region carrying moisture from the Pacific Ocean and South China Sea during April and May and reach higher latitudes during June and July (Fig. 27, 28). From April to May the northern part of the EAM region is dominated by weak westerlies with lower moisture availability and humidity carried from inland central Asia. Spatially, the change from moisture carrying easterlies to westerlies occurs in the latitude the westerly jet is positioned (Fig. 27).

Flattening of the TP, TS and MP, creates a dry zonal area over Asia stretching west to east during monsoonal months (Fig. 29). In these scenarios the westerlies dominate more than 2/3 of the EAM region. With the orography flattened completely, the easterlies and south-easterlies do not propagate to the north, and thus do not contribute as a moisture source for spring precipitation over EAM (Fig. 26). Increasing the elevation (TP1000 and TP2000 simulations), leads to a northward propagation of the westerly jet of about 2^{o}, and now the easterlies and south-easterlies propagate into higher latitudes, but with topography significantly lower than PreInd, moisture availability remains low over the whole EAM and thus not producing spring precipitation (Fig. 27, 28). In TP3000, the westerly jet reaches its northernmost position, while easterlies and south-easterlies propagate into the EAM region providing enhanced moisture available in the South. With higher topography over Asia, the pattern of moisture availability changes from being zonal (running west to east) to a more complex pattern with the south EAM region's moisture availability increasing (Fig. 27, 28). In TP4000 the simulated wind, precipitation, humidity and moisture availability begin to display a pattern that is very similar to the PreInd, and when moving to TP5000 the pattern becomes almost identical to the PreInd (Fig, 25, 26, 28). In the OligTP experiment the TP is located further South, and the westerlies are significantly weaker than in any other experiment. However, there moisture is available in the north and northwest of the EAM to be carried by the westerlies to the north of the EAM. The underlying mechanisms that control the westerly

jet's latitudinal position which in turn controls the EAM precipitation are analysed in detail by Chiang et al. (2014).

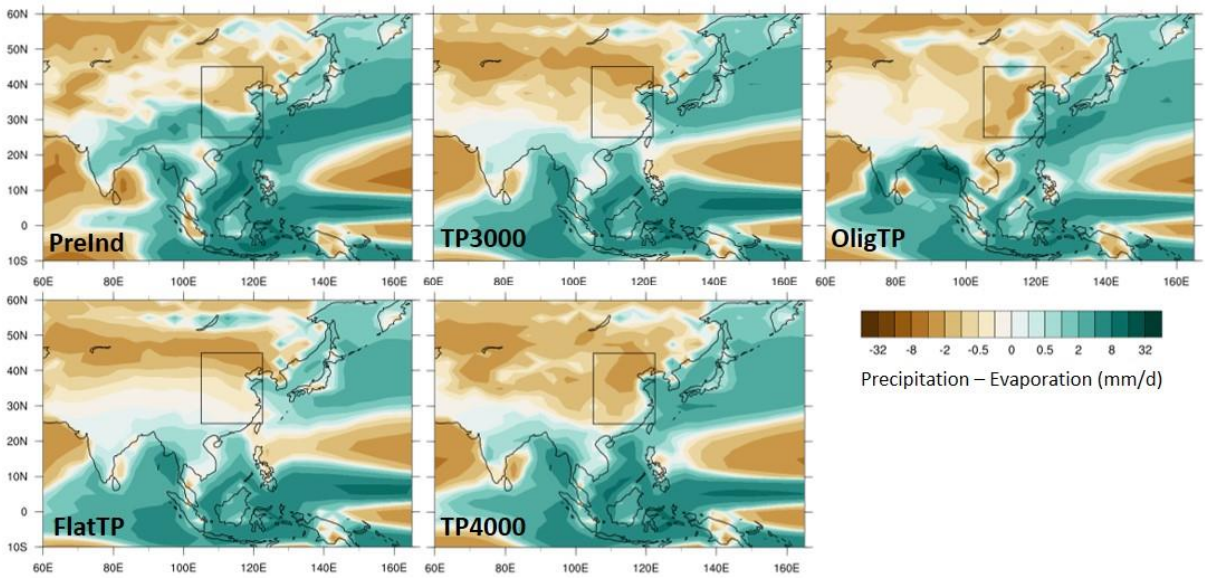

Figure 29: Moisture availability (P – E: mm/d) averaged from April to July for different experiments. For elevations less than TP3000, broad arid belts are simulated in Asia from West to East, a pattern that changes with higher elevation (TP3000 and above).

4.4 Discussion

The TP has a marked effect on the westerlies over Asia (Schiemann et al., 2009) and the seasonal migration of the westerly jet from South to North is vital to the East Asian rainfall climate (Liang and Wang, 1998). The "Jet Transition Hypothesis" (Chiang et al., 2014) suggests that changes to the position of the westerlies relative to the TP, drive rainfall changes over East Asia over geological timescales. Our simulations provide further evidence that the westerly jet transition plays an important role for the dynamics of the EAM by controlling the associated monsoonal precipitation. The northward jumps of the westerly jet coincide with the stepwise northward propagation of the EAM rainfall during monsoonal months (April to July). The westerly jet latitudinal position controls the low-level inland flow of moisture-carrying southerlies and south-easterlies over East Asia that leads to

precipitation where they converge. The lower-level southerly flow is an important factor in the spatial extent and seasonality of the EAM (Rodwell and Hoskins, 2001). There have been numerous studies deciphering the dynamics of the westerly jet and its association to the EAM climate as well as the role of the thermal and mechanical forcings from the TP (i.e. Baker et al. 2015; Chiang et al. 2015; Zhang et al. 2017, 2018), and it has been established that the high elevation over Asia alters the westerly flow, which in turn alters the EAM circulation pattern.

For elevations greater than TP3000, the pattern of atmospheric circulation is similar to the modern, with spring precipitation in the southern part of the region controlled by the moisture-carrying southerlies from the South China Sea and Pacific Ocean. This is consistent with the moisture source analysis by Baker et al. (2015). However, the EAM does not display the same characteristics when elevation is less than in experiment TP3000. Notably, with lower elevation the model simulates a change in monsoonal pattern; specifically, the absence of the first two stages of the present-day monsoon. With the westerlies flowing zonally and dominating the mid-latitudes over Central Asia, rather than splitting in the Southern and Northern branch, there is no persistent spring precipitation (stage 1) and pre-Meiyu phase (stage 2), but there is summer precipitation over the EAM reaching to the Northern part of the region (albeit weaker and spatially constrained (stages 3 and 4)). In terms of general precipitation pattern, our simulations are consistent with earlier studies that show that the uplift of the TP enhances precipitation over East Asia (Jiang et al. 2008; Zhang et al. 2007). The tipping point for the development of a modern-like circulation is seen in TP3000. This threshold is also consistent with the simulated shift from zonal arid belts to a non-zonal pattern (Fig. 29), a shift that has been suggested as an indicator for the onset of the EAM (Li et al., 2018).

Even though the land-sea thermal contrast has been suggested in the past as the necessary condition for spring rainfall over the South EAM region (Tian and Yasunari, 1998), Wu et al.

(2007) showed that the spring rainfall is formed when westerlies are split by the TP into a southern and northern branch, and cold air from the North and warm moist air from the South converge over eastern China. As shown by our simulations, the deflection of the westerlies, and the subsequent precipitation, occurs when the TP topography reaches the elevation equivalent to that used within experiment TP3000, suggesting that with elevations lower than this the EAM misses one of its most characteristic features - the spring rainfall.

Furthermore, the latitudinal position of high elevation is also an important factor that should be taken into consideration. The OligTP experiment shows that with elevation closer to the TP2000 but positioned further to the South, monsoonal circulation is more similar to the PreInd than in the TP2000 experiment, a fact that highlights the importance and necessity for enhanced constraints on the palaeogeographical history of the region to inform the boundary conditions used for climate modelling studies.

Moving forward, it will be important to study the EAM pattern in a fully palaeoclimate context, using fully realistic palaeogeographic boundary conditions that not only represent the bulk uplift that occurred in the region, but also the timing and magnitude of differential uplift of the individual regions that comprise the TP, TS and MP orogens. This is likely to provide a valuable dataset for proxy data interpretation. Insights from proxy data in the region are not limited to the intensity and/or the presence of monsoonal circulation, but also its spatial limits, seasonal variability and monsoonal phases, and fully realistic palaeo-simulations of the uplift history of the region would prove useful in terms of interpreting the palaeoclimate signals recorded in different proxy archives.

Further work using different climate models with and without realistic palaeogeographic reconstructions of the region will be necessary to evaluate the model dependency of the elevation threshold determined in this study for the onset of modern-like circulation in the region.

4.5 Conclusions

This study attempts to determine the effect of the Central Asian orogens uplift to the East Asian Monsoon (EAM) circulation. Simulations show that by uplifting the TP, TS and MP, there is an evolution towards a modern-like circulation with an elevation threshold for that change at 3000 m. Lack of high-elevation leads to the westerlies flowing zonally over Central Asia producing monsoonal precipitation limited to the summer months, whereas when elevation is set to 3000 m and above, westerlies are deflected by the TP, and the EAM circulation and associated precipitation follows the pattern seen in the present-day. Furthermore, results show that the latitudinal position of high elevation is an important factor for the EAM and they highlight the necessity for constraints on the palaeogeographical boundary conditions that will lead to a better understanding of the Asian paleoclimate and evolution. Furthermore, it is shown that the latitudinal distribution of the high elevation can be as important as the uplift in controlling the westerly jet, seasonal variability and monsoonal precipitation. This factor should be explored through a set of realistic palaeo-simulations as it has the potential to provide a highly valuable methodology for interpreting different proxy records.

Chapter 5: Key geological factors on the onset, intensification and expansion of Asian aridity

Introduction

This chapter focuses on the onset and intensification of aridity in Central Asia. A combination of the simulations already described in Chapters 3 and 4 (Table 1, Fig. 14) are used in here to explore the effect of each factor on the inland aridification. Sensitivity simulations have the advantage of allowing climate model boundary condition changes both in combination and isolation, hence making them a useful tool to differentiate between forcing factors and their impact on the climate. The results presented are based on aridity indices and climate classification in order to clearly define the arbitrary aridity threshold.

The objectives in this chapter are to determine: i) the required geological and atmospheric boundary conditions that could have led to inland Asian aridity and ii) the main forcing factor that controls Asian aridity and the factor that drove its onset.

5.1 Aridity over Asia as defined by the IPCC (2007) and De Martonne (1926) indices

The simulations carried out for this study show that flattening of the high-elevation over Asia creates ideal conditions for arid conditions to the East Asia (Fig. 30). The TP3000 experiment, shows the largest decrease in the spatial distribution of the arid environment amongst all the experiments, with most of the Central and West Asia shifting to semiarid conditions instead (Fig. 30). Doubling the CO_2 decreases the arid spatial coverage by 24%, a percentage that reaches 42% when we quadruple atmospheric CO_2 values. The influence of the CO_2 on

aridity is also evident between the OligTP and 2piCO$_2$OligTP experiments. Specifically, increasing the CO_2 values and keeping the topography constant, even though at lower latitudes results in a shrinking arid region, even though the positioning of the high elevation at lower latitudes alone causes the highest spatial extent of the arid environment among all the experiments (Fig. 31).

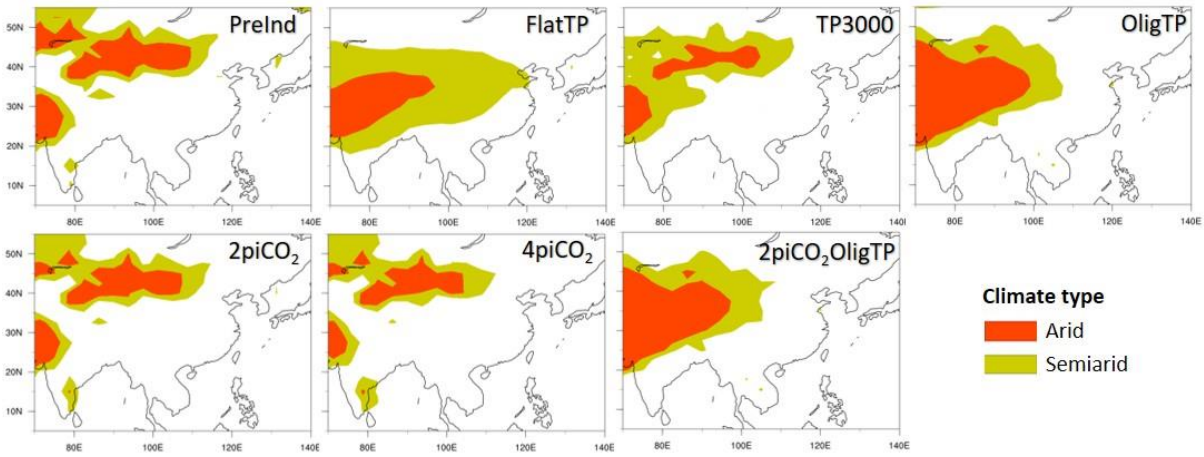

Figure 30: Arid and semiarid environments over Asia as defined by IPCC (2007) for the experiments in this study.

The similarity of the results between the two aridity indices is apparent (AI and I_{DM}). However, the De Martonne index highlights the role of higher temperatures in the spread of arid environments. Both indices agree when it comes to the shrinkage or extension of arid regions for all of the experiments, except for the FlatTP. That can be attributed to the fact that with the TP flattened, the annual average temperature over the region increases by up to 13^{o}C (Zoura et al., 2019), resulting in an overestimation of the arid region in I_{DM} when compared to the AI index (Fig. 31, 31).

For the rest of the experiments, we can see that the DM index also indicates a shrinkage of the arid regions when CO_2 values are increased (Fig. 32), while the positioning of the high elevation at lower latitudes leads to an expansion of the arid region. Furthermore, lower

elevation of the TP but positioned in the present-day latitude (TP3000), shows again a reduced spatial extent of arid environment (Fig. 32).

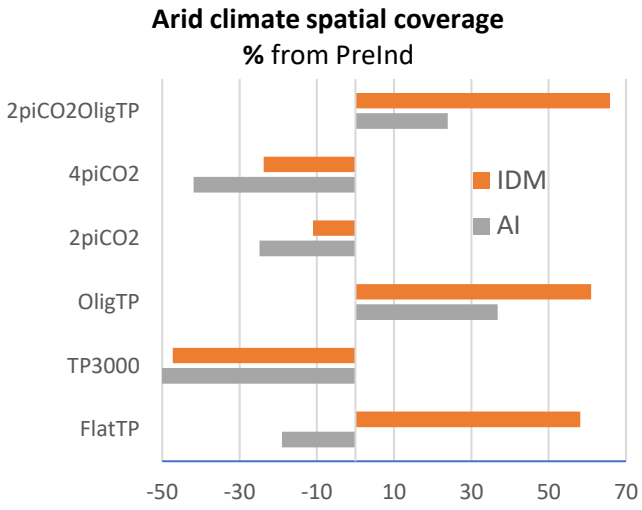

Figure 31: Percentage change (%) in the spatial coverage of arid environments over Asia between each experiment and the PreInd. Positive (negative) values mark an increase (decrease) of the spatial distribution of the arid environment.

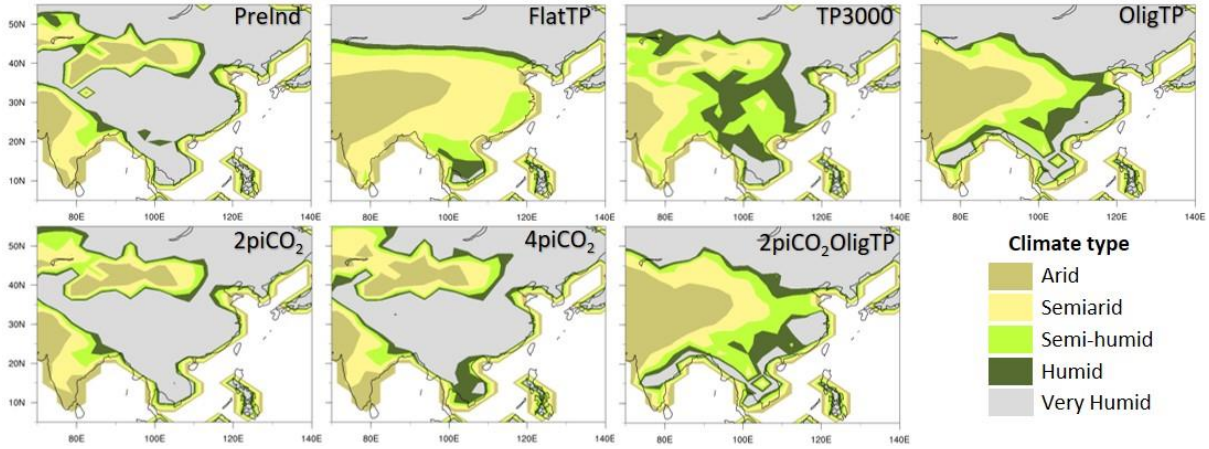

Figure 32: Environmental classification over Asia using the De Martonne (1926) index for all the experiments in this study.

5.2 Köppen climate classification

Chen and Chen (2013) used a temperature and precipitation dataset for 1901-2010 and showed that Asia is characterized by unstable climates, with stable climates limited to the region above the TP, a part of Central Asia and Southeast China, corresponding to Polar, Dry

(arid) and Mild temperature climates respectively. The PreInd simulation shows similar results for the Central Asia (Fig. 33).

Classifying the arid climate types with the Köppen classification method by using the average of the last 50 simulated years, results in a similar pattern as seen in the AI and I_{DM} indices with the main, but not significantly bigger difference, being in the spatial extent of the Cold Arid region. Again, with rising CO_2 values the Cold Arid region shrinks while the Hot Arid region propagates eastwards. Interestingly, when the TP is located at a lower latitude, increasing the CO_2 values does not correspond to an increase of the Hot Arid region as seen in experiments 2piCO2 and 4piCO2 when we compare them to the PreInd (Fig. 33). This highlights the importance that the latitudinal distribution of the TP in controlling the Asian climate, and specifically the Arid environments.

Furthermore, in terms of interannual variability, our results point out that a doubling of the CO_2 in the atmosphere causes a large part of the stable Cold Arid region over Central Asia to become unstable (70% change in spatial coverage). When CO_2 is quadrupled the whole Cold Arid region becomes unstable (Fig. 33). Instability, but spatially more limited, also characterizes the hot arid climates of Asia in the experiments where CO_2 values are increased, with the percentage of change in spatial coverage reaching 64% and 71% respectively.

Finally, in the simulations where elevation is decreased (TP3000, FlatTP), and in those that high-elevation is both decreased and located at lower latitudes (OligTP, 2piCO_2OligTP), the climatically stable regions of Asia are limited to the Hot Arid climate type and located in the west part of Asia at mid-latitudes (Fig. 33). Additionally, in all scenarios where the TP does not reach the threshold elevation of TP3000, and when it is located to lower latitudes (OligTP), Central Asia lacks a cold arid climate type. This suggests that the Cold Arid region

over Central Asia that is evident in the PreInd experiment and is similar to the modern-like one, is solely controlled by high elevation and its latitudinal distribution.

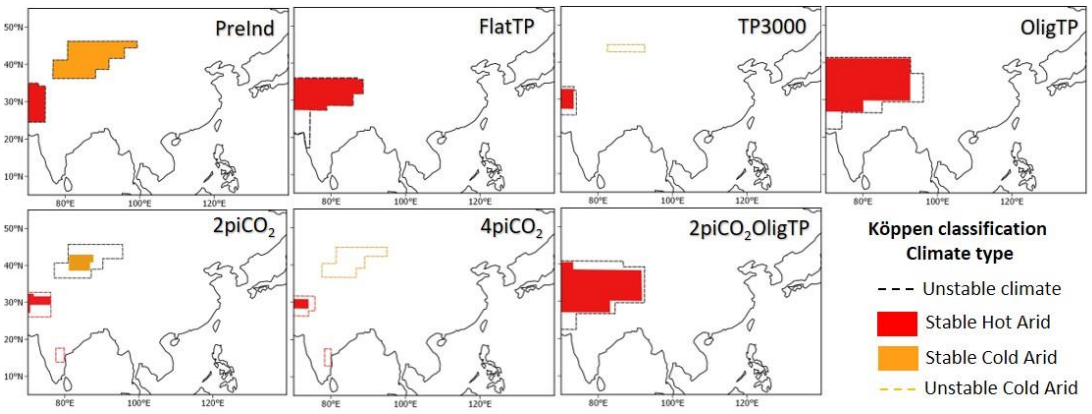

Figure 33: Spatially stable and unstable Köppen Arid (hot and cold) climate types for each experiment. The solid polygons represent hot arid and cold arid regions that are stable throughout the 50 last years of the simulations. The dashed line shows the regions that are unstable.

4. Discussion

The effects of orography on atmospheric dynamics over Asia and associated changes to aridity and Asian monsoons, have been studied extensively and are relatively well understood (i.e. Broccoli and Manabe 2002; Molnar et al. 2010). Li et al. (2018) carried out a set of Eocene simulations and showed that the existence of an uplifted TP is at least as important as a CO_2 decrease in enhancing Asian aridity. However, unconstrained factors such as palaeogeographic boundary conditions, atmospheric CO_2 values and land-sea distribution during the early Cenozoic, limit our ability to determine the timing of the aridity onset and the role that each of these factors play. Our experimental design enables the study of these factors in combination and isolation, through a series of idealised simulations to address these questions and explore the possibility of necessary threshold conditions for the onset of the Asian aridity.

The IPCC and De Martonne aridity indices provide a very useful and straightforward method for defining aridity and its spatial distribution. They both have the advantage of using

parameters that most GCMs can represent robustly and if used for realistic and not idealised simulations can be directly compared to palaeoclimate reconstructions based on proxy data. Albeit easy to use, both indices are not designed to capture interannual variability that can produce unstable climates, a feature that can be valuable as proxy interpretation. Therefore, we can address this issue by using the Köppen classification.

Simulation results show that the region characterized in the PreInd as Cold Arid is absent when topography is decreased below the TP3000 threshold or when high elevation is positioned at lower latitudes (OligTP). The underlying mechanism that drives this change is the increase of the surface temperature (by up to 13^{o}C when the TP is flattened).

Under increasing CO_2 values that lead to an increase of surface temperature, the spatial coverage of Cold Arid climate over Central Asia decreases by 23% and 42% for 2piCO2 and 4piCO2 respectively (Fig. 33). However, even with values higher than the modest estimates for atmospheric CO_2 concentrations during the Oligocene (Pagani et al., 2005), the Cold Arid climate is still present even though spatially confined when compared to the PreInd. This suggests that decreasing CO_2 values after the EOT, during the Oligocene, enhance aridity in terms of spatial coverage but as shown clearly by the OligTP-2piCO2OligTP experiments, CO_2 alone without high elevation is not a sufficient factor which can lead to the onset of aridity over Central Asia.

With elevation fixed to PreInd, and considering CO_2 change alone, the Cold Arid climate of Central Asia is becoming unstable as we move to higher CO_2 concentrations. Increased interannual variability generates climate types different from Cold Arid for 76% (2piCO2) and 100% (4piCO2) of the Cold Arid region. This could explain the disruption of aeolian deposition in Asia and the discrepancies between proxies with no continuity to record the variability.

The elevation threshold for the onset of aridity in Central Asia is the TP3000 configuration, a finding consistent with results presented in Chapter 4, that defined the elevation threshold for modern-like East Asian Monsoonal circulation at TP3000 (Zoura et al., GPC in review). Still, as the set of simulations used here are idealised and not designed to depict a specific time period during the geological time, the said elevation threshold provides an indication of a "threshold condition" rather than an absolute value for the condition itself. Nonetheless, it shows that a variety of palaeogeographic scenarios that consider all 3 major forcings (namely the TP uplift, CO_2 values and the Paratethys Sea retreat) and the range of the proposed estimates for each one can be used as a valuable tool not only to understand the dynamics and underlying mechanisms of Asian aridity during the Oligocene, but also to help constrain the boundary condition uncertainties through modelling simulations that will provide threshold values for the critical palaeoclimate changes the proxy records record.

5. Conclusions

The forcing factors of the Asian aridity onset and intensification has been a subject of debate for years. The timing of the onset has been placed from Eocene to Miocene by different studies, while the main forcing factor is yet to be determined. Here, through a series of sensitivity simulations with different elevations for the high-elevation Central Asia, including the TP, TS and MP as well as different atmospheric CO_2 concentrations, the question of the aridity onset in Central Asia is addressed. Model results show that the TP controls the onset of aridity over inland Asia, but in order to have arid conditions in Central Asia the TP should reach an elevation of at least 3000 m (TP3000 experiment). Furthermore, results show that high-elevation placed in lower latitudes is also not a sufficient condition for the onset of aridity. Finally, increasing atmospheric CO_2 values lead to increased interannual variability, which increases the spatial coverage of climatically unstable arid regions.

Chapter 6: Summary and future work

6.1 Summary of results

This thesis provided a systematic palaeoclimate modelling approach through a series of 13 sensitivity simulations with changing boundary conditions for the three key factors suggested as drivers of the climatic change in Asia. Specifically, it was the first time that the same General Circulation Model was used to study three of the factors contributing to the evolution of Asian climate at the same time. By using sensitivity simulations rather that realistic palaeosimulations, the three studied factors can be changed both in combination and isolation so that each factor's contribution to the Asian climate evolution can be studied independently. The importance of such an approach is the advantage of limiting the palaeogeographic, palaeo-CO_2 and ice-coverage uncertainties that realistic palaeosimulations have by default (i.e. the uncertainty in the latitudinal position of the TP, the uncertainty of land/sea distribution during the Early Cenozoic etc.).

Simulations showed that with increasing CO_2 values, monsoonal precipitation over the SAM and EAM is enhanced, and so is the moisture availability over those regions. Results also suggest a steeper transition from non-monsoonal to monsoonal circulation but no change in the timing of the monsoonal onset. The precipitation over the AECA during the monsoonal months shows no significant change under increasing atmospheric CO_2, however, during the non-monsoon season, the moisture availability and precipitation increase.

Removing the Greenland ice-sheet does not seem to affect the Asian climate significantly, however, under ice-free conditions monsoonal precipitation is enhanced and moisture availability increases over the South and East Asia.

Flattening of the TP drives an increase in annual temperature over the Asian landmass, while monsoonal precipitation and moisture availability both decrease in the EAM, SAM and AECA regions.

With the TP set to the Oligocene-like configuration a different response in monsoonal precipitation for the EAM and SAM is shown. Specifically, when the TP is located at lower latitudes even with elevation significantly lower than in the PreInd, the SAM precipitation is increasing but the EAM precipitation is weakening. Moreover, the AECA shows wetter conditions throughout the year. Additionally, the latitudinal distribution of the high elevation is shown to be as important as the physical uplift in controlling the westerly jet, seasonal variability and East Asian monsoonal precipitation.

With the boundary conditions for all three factors contributing to the Asian climate evolution changed, results pointed out that the climate over Asia is predominantly driven by the topography. This finding pointed out the necessity for performing more simulations focusing on the high-elevation Central Asia and how the uplift affected the Asian climate.

One of the results that stand out is the importance of high-elevation on Asian climate with simulations clearly showing that there is a threshold elevation for a shift to modern-like circulation and conditions over Asia. Evidence for the existence of a threshold elevation sufficient to produce modern-like conditions is introduced for the first time through this study and is the most prominent result.

Moreover, results suggest that aridity over Central Asia is solely controlled by the TP and its latitudinal distribution presenting with the same threshold of 3000 m for a shift to modern-like conditions for the AECA region. However, even though CO_2 seems to not be a sufficient condition for the onset of aridity, results suggest that it controls the interannual variability of the arid region.

Finally, even though this study focused on the underlaying mechanisms and dynamics of the Asian monsoons and aridity, it also focused on connecting model-derived results to possible implications in proxy interpretation, providing evidence that there is a dependency between each forcing and the hydroclimatic parameter studied. This finding should be further

explored and taken into consideration for proxy record interpretation and palaeoclimate reconstruction constraints.

6.2 Future work

The experiments carried out for this thesis were not designed to represent a specific geological period but were rather designed to provide the sensitivity of each forcing studied. But in order to understand the forcing and underlying mechanisms that drove the climatic change over Asia during the Cenozoic in more detail, it is necessary to perform an additional series of fully realistic palaeo simulations.

Firstly, this will give the ability to study the effect of the Paratethys Sea retreat, one of the suggested major forcing factors for climate change over Asia that was not included in this study to avoid any biases introduced by land-sea distribution uncertainties. Simulating the land/sea distribution rearrangement during the Early Cenozoic due to the Paratethys Sea retreat from Central Asia, should be one of the priorities for any efforts to model the Asian Climate during this period. Moreover, as the Paratethys Sea spatial extent, bathymetry and timing of the retreat are largely unconstrained, simulations should be designed to include a range of different reconstructions for the Paratethys Sea boundary conditions.

Secondly, it is essential to perform an extended series of realistic palaeogeographic reconstructions that will include the differential TP uplift and considers more than one of the proposed scenarios of uplift and associated palaeoelevation. With recent geological studies suggesting that part of the TP had reached modern-like elevation during the Early Cenozoic, it is necessary to use new palaeoelevation boundary conditions to be compared with simulations that use reconstructions that place the TP at elevations significantly lower (up to 1500 m) than the newly suggested ones. The necessity for using updated palaeoelevation is also pointed out by the threshold elevation for modern-like circulation shown in this study

as a difference of up to 1500 m between the reconstructed TP palaeoelevations, can lead to completely different simulated palaeoclimates for the same time-period (i.e. modern-like monsoonal circulation vs. broad zonal arid bands).

The palaeogeographic, land-sea distribution, atmospheric CO_2 concentration and ice-sheet coverage boundary conditions, especially for the largely unconstrainted early Cenozoic, should be designed to cover a wide range of scenarios that take into account most of the proxy reconstructions, with emphasis on the recent and better constrained proxy records produced by advancements in dating methods, analysis techniques and calibration methods. For example, covering the whole range of suggested CO_2 values during the EOT (1700 – 450 ppm) with a small interval; taking into account stepwise building of the ice-sheets in both Greenland and Antarctica; using different orbital forcing parameters etc.

A systematic approach like this will provide results directly comparable to proxy data, advancing our understanding on the mechanisms controlling the Asian climate. Direct comparison of a variety of simulated palaeoclimates with proxy records, will give the ability to further constraint some of the uncertainties by eliminating scenarios that do not simulate palaeoclimates consistent with the proxy reconstructions. Additionally, this will provide the ability to fully factorize boundary condition changes to determine the effect of individual boundary conditions.

However, as the parameterizations used in GCMs vary and there are certain biases in each one, simulations with consistent boundary conditions using a wide range of coupled GCMs should be used in order to quantify such biases and associated uncertainties in the representation of Asian climate. A model intercomparison project specifically designed for the Early Cenozoic following the methodology and approach of intercomparison projects for different time periods (i.e. Pliocene Model Intercomparison Project), would not only help to constrain the model dependency on the threshold conditions (such as the uplift or the

atmospheric CO_2 values), but also provide a better understanding of the complex climate dynamics over Asia.

References

Alyea, J. (1972). *Numerical simulation of an ice age paleoclimate.* Colorado, USA: Atm. Sci. Pap. No 193 Dept. Atm. Sci., Colorado State Univ.

An, Z., Kutzbach, J. E., Prell, W. L., & Porter, S. C. (2001). Evolution of Asian monsoons and phased uplift of the Himalaya-Tibetan plateau since Late Miocene times. *Nature*, *411*, 62–66. Retrieved from www.nature.com

Anagnostou, E., John, E. H., Edgar, K. M., Foster, G. M., Ridgwell, A., Inglis, G. N., … Pearson, P. N. (2016). Changing atmospheric CO_2 concentration was the primary driver of early Cenozoic climate. *Nature*, *533*, 380–398. https://doi.org/10.1038/nature17423

Annamalai, H., Hamilton, K., & Sperber, K. R. (2007). The South Asian Summer Monsoon and Its Relationship with ENSO in the IPCC AR4 Simulations. *Journal of Climate*, *20*(6), 1071–1092. https://doi.org/10.1175/JCLI4035.1

Ao, H., Roberts, A. P., Dekkers, M. J., Liu, X., Rohling, E. J., Shi, Z., … Zhao, X. (2016). Late Miocene-Pliocene Asian monsoon intensification linked to Antarctic ice-sheet growth. *Earth and Planetary Science Letters*. https://doi.org/10.1016/j.epsl.2016.03.028

Baker, A. J., Sodemann, H., Baldini, J. U. L., Breitenbach, S. F. M., Johnson, K. R., van Hunen, J., & Pingzhong, Z. (2015). Seasonality of westerly moisture transport in the East Asian summer monsoon and its implications for interpreting precipitation δ18O. *Journal of Geophysical Research*, *120*, 5850–5862. https://doi.org/10.1002/2014JD022919

Barrett, P. J. (1996). Antarctic paleoenvironment through Cenozoic times: A review. *Terra Antarctic*, *3*, 103–119.

Beerling, D. J., & Royer, D. L. (2011). Convergent Cenozoic CO_2 history. *Nature Geoscience*. https://doi.org/10.1038/ngeo1186

Bosboom, R., Dupont-Nivet, G., Grothe, A., Brinkhuis, H., Villa, G., Mandic, O., … Guo, Z. J.

(2014). Timing, cause and impact of the late Eocene stepwise sea retreat from the Tarim Basin (west China). *Palaeogeography, Palaeoclimatology, Palaeoecology*. https://doi.org/10.1016/j.palaeo.2014.03.035

Bosboom, R. E., Dupont-Nivet, G., Grothe, A., Brinkhuis, H., Villa, G., Mandic, O., … Krijgsman, W. (2014). Linking Tarim Basin sea retreat (west China) and Asian aridification in the late Eocene. *Basin Research*, *26*, 621–640. https://doi.org/10.1111/bre.12054

Broccoli, A. J., & Manabe, S. (2002). The Effects of Orography on Midlatitude Northern Hemisphere Dry Climates. *Journal of Climate*. https://doi.org/10.1175/1520-0442(1992)005<1181:teooom>2.0.co;2

Carter, A., Riley, T. R., Hillenbrand, C. D., & Rittner, M. (2017). Widespread Antarctic glaciation during the Late Eocene. *Earth and Planetary Science Letters*, *458*, 49–57. https://doi.org/10.1016/j.epsl.2016.10.045

Cattle, H., Crossley, J., Drewry, D. J., Wadhams, P., Dowdeswell, J. A., & Schofield, A. N. (1995). Modelling Arctic climate change. *Philosophical Transactions of the Royal Society of London. Series A: Physical and Engineering Sciences*, *352*(1699), 201–213. https://doi.org/10.1098/rsta.1995.0064

Caves, J. K., Winnick, M. J., Graham, S. A., Sjostrom, D. J., Mulch, A., & Chamberlain, C. P. (2015). Role of the westerlies in Central Asia climate over the Cenozoic. *Earth and Planetary Science Letters*. https://doi.org/10.1016/j.epsl.2015.07.023

Chen, D., & Chen, H. W. (2013). Using the Köppen classification to quantify climate variation and change: An example for 1901-2010. *Environmental Development*. https://doi.org/10.1016/j.envdev.2013.03.007

Cherchi, A., Alessandri, A., Masina, S., & Navarra, A. (2011). Effects of increased CO_2 levels on monsoons. *Climate Dynamics*. https://doi.org/10.1007/s00382-010-0801-7

Chiang, J. C. H., Fung, I., Wu, C.-H., Cai, Y., Edman, J., Liu, Y., … Labrousse, C. (2014). Role of seasonal transitions and westerly jets in East Asian paleoclimate. *Quaternary Science Reviews*, *108*, 111–129. https://doi.org/10.1016/j.quascirev.2014.11.009

Chou, C., Neelin, J. D., Chen, C. A., & Tu, J. Y. (2009). Evaluating the "rich-get-richer" mechanism in tropical precipitation change under global warming. *Journal of Climate*. https://doi.org/10.1175/2008JCLI2471.1

Clift, P. D., & Plumb, R. A. (2008). *The Asian monsoon: Causes, history and effects*. *The Asian Monsoon: Causes, History and Effects*. Cambridge University Press. https://doi.org/10.1017/CBO9780511535833

Coleman, M., & Hodges, K. (1995). Evidence for Tibetan plateau uplift before 14 Myr ago from a new minimum age for east-west extension. *Nature*. https://doi.org/10.1038/374049a0

Council, N. R. (2008). *Antarctica: A Keystone in a changing world*. Washington, DC: The National Academies Press. https://doi.org/10.1016/S0920-5446(08)70043-8

Cox, P. M., Betts, R. A., Bunton, C. B., Essery, R. L. H., Rowntree, P. R., & Smith, J. (1999). The impact of new land surface physics on the GCM simulation of climate and climate sensitivity. *Climate Dynamics*, *15*, 183–203. https://doi.org/10.1007/s003820050276

Coxall, H. K., & Wilson, P. A. (2011). Early Oligocene glaciation and productivity in the eastern equatorial Pacific: Insights into global carbon cycling. *Paleoceanography*, *26*(2). https://doi.org/10.1029/2010PA002021

Coxall, H. K., Wilson, P. A., Palike, H., Lear, C. H., & Backman. (2005). Rapid stepwise onset of Antarctic glaciation and deeper calcite compensation in the Pacific Ocean. *Nature*, *433*, 53–57. https://doi.org/10.1038/nature03186

Cramer, B. S., Toggweiler, J. R., Wright, J. D., Katz, M. E., & Miller, K. G. (2009). Ocean

overturning since the Late Cretaceous: Inferences from a new benthic foraminiferal isotope compilation. *Paleoceanography*, *24*(4). https://doi.org/10.1029/2008PA001683

Currie, B. S., Rowley, D. B., & Tabor, N. J. (2005). Middle Miocene paleoaltimetry of southern Tibet: Implications for the role of mantle thickening and delamination in the Himalayan orogen. *Geology*. https://doi.org/10.1130/G21170.1

Cyr, A. J., Currie, B. S., & Rowley, D. B. (2005). Geochemical Evaluation of Fenghuoshan Group Lacustrine Carbonates, North-Central Tibet: Implications for the Paleoaltimetry of the Eocene Tibetan Plateau. *The Journal of Geology*. https://doi.org/10.1086/431907

Dabang, J., Huijun, W., & Xianmei, L. (2005). Evaluation of East Asian climatology as simulated by seven coupled models. *Advances in Atmospheric Sciences*, *22*(4), 479–495. https://doi.org/10.1007/bf02918482

de Martonne, E. (1926). Traité de Géographie Physique. *Geologiska Föreningen i Stockholm Förhandlingar*, *48*(1), 101. https://doi.org/10.1080/11035892609445647

de Noblet, N. (1997). Modelling late-Quaternary palaeoclimates and palaeobiomes. In B. Huntley, W. Cramer, A. V Morgan, H. C. Prentice, & J. R. M. Allen (Eds.), *Past and Future Rapid Environmental Changes* (pp. 31–52). Berlin, Heidelberg: Springer Berlin Heidelberg.

DeCelles, P. G., Quade, J., Kapp, P., Fan, M., Dettman, D. L., & Ding, L. (2007). High and dry in central Tibet during the Late Oligocene. *Earth and Planetary Science Letters*. https://doi.org/10.1016/j.epsl.2006.11.001

DeConto, R. M., & Pollard, D. (2003). A coupled climate-ice sheet modeling approach to the Early Cenozoic history of the Antarctic ice sheet. In *Palaeogeography, Palaeoclimatology, Palaeoecology*. https://doi.org/10.1016/S0031-0182(03)00393-6

DeConto, R. M., Pollard, D., Wilson, P. A., Palike, H., Lear, C. H., & Pagani, M. (2008). Thresholds for Cenozoic bipolar glaciation. *Nature*, *455*, 652–657. https://doi.org/10.1038/nature07337

Dong, X., Ding, Z., Yang, S., Luo, P., Wang, X., & Ji, J. (2013). Synchronous drying and cooling in central Asia during late Oligocene. *Chinese Science Bulletin*, *58*(25), 3119–3124. https://doi.org/10.1007/s11434-013-5821-3

Dupont-Nivet, G., Hoom, C., & Konert, M. (2008). Tibetan uplift prior to the Eocene-Oligocene climate transition: Evidence from pollen analysis of the Xining Basin. *Geology*. https://doi.org/10.1130/G25063A.1

Dupont-Nivet, G., Krijgsman, W., Langereis, C. G., Abels, H. A., Dai, S., & Fang, X. (2007a). Tibetan plateau aridification linked to global cooling at the Eocene-Oligocene transition. *Nature*. https://doi.org/10.1038/nature05516

Dupont-Nivet, G., Krijgsman, W., Langereis, C. G., Abels, H. A., Dai, S., & Fang, X. (2007b). Tibetan plateau aridification linked to global cooling at the Eocene–Oligocene transition. *Nature*, *445*(7128), 635–638. https://doi.org/10.1038/nature05516

Eldrett, J. S., Harding, I. C., Wilson, P. A., Butler, E., & Roberts, A. P. (2007). Continental ice in Greenland during the Eocene and Oligocene. *Nature*, *446*, 176–179. https://doi.org/10.1038/nature05591

England, P., & Searle, M. (1986). The Cretaceous-tertiary deformation of the Lhasa Block and its implications for crustal thickening in Tibet. *Tectonics*. https://doi.org/10.1029/TC005i001p00001

Escutia, C., De Santis, L., Donda, F., Dunbar, R. B., Cooper, A. K., Brancolini, G., & Eittreim, S. L. (2005). Cenozoic ice sheet history from East Antarctic Wilkes Land continental margin sediments. *Global and Planetary Change*, *45*, 51–81. https://doi.org/10.1016/j.gloplacha.2004.09.010

Francis, J. E., Marenssi, S., Levy, R., Hambrey, M., Thorn, V. C., Mohr, B., … DeConto, R. (2009). From Greenhouse to Icehouse - The Eocene/Oligocene in Antarctica. *Developments in Earth and Environmental Sciences*. https://doi.org/10.1016/S1571-9197(08)00008-6

Gadgil, S. (2003). T HE I NDIAN M ONSOON AND I TS V ARIABILITY. *Annual Review of Earth and Planetary Sciences*. https://doi.org/10.1146/annurev.earth.31.100901.141251

Gao, X., & Giorgi, F. (2008). Increased aridity in the Mediterranean region under greenhouse gas forcing estimated from high resolution simulations with a regional climate model. *Global and Planetary Change*. https://doi.org/10.1016/j.gloplacha.2008.02.002

Garzione, C. N., Dettman, D. L., Quade, J., DeCelles, P. G., & Butler, R. F. (2000). High times on the Tibetan Plateau Paleoelevation of the Thakkhola graben, Nepal. *Geology*, *28*(4), 339–342.

Goldner, A., Herold, N., & Huber, M. (2014). Antarctic glaciation caused ocean circulation changes at the Eocene-Oligocene transition. *Nature*, *511*(7511), 574–577. https://doi.org/10.1038/nature13597

Gordon, C., Cooper, C., Senior, C. A., Banks, H., Gregory, J. M., Johns, T. C., … Wood, R. A. (2000). The simulation of SST, sea ice extents and ocean heat transports in a version of the Hadley Centre coupled model without flux adjustments. *Climate Dynamics*, *16*, 147–168. https://doi.org/10.1007/s003820050010

Gregory, D., Shutts, G. J., & Mitchell, J. R. (1998). A new gravity-wave-drag scheme incorporating anisotropic orography and low-level wave breaking: Impact upon the climate of the UK Meteorological Office Unified Model. *Quarterly Journal of the Royal Meteorological Society*, *124*(546), 463–493. https://doi.org/10.1002/qj.49712454606

Gregory, J. M., & Mitchell, J. F. B. (1997). The climate response to CO_2 of the Hadley Centre

coupled AOGCM with and without flux adjustment. *Geophysical Research Letters*, *24*(15), 1943–1946.

Guo, Z., Dupont-Nivet, G., Abels, H. A., Bosboom, R. E., Hoorn, C., & van den Berg, B. C. J. (2014). Aridification in continental Asia after the Middle Eocene Climatic Optimum (MECO). *Earth and Planetary Science Letters*. https://doi.org/10.1016/j.epsl.2013.12.014

Guo, Z. T., Ruddiman, W. F., Hao, Q. Z., Wu, H. B., Qiao, Y. S., Zhu, R. X., … Llu, T. S. (2002). Onset of Asian desertification by 22 Myr ago inferred from loess deposits in China. *Nature*, *416*(6877), 159–163. https://doi.org/10.1038/416159a

Guo, Z. T., Sun, B., Zhang, Z. S., Peng, S. Z., Xiao, G. Q., Ge, J. Y., … Wei, J. J. (2008). A major reorganization of Asian climate by the early Miocene. *Climate of the Past*. https://doi.org/10.5194/cp-4-153-2008

Hansen, J., Sato, M., Kharecha, P., Beerling, D. J., Berner, R., Masson-Delmotte, V., … Zachos, J. C. (2008). Target Atmospheric CO_2: Where Should Humanity Aim? James. *Open Atmos. Sci. J.*, *2*, 217–231. https://doi.org/10.2174/1874282300802010217

Haywood, A. M., & Valdes, P. J. (2004). Modelling Pliocene warmth: contribution of atmosphere, oceans and cryosphere. *Earth and Planetary Science Letters*, *218*(3), 363–377. https://doi.org/https://doi.org/10.1016/S0012-821X(03)00685-X

Haywood, A. M., Valdes, P. J., Aze, T., Barlow, N., Burke, A., Dolan, A. M., … Voss, J. (2019). What can Palaeoclimate Modelling do for you? *Earth Systems and Environment*, *3*(1), 1–18. https://doi.org/10.1007/s41748-019-00093-1

Henderiks, J., & Pagani, M. (2008). Coccolithophore cell size and the Paleogene decline in atmospheric CO_2. *Earth and Planetary Science Letters*, *269*(3–4), 576–584. https://doi.org/10.1016/j.epsl.2008.03.016

Heureux, A. M. C., & Rickaby, R. E. M. (2015). Refining our estimate of atmospheric CO_2 across the eocene-Oligocene climatic transition. *Earth and Planetary Science Letters*. https://doi.org/10.1016/j.epsl.2014.10.036

Hodges, K. V. (2000). Tectonics of the Himalaya and southern Tibet from two perspectives. *GSA Bulletin*, *112*(3), 324–350.

Holbourn, A. E., Kuhnt, W., Clemens, S. C., Kochhann, K. G. D., Jöhnck, J., Lübbers, J., & Andersen, N. (2018). Late Miocene climate cooling and intensification of southeast Asian winter monsoon. *Nature Communications*, *9*(1), 1584. https://doi.org/10.1038/s41467-018-03950-1

Holbourn, A., Kuhnt, W., Kochhann, K. G. D., Andersen, N., & Sebastian Meier, K. J. (2015). Global perturbation of the carbon cycle at the onset of the Miocene Climatic Optimum. *Geology*, *43*(2), 123–126. https://doi.org/10.1130/G36317.1

Holbourn, A., Kuhnt, W., Lyle, M., Schneider, L., Romero, O., & Andersen, N. (2014). Middle Miocene climate cooling linked to intensification of eastern equatorial Pacific upwelling. *Geology*, *42*(1), 19–22. https://doi.org/10.1130/G34890.1

Holbourn, A., Kuhnt, W., Schulz, M., & Erlenkeuser, H. (2005). Impacts of orbital forcing and atmospheric carbon dioxide on Miocene ice-sheet expansion. *Nature*. https://doi.org/10.1038/nature04123

Hollis, C. J., Handley, L., Crouch, E. M., Morgans, H. E. G., Baker, J. A., Creech, J., … Pancost, R. D. (2009). Tropical sea temperatures in the high-latitude South Pacific during the Eocene. *Geology*, *37*(2), 99–102. https://doi.org/10.1130/G25200A.1

Hollis, C. J., Taylor, K. W. R., Handley, L., Pancost, R. D., Huber, M., Creech, J. B., … Zachos, J. C. (2012). Early Paleogene temperature history of the Southwest Pacific Ocean: Reconciling proxies and models. *Earth and Planetary Science Letters*, *349–350*, 53–66. https://doi.org/https://doi.org/10.1016/j.epsl.2012.06.024

Hong, B., Gasse, F., Uchida, M., Hong, Y., Leng, X., Shibata, Y., … Wang, Y. (2014). Increasing summer rainfall in arid eastern-Central Asia over the past 8500 years. *Scientific Reports*. https://doi.org/10.1038/srep05279

Huber, M., & Goldner, A. (2012, January 30). Eocene monsoons. *Journal of Asian Earth Sciences*. https://doi.org/10.1016/j.jseaes.2011.09.014

Inness, P. M., & Slingo, J. M. (2003). Simulation of the Madden-Julian Oscillation in a Coupled General Circulation Model. Part I: Comparison with Observations and an Atmosphere-Only GCM. *Journal of Climate*, *16*(3), 345–364.

IPCC. (2002). Climate change 2001: the scientific basis. Contribution of Working Group 1 to the Third Assessment Report of the Intergovernmental Panel on Climate Change, edited by J. T. Houghton, Y. Ding, D. J. Griggs, M. Noguer, P. J. van der Linden, X. Da. *International Journal of Climatology*, *22*(9), 1144. https://doi.org/10.1002/joc.763

IPCC. (2007). *Climate change 2007: Synthesis Report. Contribution of Working Groups I, II and III to the Fourth Assessment Report of the Intergovermental Panel on Climate Change*. Geneva, Switzerland.

Jagniecki, E. A., Lowenstein, T. K. T. K., Jenkins, D. M., & Demicco, R. V. (2015). Eocene atmospheric CO_2 from the nahcolite proxy. *Geology*, *43*(12), 1075–1078. https://doi.org/10.1130/G36886.1

Jiang, D., Ding, Z., Drange, H., & Gao, Y. (2008). Sensitivity of East Asian climate to the progressive uplift and expansion of the Tibetan Plateau under the mid-Pliocene boundary conditions. *Advances in Atmospheric Sciences*, *25*, 709–722. https://doi.org/10.1007/s00376-008-0709-x

Jiang, D., Wang, H., & Lang, X. (2005). Evaluation of East Asian climatology as simulated by seven coupled models. *Advances in Atmospheric Sciences*, *22*(4), 479–495.

Jovane, L., Florindo, F., Acton, G., Ohneiser, C., Sagnotti, L., Strada, E., … Passchier, S. (2019). Miocene Glacial Dynamics Recorded by Variations in Magnetic Properties in the ANDRILL-2A Drill Core. *Journal of Geophysical Research: Solid Earth*, *124*(3), 2297–2312. https://doi.org/10.1029/2018JB016865

Kapp, P., DeCelles, P. G., Gehrels, G. E., Heizler, M., & Ding, L. (2007). Geological records of the Lhasa-Qiangtang and Indo-Asian collisions in the Nima area of central Tibet. *Bulletin of the Geological Society of America*. https://doi.org/10.1130/B26033.1

Kathayat, G., Cheng, H., Sinha, A., Yi, L., Li, X., Zhang, H., … Edwards, L. (2017). The Indian monsoon variability and civilization changes in the Indian subcontinent. *Science Advances*. https://doi.org/10.1126/sciadv.1701296

Köppen, W. (1936). Das geographische System der Klimate. In W. Köppen & R. Geiger (Eds.), *Handbuch der Klimatologie* (pp. 1–44). Berlin: Verlag von Gebruder Borntraeger. Retrieved from www.borntraeger-cramer.com

Lease, R. O., Burbank, D. W., Gehrels, G. E., Wang, Z., & Yuan, D. (2007). Signatures of mountain building: Detrital zircon U/Pb ages from northeastern Tibet. *Geology*. https://doi.org/10.1130/G23057A.1

Lee, S. Y., Chiang, J. C. H., & Chang, P. (2015). Tropical Pacific response to continental ice sheet topography. *Climate Dynamics*, *44*, 2429–2446. https://doi.org/10.1007/s00382-014-2162-0

Lei, Y., Hoskins, B., & Slingo, J. (2014). Natural variability of summer rainfall over China in HadCM3. *Climate Dynamics*, *42*(1–2), 417–432. https://doi.org/10.1007/s00382-013-1726-8

Leier, A. L., DeCelles, P. G., Kapp, P., & Gehrels, G. E. (2007). Lower Cretaceous Strata in the Lhasa Terrane, Tibet, with Implications for Understanding the Early Tectonic History of the Tibetan Plateau. *Journal of Sedimentary Research*.

https://doi.org/10.2110/jsr.2007.078

Li, J., Ding, Y., Wu, G., Chang, C.-P., Liu, J., Wu, Z., & Wang, B. (2008). How to Measure the Strength of the East Asian Summer Monsoon. *Journal of Climate*. https://doi.org/10.1175/2008jcli2183.1

Li, X., Zhang, R., Zhang, Z., & Yan, Q. (2018a). Do climate simulations support the existence of East Asian monsoon climate in the Late Eocene? *Palaeogeography, Palaeoclimatology, Palaeoecology*, *509*, 47–57. https://doi.org/10.1016/j.palaeo.2017.12.037

Li, X., Zhang, R., Zhang, Z., & Yan, Q. (2018b). Do climate simulations support the existence of East Asian monsoon climate in the Late Eocene? *Palaeogeography, Palaeoclimatology, Palaeoecology*. https://doi.org/10.1016/j.palaeo.2017.12.037

Li, X., Zhang, R., Zhang, Z., & Yan, Q. (2018c). What enhanced the aridity in Eocene Asian inland: Global cooling or early Tibetan Plateau uplift? *Palaeogeography, Palaeoclimatology, Palaeoecology*. https://doi.org/10.1016/j.palaeo.2017.10.029

Liang, X. Z., & Wang, W. C. (1998). Associations between China monsoon rainfall and tropospheric jets. *Quarterly Journal of the Royal Meteorological Society*, *124*(552), 2597–2623. https://doi.org/10.1256/smsqj.55203

Licht, A., Cappelle, M. van, Abels, H. A., Ladant, J. B., Trabucho-Alexandre, J., France-Lanord, C., … Jaeger, J. J. (2014). Asian monsoons in a late Eocene greenhouse world. *Nature*, *513*, 501–513. https://doi.org/10.1038/nature13704

Licht, A., Dupont-Nivet, G., Pullen, A., Kapp, P., Abels, H. A., Lai, Z., … Giesler, D. (2016). Resilience of the Asian atmospheric circulation shown by Paleogene dust provenance. *Nature Communications*. https://doi.org/10.1038/ncomms12390

Lippert, P. C., van Hinsbergen, D. J. J., & Dupont-Nivet, G. (2014). Early Cretaceous to

present latitude of the central proto-Tibetan Plateau: A paleomagnetic synthesis with implications for Cenozoic tectonics, paleogeography, and climate of Asia. *The Geological Society of America*, *Special pa*, 1–29. https://doi.org/10.1130/2014.2507(01)

Liu, X. D., & Dong, B. W. (2013). Influence of the Tibetan Plateau uplift on the Asian monsoon-arid environment evolution. *Chinese Science Bulletin*, *58*(34), 4277–4291. https://doi.org/10.1007/s11434-013-5987-8

Liu, X., Dong, B., Yin, Z.-Y., Smith, R. S., & Guo, Q. (2017). Continental drift and plateau uplift control origination and evolution of Asian and Australian monsoons. *Scientific Reports*, *7*(1), 40344. https://doi.org/10.1038/srep40344

Liu, X., Dong, B., Yin, Z. Y., Smith, R. S., & Guo, Q. (2019). Continental drift, plateau uplift, and the evolutions of monsoon and arid regions in Asia, Africa, and Australia during the Cenozoic. *Science China Earth Sciences*. https://doi.org/10.1007/s11430-018-9337-8

Liu, X., & Yin, Z.-Y. (2002). Sensitivity of East Asian monsoon climate to the uplift of the Tibetan Plateau. *Palaeogeography, Palaeoclimatology, Palaeoecology*, *183*, 223–245. Retrieved from www.elsevier.com/locate/palaeo

Lu, H., Wang, X., & Li, L. (2010). Aeolian sediment evidence that global cooling has driven late Cenozoic stepwise aridification in central Asia. *Geological Society, London, Special Publications*, *342*(1), 29. https://doi.org/10.1144/SP342.4

Lu, H. Y., & Guo, Z. (2014, January 1). Evolution of the monsoon and dry climate in East Asia during late Cenozoic: A review. *Science China Earth Sciences*. Science in China Press. https://doi.org/10.1007/s11430-013-4790-3

Lunt, D. J., Flecker, R., & Clift, P. D. (2010). The impacts of Tibetan uplift on palaeoclimate proxies. *Geological Society, London, Special Publications*.

https://doi.org/10.1144/sp342.16

Lunt, D. J., Ross, I., Hopley, P. J., & Valdes, P. J. (2007). Modelling Late Oligocene C4 grasses and climate. *Palaeogeography, Palaeoclimatology, Palaeoecology*, *251*(2), 239–253. https://doi.org/https://doi.org/10.1016/j.palaeo.2007.04.004

Manabe, S., & Hahn, D. G. (1977). Simulation of the tropical climate of an ice age. *Journal of Geophysical Research (1896-1977)*, *82*(27), 3889–3911. https://doi.org/10.1029/JC082i027p03889

Markwick, P. J. (2007). The palaeogeographic and palaeoclimatic significance of climate proxies for data-model comparisons. *Deep-Time Perspectives on Climate Change: Marrying the Signal from Computer Models and Biological Proxies*, 251–312.

Meyer, B., Tapponnier, P., Bourjot, L., Métivier, F., Gaudemer, Y., Peltzer, G., … Zhitai, C. (1998). Crustal thickening in Gansu-Qinghai, lithospheric mantle subduction, and oblique, strike-slip controlled growth of the Tibet Plateau. *Geophysical Journal International*. https://doi.org/10.1046/j.1365-246X.1998.00567.x

Miao, Y., Wu, F., Chang, H., Fang, X., Deng, T., Sun, J., & Jin, C. (2016). A Late-Eocene palynological record from the Hoh Xil Basin, northern Tibetan Plateau, and its implications for stratigraphic age, paleoclimate and paleoelevation. *Gondwana Research*, *31*, 241–252. https://doi.org/https://doi.org/10.1016/j.gr.2015.01.007

Miao, Y., Wu, F., Herrmann, M., Yan, X., & Meng, Q. (2013). Late early Oligocene East Asian summer monsoon in the NE Tibetan Plateau: Evidence from a palynological record from the Lanzhou Basin, China. *Journal of Asian Earth Sciences*. https://doi.org/10.1016/j.jseaes.2013.07.003

Miller, K. G., Wright, J. D., Katz, M. E., Wade, B. S., Browning, J. V., Cramer, B. S., & Rosenthal, Y. (2009). Climate threshold at the Eocene-Oligocene transition: Antarctic ice sheet influence on ocean circulation. *The Geological Society of America*, *Special pa*,

169–178. https://doi.org/10.1130/2009.2452(11)

Molnar, P., Boos, W. R., & Battisti, D. S. (2010a). Orographic Controls on Climate and Paleoclimate of Asia: Thermal and Mechanical Roles for the Tibetan Plateau. *Annual Review of Earth and Planetary Sciences*. https://doi.org/10.1146/annurev-earth-040809-152456

Molnar, P., Boos, W. R., & Battisti, D. S. (2010b). Orographic Controls on Climate and Paleoclimate of Asia: Thermal and Mechanical Roles for the Tibetan Plateau. *Annual Review of Earth and Planetary Sciences*, *38*, 77–102. https://doi.org/10.1146/annurev-earth-040809-152456

Molnar, P., England, P., & Martinod, J. (1993). Mantle dynamics, uplift of the Tibetan Plateau and the Indian monsoon. *Reviews of Geophysics*, *31*(4), 357–396.

Molnar, P., & Stock, J. M. (2009). Slowing of India's convergence with Eurasia since 20 Ma and its implications for Tibetan mantle dynamics. *Tectonics*. https://doi.org/10.1029/2008TC002271

Moran, K., Backman, J., Brinkhuis, H., Clemens, S. C., Cronin, T., Dickens, G. R., … Kristoffersen, Y. (2006). The Cenozoic palaeoenvironment of the Arctic Ocean. *Nature*, *441*, 601–605. https://doi.org/10.1038/nature04800

Murphy, M.A, Yin, An, Harrison, T.M., Harrison, Durr, S.B, Z, Chen, Ryerson, F.J., Kidd, W.S.F., X, Wang, X, Z. (1997). Did the Indo-Asian collision alone create the Tibetan plateau? *Geology*, *25*(8), 719–722. https://doi.org/10.1130/0091-7613(1997)025<0719:DTIACA>2.3.CO;2

Najman, Y., Pringle, M., Godin, L., & Oliver, G. (2001). Dating of the oldest continental sediments from the Himalayan foreland basin. *Nature*, *410*, 194–197.

Normile, D. (2007). Getting at the roots of killer dust storms. *Science*.

https://doi.org/10.1126/science.317.5836.314

Pagani, M., Zachos, J. C., Freeman, K. H., Tipple, B., & Bohaty, S. (2005). Marked decline in atmospheric carbon dioxide concentrations during the Paleogene. *Science*, *309*, 600–603. https://doi.org/10.1126/science.1113485

Parthasarathy, B., Munot, A. A., & Kothawale, D. R. (1994). All-India monthly and seasonal rainfall series: 1871-1993. *Theoretical and Applied Climatology*. https://doi.org/10.1007/BF00867461

Pearson, P. N., Foster, G. L., & Wade, B. S. (2009a). Atmospheric carbon dioxide through the Eocene-Oligocene climate transition. *Nature*, *461*, 1110–1114. https://doi.org/10.1038/nature08447

Pearson, P. N., Foster, G. L., & Wade, B. S. (2009b). Atmospheric carbon dioxide through the Eocene-Oligocene climate transition. *Nature*. https://doi.org/10.1038/nature08447

Pearson, P. N., & Palmer, M. R. (2000). Atmospheric carbon dioxide concentrations over the past 60 million years. *Nature*, *406*, 695–699. https://doi.org/10.1038/35021000

Pope, V. D., Gallani, M. L., Rowntree, P. R., & Stratton, R. A. (2000). The impact of new physical parametrizations in the Hadley Centre climate model: HadAM3. *Climate Dynamics*, *16*(2–3), 123–146. https://doi.org/10.1007/s003820050009

Pope, V. D., Pamment, J. A., Jackson, D. R., & Slingo, A. (2001). The Representation of Water Vapor and Its Dependence on Vertical Resolution in the Hadley Centre Climate Model. *Journal of Climate*, *14*(14), 3065–3085. https://doi.org/10.1175/1520-0442(2001)014<3065:TROWVA>2.0.CO;2

Prell, W. L., Niitsuma, N., & Al., E. (1991). ODP Leg 117. *Proc. ODP, Init. Repts.*, *117*.

Quan, C., Han, S., Utescher, T., Zhang, C., & Liu, Y. S. C. (2013). Validation of temperature-

precipitation based aridity index: Paleoclimatic implications. *Palaeogeography, Palaeoclimatology, Palaeoecology*. https://doi.org/10.1016/j.palaeo.2013.05.008

R. Lewis, A., Marchant, D., Ashworth, A., R. Hemming, S., & Machlus, M. (2007). *Major middle Miocene climate change and the extinction of tundra communities: Evidence from the Transantarctic Mountains*.

Ramage, C. S. (1971). *Monsoon meteorology*. Academic Press, New York.

Ramstein, G., Fluteau, F., Besse, J., & Joussaume, S. (1997). Effect of orogeny, plate motion and land-sea distribution on Eurasian climate change over the past 30 million years. *Nature*, *386*(6627), 788–795. https://doi.org/10.1038/386788a0

Rea, D. K. (1994). The paleoclimatic record provided by eolian deposition in the deep sea: The geologic history of wind. *Reviews of Geophysics*. https://doi.org/10.1029/93RG03257

Rodwell, M. J., & Hoskins, B. J. (2001). Subtropical Anticyclones and Summer Monsoons. *Journal of Climate*, *14*(15), 3192–3211. https://doi.org/10.1175/1520-0442(2001)014<3192:SAASM>2.0.CO;2

Rögl, F. (1998). Palaeogeographic Considerations for Mediterranean and Paratethys Seaways (Oligocene to Miocene). *Annalen Des Naturhistorischen Museums in Wien*, *99A*(April), 279–310.

Rögl, F. (1999). MEDITERRANEAN AND PARATETHYS. FACTS AND HYPOTHESES OF AN OLIGOCENE TO MIOCENE PALEOGEOGRAPHY (SHORT OVERVIEW). *Geologica Carpathica*, *50*(4), 339–349.

Roth-Nebelsick, A., Grein, M., Utescher, T., & Konrad, W. (2012). Stomatal pore length change in leaves of Eotrigonobalanus furcinervis (Fagaceae) from the Late Eocene to the Latest Oligocene and its impact on gas exchange and CO 2 reconstruction. *Review*

of Palaeobotany and Palynology, *174*, 106–112. https://doi.org/10.1016/j.revpalbo.2012.01.001

Rowley, D. B. (1996). Age of initiation of collision between India and Asia: A review of stratigraphic data. *Earth and Planetary Science Letters*, *145*, 1–13.

Rowley, D. B., & Currie, B. S. (2006). Palaeo-altimetry of the late Eocene to Miocene Lunpola basin, central Tibet. *Nature*, *439*, 677–681. https://doi.org/10.1038/nature04506

Rowley, D. B., Pierrehumbert, R. T., & Currie, B. S. (2001). A new approach to stable isotope-based paleoaltimetry: implications for paleoaltimetry and paleohypsometry of the High Himalaya since the Late Miocene. *Earth and Planetary Science Letters*, *5836*, 1–17. Retrieved from www.elsevier.com/locate/epsl

Royer, D. L., Berner, R. A., Beerling, D. J., Berner, R., & Ž Beerling, S. D. (2001). *Phanerozoic atmospheric CO change: evaluating geochemical 2 and paleobiological approaches*. *Earth-Science Reviews* (Vol. 54). Retrieved from www.elsevier.comrlocaterearscirev

Rubel, F., & Kottek, M. (2010). Observed and projected climate shifts 1901-2100 depicted by world maps of the Köppen-Geiger climate classification. *Meteorologische Zeitschrift*, *19*(2), 135–141. https://doi.org/10.1127/0941-2948/2010/0430

Schiemann, R., Lüthi, D., & Schär, C. (2009a). Seasonality and interannual variability of the westerley jet in the Tibetan Plateau region. *Journal of Climate*, *22*(11), 2940–2957. https://doi.org/10.1175/2008JCLI2625.1

Schiemann, R., Lüthi, D., & Schär, C. (2009b). Seasonality and interannual variability of the westerley jet in the Tibetan Plateau region. *Journal of Climate*, *22*, 2940–2957. https://doi.org/10.1175/2008JCLI2625.1

Shukla, A., Mehrotra, R. C., Spicer, R. A., Spicer, T. E. V., & Kumar, M. (2014). Cool

equatorial terrestrial temperatures and the South Asian monsoon in the Early Eocene: Evidence from the Gurha Mine, Rajasthan, India. *Palaeogeography, Palaeoclimatology, Palaeoecology*, *412*, 187–198. https://doi.org/10.1016/j.palaeo.2014.08.004

Smith, R. N. B. (1990). A scheme for predicting layer clouds and their water content in a general circulation model. *Quarterly Journal of the Royal Meteorological Society*, *116*(492), 435–460. https://doi.org/10.1002/qj.49711649210

Solomon, S., Qin, D., Manning, M., Chen, Z., Marquis, M., Averyt, K. B., … Miller, H. L. (2007). Global climate projections. In S. Solomon, D. Qin, M. Manning, Z. Chen, M. Marquis, K. B. Averyt, … H. L. Miller (Eds.), *Climate Change 2007: The Physical Science Basis. Contribution of Working Group I to the Fourth Assessment Report of the Intergovernmental Panel on Climate Change*. Cambridge University Press.

Spicer, R. A., Harris, N. B. W., Widdowson, M., Herman, A. B., Guo, S., Valdes, P. J., … Kelley, S. P. (2003). Constant elevation of southern Tibet over the past 15 million years. *Nature*. https://doi.org/10.1038/nature01356

Spicer, R., Yang, J., Herman, A., Kodrul, T., Aleksandrova, G., Maslova, N., … Jin, J.-H. (2017). Paleogene monsoons across India and South China: Drivers of biotic change. *Gondwana Research*, *49*, 350–363. https://doi.org/https://doi.org/10.1016/j.gr.2017.06.006

Srivastava, G., Spicer, R. A., Spicer, T. E. V., Yang, J., Kumar, M., Mehrotra, R., & Mehrotra, N. (2012). Megaflora and palaeoclimate of a Late Oligocene tropical delta, Makum Coalfield, Assam: Evidence for the early development of the South Asia Monsoon. *Palaeogeography, Palaeoclimatology, Palaeoecology*, *342–343*, 130–142. https://doi.org/10.1016/j.palaeo.2012.05.002

Steinthorsdottir, M., Porter, A. S., Holohan, A., Kunzmann, L., Collinson, M., & McElwain, J.

C. (2016). Fossil plant stomata indicate decreasing atmospheric CO 2 prior to the Eocene-Oligocene boundary. *Climate of the Past*, *12*(2), 439–454. https://doi.org/10.5194/cp-12-439-2016

Steinthorsdottir, M., Vajda, V., & Pole, M. (2019). Significant transient pCO 2 perturbation at the New Zealand Oligocene-Miocene transition recorded by fossil plant stomata. *Palaeogeography, Palaeoclimatology, Palaeoecology*, *515*, 152–161. https://doi.org/10.1016/j.palaeo.2018.01.039

Su, F., Duan, X., Chen, D., Hao, Z., & Cuo, L. (2013). Evaluation of the global climate models in the CMIP5 over the Tibetan Plateau. *Journal of Climate*, *26*(10), 3187–3208. https://doi.org/10.1175/JCLI-D-12-00321.1

Sun, B. N., Wang, Q. J., Konrad, W., Ma, F. J., Dong, J. L., & Wang, Z. X. (2017). Reconstruction of atmospheric CO_2 during the Oligocene based on leaf fossils from the Ningming Formation in Guangxi, China. *Palaeogeography, Palaeoclimatology, Palaeoecology*, *467*, 5–15. https://doi.org/10.1016/j.palaeo.2016.09.015

Sun, J., Gong, Z., Tian, Z., Jia, Y., & Windley, B. (2015). Late Miocene stepwise aridification in the Asian interior and the interplay between tectonics and climate. *Palaeogeography, Palaeoclimatology, Palaeoecology*. https://doi.org/10.1016/j.palaeo.2015.01.001

Sun, X., & Wang, P. (2005). How old is the Asian monsoon system? - Palaeobotanical records from China. *Palaeogeography, Palaeoclimatology, Palaeoecology*, *222*(3–4), 181–222. https://doi.org/10.1016/j.palaeo.2005.03.005

Tang, Z., Yang, S., Qiao, Q., Yin, F., Huang, B., & Ding, Z. (2016). A high-resolution geochemical record from the Kuche depression: Constraints on early Miocene uplift of South Tian Shan. *Palaeogeography, Palaeoclimatology, Palaeoecology*, *446*, 1–10. https://doi.org/10.1016/j.palaeo.2016.01.020

Tapponnier, P. (2001). Oblique Stepwise Rise and Growth of the Tibet Plateau. *Science*,

294(5547), 1671–1677. https://doi.org/10.1126/science.105978

Taylor, M., & Yin, A. (2009). Active structures of the Himalayan-Tibetan orogen and their relationships to earthquake distribution, contemporary strain field, and Cenozoic volcanism. *Geosphere*. https://doi.org/10.1130/ges00217.1

Tian, S.-F., & Yasunari, T. (1998). Climatological Aspects and Mechanism of Spring Persistent Rains over Central China. *Journal of the Meteorological Society of Japan*, *76*, 57–70. https://doi.org/10.2151/jmsj1965.76.1_57

Tindall, J., Flecker, R., Valdes, P., Schmidt, D. N., Markwick, P., & Harris, J. (2010). Modelling the oxygen isotope distribution of ancient seawater using a coupled ocean–atmosphere GCM: Implications for reconstructing early Eocene climate. *Earth and Planetary Science Letters*, *292*(3), 265–273. https://doi.org/https://doi.org/10.1016/j.epsl.2009.12.049

Tripati, A., & Darby, D. (2018). Evidence for ephemeral middle Eocene to early Oligocene Greenland glacial ice and pan-Arctic sea ice. *Nature Communications*, *1038*(9). https://doi.org/10.1038/s41467-018-03180-5

Turner, a. G., Inness, P. M., & Slingo, J. M. (2005). The role of the basic state in the ENSO–monsoon relationship and implications for predictability. *Quarterly Journal of the Royal Meteorological Society*, *131*(607), 781–804. https://doi.org/10.1256/qj.04.70

TURNER, A., SPERBER, K. R., SLINGO, J., MEEHL, G., MECHOSO, C. R., KIMOTO, M., & GIANNINI, A. (2011). MODELLING MONSOONS: UNDERSTANDING AND PREDICTING CURRENT AND FUTURE BEHAVIOUR. In *The Global Monsoon System* (Vol. Volume 5, pp. 421–454). WORLD SCIENTIFIC. https://doi.org/doi:10.1142/9789814343411_0025

Ueda, H., Iwai, A., Kuwako, K., & Hori, M. E. (2006). Impact of anthropogenic forcing on the Asian summer monsoon as simulated by eight GCMs. *Geophysical Research Letters*, *33*(6). https://doi.org/10.1029/2005GL025336

Wang, B. (2005). Global Monsoon System : Research and Forecast. *WMO Report*, *1266*(1266), 0–552.

Wang, B., Ding, Q., Fu, X., Kang, I. S., Jin, K., Shukla, J., & Doblas-Reyes, F. (2005). Fundamental challenge in simulation and prediction of summer monsoon rainfall. *Geophysical Research Letters*, *32*(15). https://doi.org/10.1029/2005GL022734

Wang, B., & Fan, Z. (1999). Choice of South Asian Summer Monsoon Indices. *Bulletin of the American Meteorological Society*. https://doi.org/10.1175/1520-0477(1999)080<0629:COSASM>2.0.CO;2

Wang, C., Hong, H., Li, Z., Yin, K., Xie, J., Liang, G., … Zhang, K. (2013). The Eocene–Oligocene climate transition in the Tarim Basin, Northwest China: Evidence from clay mineralogy. *Applied Clay Science*, *74*, 10–19. https://doi.org/10.1016/j.clay.2012.09.003

Wang, C., Zhao, X., Liu, Z., Lippert, P. C., Graham, S. A., Coe, R. S., … Li, Y. (2008). Constraints on the early uplift history of the Tibetan Plateau. *Proceedings of the National Academy of Sciences*, *105*(13), 4987–4992. https://doi.org/10.1073/pnas.0703595105

Webster, P. J., Magana, V. O., Palmer, T. N., Shukla, J., Tomas, R. A., Yanai, M., & Yasunari, T. (1998). *Monsoons: Processes, predictability, and the prospects for prediction*. *Journal of Geophysical Research* (Vol. 103).

Webster, P. J., & Yang, S. (1992). *Monsoon and ENSO: Selectively interactive systems*. *Mefeorol. Soc* (Vol. 118).

Williams, J., Barry, R. G., & Washington, W. M. (1974). Simulation of the Atmospheric Circulation Using the NCAR Global Circulation Model with Ice Age Boundary Conditions. *Journal of Applied Meteorology*, *13*(3), 305–317.

Willmes, C., Becker, D., Brocks, S., Hütt, C., & Bareth, G. (2017). High Resolution Köppen-

Geiger Classifications of Paleoclimate Simulations. *Transactions in GIS*. https://doi.org/10.1111/tgis.12187

Winkler, A., Wolf-Welling, T., Stattegger, K., & Thiede, J. (2002). Clay mineral sedimentation in high northern latitude deep-sea basins since the Middle Miocene (ODP Leg 151, NAAG). *International Journal of Earth Sciences*, *91*(1), 133–148. https://doi.org/10.1007/s005310100199

Wu, G., Liu, Y., Wang, T., Wan, R., Liu, X., Li, W., … Liang, X. (2007). The Influence of Mechanical and Thermal Forcing by the Tibetan Plateau on Asian Climate. *Journal of Hydrometeorology*, *8*, 770–789. https://doi.org/10.1175/jhm609.1

Yin, A. (2010). Cenozoic tectonic evolution of Asia: A preliminary synthesis. *Tectonophysics*. https://doi.org/10.1016/j.tecto.2009.06.002

Yin, A., Dang, Y. Q., Wang, L. C., Jiang, W. M., Zhou, S. P., Chen, X. H., … McRivette, M. W. (2008). Cenozoic tectonic evolution of Qaidam basin and its surrounding regions (Part 1): The southern Qilian Shan-Nan Shan thrust belt and northern Qaidam basin. *Bulletin of the Geological Society of America*. https://doi.org/10.1130/B26180.1

Yin, A., & Harrison, T. M. (2000). Geologic Evolution of the Himalayan-Tibetan Orogen. *Annual Reviews of Earth and Planetary Sciences*, *28*, 211–280. https://doi.org/10.1080/01947641003598252

Yin, A., Nie, S., Craig, P., Harrison, T. M., Ryerson, F. J., Xianglin, Q., & Geng, Y. (1998). Late Cenozoic tectonic evolution of the southern Chinese Tian Shan. *Tectonics*, *17*, 1–27. https://doi.org/10.1029/97TC03140

Zachos, J.C., Dickens G.R., Zeebe, R. E. (2008). An early Cenozoic perspective on greenhouse warming and carbon-cycle dynamics. *Nature*, *451*.

Zachos, J. C., Breza, J. R., & Sherwood, W. W. (1992). Early oligocene ice sheet expansion on

antarctica: Stable isotope and sedimentological evidence from Kerguelen Plateau, southern Indian Ocean. *Geology*, *20*, 569–573.

Zachos, J. C., Pagani, M., Sloan, L., Thomas, E., & Billups, K. (2001). Trends, Rhythms, and Aberrations in Global Climate 65 Ma to Present. *Science*, *292*, 686–693.

Zhang, Q., Liu, Y., Wang, T., Wang, Z., Liang, X., Li, W., … Wan, R. (2007). The Influence of Mechanical and Thermal Forcing by the Tibetan Plateau on Asian Climate. *Journal of Hydrometeorology*, *8*, 770–789. https://doi.org/10.1175/jhm609.1

Zhang, R., Jiang, D., Ramstein, G., Zhang, Z., Lippert, P. C., & Yu, E. (2018). Changes in Tibetan Plateau latitude as an important factor for understanding East Asian climate since the Eocene: A modeling study. *Earth and Planetary Science Letters*. https://doi.org/10.1016/j.epsl.2017.12.034

Zhang, R., Jiang, D., Zhang, Z., Cheng, Z., & Zhang, Q. (2017). Comparison of the climate effects of surface uplifts from the northern Tibetan Plateau, the Tianshan, and the Mongolian Plateau on the East Asian climate. *Journal of Geophysical Research*, *122*, 7949–7970. https://doi.org/10.1002/2017JD026470

Zhang, Y. G., Pagani, M., Liu, Z., Bohaty, S. M., & DeConto, R. M. (2013). A 40-million-year history of atmospheric CO_2. *Philosophical Transactions of the Royal Society A: Mathematical, Physical and Engineering Sciences*, *371*. https://doi.org/10.1098/rsta.2013.0096

Zhongshi, Z., Wang, H., Guo, Z., & Jiang, D. (2007). What triggers the transition of palaeoenvironmental patterns in China, the Tibetan Plateau uplift or the Paratethys Sea retreat? *Palaeogeography, Palaeoclimatology, Palaeoecology*. https://doi.org/10.1016/j.palaeo.2006.08.003

Zoura, D., Hill, D. J., Dolan, A. M., Hunter, S. J., Tang, Z., & Haywood, A. M. (2019). Atmospheric carbon dioxide, ice sheet and topographic constraints on palaeo

moisture availability in Asia. *Earth and Planetary Science Letters*, *519*, 12–27. https://doi.org/10.1016/j.epsl.2019.04.035